Development, characterization, and performance analysis of eggshell derived calcium phosphate

Thesis Submitted

By

Dalia Acharjee

(D-7/ISLM/06/17)

Doctor of Philosophy (Engineering)

SCHOOL OF BIO-SCIENCE & ENGINEERING
FACULTY COUNCIL OF ENGINEERING & TECHNOLOGY
JADAVPUR UNIVERSITY
KOLKATA, INDIA

2023

JADAVPUR UNIVERSITY
KOLKATA-700032, INDIA

1. Title of the thesis:

"Development, characterization and performance analysis of eggshell derived calcium phosphate"

2. Name, Designation & Institution of Supervisors:

Dr. Piyali Basak

Associate Professor

School of Bio-science and Engineering

Jadavpur University

Kolkata-700032

&

Dr.Sukumar Roy

Professor

Department of Biomedical Engineering

Netaji Subhas Engineering College

Techno City,Garia

Kolkata-700152

&

Dr. Samit Kumar Nandi

Professor

Department of Veterinary Surgery & Radiology

West Bengal University of Animal and Fishery Science

Kolkata-700037

CERTIFICATE FROM THE SUPERVISOR/S

This is to certify that the thesis entitled **"Development, characterization and performance analysis of eggshell derived calcium phosphate** "submitted by Dalia Acharjee, who got her name registered on 10/01/2017 for the award of **Ph.D.(Engineering) degree** of **Jadavpur University**, is absolutely based upon her own work under the supervision of **Dr. Piyali Basak , Dr. Sukumar Roy and Dr. Samit Kumar Nandi,** and that neither her thesis nor any part of the same has been submitted for any degree / diploma or any other academic award anywhere before.

Piyali Basak. 27th Dec 2023

Dr. Piyali Basak

Associate Professor
School of Bio-science & Engineering
Jadavpur University
Kolkata-700032

Samit Kumar Nandi 27/12/23

Dr. Samit Kumar Nandi

Professor
Department of Veterinary Surgery & Radiology, West Bengal University of Animal and Fishery Science, Kolkata-700037

Sukumar Roy
27/12/2023

Dr. Sukumar Roy

Professor
Department of Biomedical Engineering
Netaji Subhas Engineering College
Techno City, Garia
Kolkata-700152

"Statement of Originality"

I, DALIA ACHARJEE(D-7/ISLM/06/17)registered on 10/01/2017do hereby declare that this thesis entitled "Development, Characterization, and performance analysis of eggshell derived calcium phosphate" contains literature survey and original research work done by the undersigned candidate as part of Doctoral studies.

All information in this thesis have been obtained and presented in accordance with existing academic rules and ethical conduct. I declare that, as required by these rules and conduct, I have fully cited and referred all materials and results that are not original to this work.

I also declare that I have checked this thesis as per the "Policy on Anti Plagiarism, Jadavpur University, 2019", and the level of similarity as checked by iThenticate software is10%.

Dalia Acharjee
Signature of Candidate:

Date : 27.12.2023

Certified by Supervisor(s):

(Signature with date, seal)

1. Piyali Basak. 27th Dec 2023

DR. PIYALI BASAK
ASSOCIATE PROFESSOR
SCHOOL OF BIOSCIENCE & ENGG.
JADAVPUR UNIVERSITY
KOLKATA - 700032

2. Sukumar Roy 27th Dec. 2023

Dr. SUKUMAR ROY
Professor : Dept. of Biomedical Engineering
Netaji Subhas Engineering College
Techno City, Garia
Kolkata-700 152

3. Samit Kumar Nandi 27th Dec 2023

Dr. S. K. Nandi
Professor
Dept. of Veterinary Surgery & Radiology
F/O Veterinary & Animal Sciences
W.B.U.A.F.S., 37, K.B. Sarani, Kol-37

DEDICATION

To my Father Dibakar Acharjee and to my mother Chitra Acharjee for all your love, patience, and encouragement over the years.

To my supervisors Dr. Piyali Basak, Dr. Sukumar Roy, Dr. Samit Kumar Nandi without you I would not be where I am today. Thank you for always being only a phone call away!

To my friend Dr. Sujan Krishna Samanta, encourage and help all the time in my journey. Thank you for your co-operation.

To my Husband Mr. Biplab Dey, for all your love and support. Thank you for sharing this journey with

PREFACE

This thesis is the result of my own work and includes nothing which is the outcome of work done in collaboration, except where specifically indicated in the text and acknowledgements. The research was conducted primarily at the School of Bio-Science and Engineering, Jadavpur University , at the laboratories of Netaji Subhas Engineering College, Techno City,Garia, Kolkata-700152 and laboratories of West Bengal university of animal and Fishery Science, Kolkata and Central Research Facility, IIT-Kharagpur during the years from 2017 to 2023, under the supervision of Dr Piyali Basak school of Bio-science and engineering , Jadavpur University ,Dr. Sukumar Roy ,Department of Biomedical Engineering Netaji Subhas Engineering College, Techno City,Garia , Kolkata-700152 and Dr. Samit Kumar Nandi, Department of Veterinary Surgery & Radiology, West Bengal University of Animal and Fishery Science, Kolkata.

No part of this thesis has already been or is being concurrently submitted for any degree, diploma or other qualification.

Acknowledgement

First and foremost I would like to express my deepest regards and respect to the most important person of my thesis advisor ***Dr. Piyali Basak, School of Bio-science & Engineering, Jadavpur University,*** for her esteemed guidance, invaluable suggestions, constant encouragement at every stage of my work. She has not only been my guide but more like a friend to me. Without her assistance it would not be possible to complete the work. My heart will always bear respectful gratitude to her.

I express my gratitude to my co-guide ***Dr. Sukumar Roy, Department of Biomedical Engineering Netaji Subhas Engineering College, Techno City, Garia, Kolkata-700152***,for his continuous support,sharing valuable documents relating to the work, giving suggestion and solving different problems faces during the journey.

My deepest gratitude goes to my co-guide ***Dr. Samit Kumar Nandi, Department of Veterinary Surgery & Radiology, West Bengal University of Animal & Fishery Science, Kolkata***. I am very grateful for his tremendous help and kind support behind this research. He has educated me on different aspects of animal trials. The thesis work would never be possible without his help.

I express my indebtness to ***Director, Netaji Subhash Engineering College, and Techno India Group*** *for giving me opportunities to go with this work.*

During my research, ***Dr.*** **Sujan Krishna Samanta,** ***Department of Biomedical Engineering Netaji Subhas Engineering College, Techno City, Garia*** helped me a lot for sample preparation. I would like to give my sincere thanks to ***Dr.*** **Sujan Krishna Samanta** for his kind help. I offer my cordial thanks to***, Biswanath Kundu, CGCRI, Kolkata***, for providing all the necessary help and technical support during my work. I would like to express my appreciation to ***Dr. Mangal Roy and Santanu Mondal, Department of Metallurgical and Materials Engineering, IIT, Kharagpur****, India for extending their help in material characterization and in vivo studies.*

I would like to acknowledge ***Pratik, Pranabesh***,***Tathagata*** for being more like a family member to me during my entire research work. Last but certainly not the least, I would like to thank my ***mother*** and all other family members for their immense support and constant enthusiasm whenever I tried to tread a lesser walked lane. Without their help I could have never achieved anything in any sphere of life.

(Dalia Acharjee)
School of Bio-Science & Engineering, JU

Abstract

To meet up everyday food requirement with ever increasing population in the world, a huge amount of egg shell wastes is given rise to everywhere from house hold kitchen to various food processing units. Egg shell contains large amount of calcium ion. By using egg shell hydroxyapatite ceramic have been prepared. Hydroxyapatite plays a significant role in several biomedical application for their marked bioactivity. In bone grafting, it is used for treating bone defects caused by wounds or osteoporosis. In the present work an in-depth and systematic study of different doped variants (Zinc, Magnesium and Titanium) of hydroxyapatite by using laboratory grade calcium hydroxide (synthetic source) and egg shell (Biogenic source) was done. We have prepared Pure HAp (synthetic source) with its six variants and egg shell HAp (Biogenic source) with six variants. Total fourteen variants were prepared and a comparative assessment was done. We have tried to investigate some important features which are the prerequisite for their application. These include green density, Sintered density, lattice parameter study, mechanical properties, contacts behavior with SBF, hemolytic characteristics, and its cytotoxic nature. The capability of new apatite development on the surface of PureHAp shell HAp and their variants were also considered and compared by using Simulated Body Fluid (SBF) to observe their interaction with human body fluid. The focus of our work is to study the performances of eggshell sourced hydroxyapatite and their doped variants over pure HAp and their dopants on bone regeneration. The pure and doped samples were implanted in femoral bone defect model (rabbit) to assess bone regeneration. Bone regeneration was assessed after 1- and 2-month post-implantation on the basis of clinical radiological, histological, fluorochrome labelling and scanning electron microscopy (SEM). Radiological and fluorochrome labelling study showed reduced size of 5% Ti-Egg shell HAp implant vis-à-vis more new bone formation as compared to other groups. less interfacial gap between the implant and bone were also observed in SEM study. However, all the doped materials are suitable as bone grafting material and have potential for application in bone tissue engineering. It may be concluded that-egg shell dopant implants stimulates prompt new bone formation and presents an exciting possibility for orthopedic reconstructive procedures.

TABLE OF CONTENTS

LIST OF TABLES

LIST OF FIGURES

LIST OF ABBREVIATIONS

HAP	Hydroxyapatite
ASTM	American Society for Testing and Materials
Ca-P	Calcium Phosphate
SEM	Scanning Electron Microscope
FTIR	Fourier Transform Infrared Spectroscopy
GPa	Giga Pascal
BMP	Bone Morphogenetic Protein
TGF	Transforming Growth Factor
JCPDS	Joint Committee On Powder Diffraction Standards
OD	Optical Density
OTC	Oxy-tetracycline dihydrate
SBF	Simulated Body Fluid
SD	Standard Deviation
1M	One Month
2M	Two Month
XRD	X-Ray Diffraction
PBMC	Peripheral Blood Mononuclear Cell

HC	Haversian Canal
BII	Bone-Implant-Interfaces

LIST OF PUBLICATIONS

Journal publications

1)Dalia Acharjee, Santanu Mandal, Sujan Krishna Samanta, Mangal Roy, Biswanath Kundu, Sukumar Roy, Piyali Basak and Samit K. Nandi, In Vitro and In Vivo Bone Regeneration Assessment of Titanium-Doped Waste Eggshell-Derived Hydroxyapatite in the Animal Model, *ACS Biomater. Sci. Eng.* 2023, 9, 8, 4673–4685, https://doi.org/10.1021/acsbiomaterials.3c00060

2) Dalia Acharjee, SujanKrishnaSamanta, Sourav Debnath, Piyali Basak, Sukumar Roy, Samit Kumar Nandi, In-Vitro characterization of Magnesium doped Hydroxyapatite developed from calcium hydroxide and waste eggshell, Journal for Basic Sciences, ISSN NO: 1006-8341

3) Dalia Acharjee, SujanKrishnaSamanta, Mayukh Das, Piyali Basak, Sukumar Roy, Study on Structure and Properties of Crystalline Hydroxyapatite obtained from Biological and Synthetic Sources, 978-1-7281-7340-5/20/$31.00 ©2020 IEEE

4) Dalia Acharjee, SujanKrishnaSamanta, Piyali Basak, Sukumar Roy, Samit Kumar Nandi, In Vitro Performance Analysis of Ti- and Zn-Doped Hydroxyapatite Made from Waste Eggshells, Sustainable Advanced Technologies for Industrial Pollution Control, Springer Proceedings in Earth and Environmental Sciences, https://doi.org/10.1007/978-3-031-37596-5

5) Dalia Acharjee, SujanKrishnaSamanta, Sourav Debnath, Piyali Basak, Sukumar Roy, Samit Kumar Nandi, Bio-Sourced Hydroxyapatite is Better Bioactive than its Synthetic Grade: A Comparative Assessment of Ti and Zn Doped Hydroxyapatite Derived from Bio and Synthetic Sources, Journal of Mines, Metals and Fuels, 71(11): 0-0; 2023. DOI: 10.18311/jmmf/2023/, Print ISSN : 0022-2755.

List of Patents: Nil

List of presentations in national/international

1)Study on Structure and Properties of Crystalline Hydroxyapatite obtained from Biological and Synthetic Sources, , 2020 IEEE International Conference for Convergence in Engineering,Netaji Subhash Engineering college,Garia

2)In Vitro Performance Analysis of Ti- and Zn-Doped Hydroxyapatite Made from Waste Eggshells, Sustainable Advanced Technologies for Industrial Pollution Control Proceedings of ATIPC 2022, Civil Engineering Department, Indian Institute of Engineering Science and Technology, Shibpur, P.O.- Botanic Garden Howrah - 711 103, West Bengal, India

1. INTRODUCTION

1.1 Introduction

In the past few decades, bone grafting surgeries have become increasingly common because of various bone defects, which are about two million worldwide [1]. Along with bone-related diseases, the increasing number of sports injuries and accidents have accelerated the requirement for bone tissue replacement [2]. In this regard, the methodologies commonly used for bone regeneration are autografting or allografting. However, those processes involve different limitations such as shortage of material, donor site morbidity, disease transmission risk, inappropriate immune response, etc. [3]. Those limitations triggered huge research interest in bone tissue engineering towards the development of various synthetic biocompatible materials based on metals, polymers, and ceramics. This study focuses on the naturally available bio ceramic, as it possesses many trace elements that are beneficial for tissue ingrowth.

1.2 Bioceramic

Repair and reconstruction of damaged or diseased body parts can be accomplished with biocompatible ceramics [4]. They have found wide applications in the biomedical field as biocompatible materials, such as tooth replacement, knee replacements, hip replacements, ligaments, tendons, spinal fusions, periodontium repairs, maxillofacial reconstruction, jaw stabilization, and augmentation temporary bone fillers following tumor removal, and carbon coatings in prosthetic heart valves that are thrombo-resistant [5.6]. The characteristics of bio-ceramics can be classified according to their origin, tissue response, crystallinity, and composition [7].

1. Based on Origin:
   - ❖ Natural Materials: Teeth, Bones, Biogenic Silica, Mollusk Shells & Natural Pearls
   - ❖ Synthetic Materials: Calcium Phosphate, Bioglass & Hydroxyapatite (HAp)

2. Based on Tissue Responses:
   - ❖ Bioactive Materials: Calcium Phosphate, Bioglass & Hydroxyapatite (HAp)
   - ❖ Bioinert Materials: Glassy Carbon and alumina

3. Based on Composition:
   - ❖ Aluminum Materials: Alumina & Aluminosilicates
   - ❖ Zirconium Materials: Zircon, Cubic Zirconia, & Tetragonal Zirconia
   - ❖ Carbon Materials: Graphite and vitreous Carbon
   - ❖ Calcium Phosphate Materials: Amorphous Calcium Phosphate, β-Tricalcium Phosphate, Biphasic Calcium Phosphate, HAp, and fluorapatite
   - ❖ Silica Materials: Tricalcium Silicate

4. Based on Crystallinity:
   - ❖ Crystalline Materials: Aluminosilicates, HAp, Fluorapatite, & Zirconia
   - ❖ Amorphous Materials: Amorphous Calcium Phosphate, & Bioglass

Among these materials, hydroxyapatite has gained significant interest for its biocompatibility, osteoconductive, and chemical alikeness to the bone's inorganic component. Besides, a substantial portion (60-70%) of natural bone contains hydroxyapatite.

1.3 Hydroxyapatite (HAp)

A precursor of octacalcium phosphate, it has a calcium-to-phosphorus ratio of 1.67 and is an important inorganic component of teeth and bones. The chemical formula for this compound is $Ca_{10}(PO_4)_6(OH)_2$ and it has a hexagonal structure. There are three phosphate tetrahedral cells per unit cell occupying the void spaces between two hexagons [8].

Table 1.1 Mechanical and Physical Properties of Hydroxyapatite

Elastic Modulus (GPa)	40 - 117
Compressive Strength (MPa)	294
Bending Strength (MPa)	147
Vickers Hardness (GPa)	3.43
Poisson's ratio	0.27
Density (g/cm^3)	3.167

Because of its bioactive and bioresorbable properties and extensive effect in physiological and biological environments, HAp has gained more research interest in scientists to synthesize in the laboratory [9]. Several methods have been used for the synthesis of HAp. These are hydrothermal, chemical precipitation, sol-gel, multiple emulsion, biomimetic deposition, electro-deposition method, etc. [10]. There are differences in the absorption rate of the biological apatite layer of synthesized HAp and of natural apatite. It contains trace elements like Na^+, Mg^{2+}, Zn^{2+}, K^+, Ba^{2+}, Si^{2+}, F^-, and CO_3^{-2} and particles are in the nano range, which provides larger surface areas, mechanical ductility, and uniform distribution of grain size in physiological conditions [11]. To enhance the performance properties of synthetic HAp or mimic natural apatite components, researchers researched and developed it from natural ingredients [12, 13].

1.3.1 HAp Prepared from Natural Sources

HAp is extracted or prepared from a variety of natural sources or wastes. It may be from mammalian bone (bovine, horse, or camel), marine or aquatic sources (fish bone and scale), shells (cockle, calm, eggshell, seashell), plants, and mineral sources (limestone). In studies of HAp prepared from natural sources, it is non-stoichiometric. HAp prepared from natural sources is responsible for the reduction of environmental pollution, and production cost and would be sustainable too. As a result, this contributes to the economy, the environment, and the general health of the population. Mammalian bone, specifically the cortical part, is used as a research model because it resembles human bone morphologically and structurally. Much literature demonstrated the preparation of HAp from bovine bone. One literature

showed that a nano-sized HAp was prepared from bovine bone through a vibro-milling process [14]. Whereas others extracted it mainly from three different processes: subcritical water, thermal decomposition, and alkaline hydrothermal process [15]. The three processes are cheap and simple and the thermal decomposition process gives better HAp nanorods. Increasing consumption of fish in our daily day life causes a huge amount of fish scale and fish bone wastage. With a rich source of calcium, phosphate, and carbonate, it made sense to use it to make HAp, which will aid in waste management. Different literature showed a detailed study of HAp prepared by using these fish wastes. Some researchers followed the alkaline hydrolysis method [16] and made HAp. As per the Environmental Protection Agency eggshell wastes ranked as the 15^{th} major food industrial problem [17]. Eggshell consists of three-layer namely lamellar, cuticle, and spongeous. The spongeous and lamellar layers form a matrix bonded with protein fibers and calcium carbonate crystal (1:50). The matrix crystal surrounds the calcium carbonate crystal and passes through it. It increases the mechanical strength of eggshell [18, 19]. A major organic component of matrices is mucopolysaccharide protein (chondroitin sulphate A and B), plus glucosamine, galactosamine, fucose, manose, and silica. The inorganic components are calcium carbonate (94%), calcium phosphate, and magnesium carbonate. The eggshell contains a substantial amount of calcium carbonate, which can be used for a variety of food products as well as industrial applications, such as milk tablets enriched with eggshell powder, lactose-free milk for lactose-intolerant individuals, calcium supplements, bone graft substitutes, dentistry, pharmaceutical industry/excipients, heavy metal removal, and catalytic applications [17].

1.3.2 Hydroxyapatite Composites with Porous Blocks

HAp is osteoconductive but not osteoinductive. It has poor resistance to bacterial growth on the implant surface. There is no load-bearing capacity of pure synthetic HAp that can be used in implant applications. The researchers tried to sort out the problems by incorporating some ions in the structure preferably carbonate (carbonated hydroxyapatite), as it presents abundantly in human and animal bone [20, 21]. To improve its load-bearing capacities, carbon nanotubes and different metal oxides are used (alumina, zirconia, titanium). However, its application has limitations as they are bioinert and non-biocompatible. Many have studied and prepared HAp whiskers as they are biocompatible and have better mechanical properties but one limitation is thermally unstable. Another way is to make a composite by adding polymer and cross-linking agent. CHA (carbonated hydroxyapatite) can be doped with trace elements Zn^{2+}, Na+, Ti^{4+}, $Sr^{2+,}$ and Mg^{2+}. This sort of co-doping may affect crystallite size, crystallinity levels, lattice parameters, solubility, morphology, thermal stability, and bioactivity of the ceramic. In addition to promoting bone metabolism and growth, zinc ions contribute to the development of the body's physiological systems. The Zn-doped HAp showed better MG63 cell response and proliferation compared to the undoped HAp. A scaffold material implanted into the body must have interconnected pores for tissue to grow through them and for the implant to be biologically fixed to the host body. Researchers have studied numerous processes and materials for the formation of porous blocks. It is beneficial for mineralized bone cell growth to have pores larger than 150 m [23]. The densification and grain size of the bulk HAp influences the mechanical properties. The sintering temperature of $900\text{-}1150^{0}$C is ideal for densification of scaffolds. The strength of the material decreases when the HAp is converted into tricalcium phosphate above the temperature. Different

processes were applied to get a porous scaffold like mixing rod-shaped and spherical-shaped HAp with polyacrylamide solids with slow stirring then a uniform slurry mixture was obtained by stirring at a high speed for 1 hour. It was seen that r-HAp (rod-shaped hydroxyapatite) would get grain dissolution before grain growth and s-HAp (spherical-shaped hydroxyapatite) get surface dissolution during sintering. When these combinations are mixed and sintered, the grain growth is restricted by s-HAp. Alternatively dissolved r-HAp on surfaces causes grain growth and maintains scaffold structure [24]. Few researchers made porous blocks by using porogens/porosifiers. When heated the samples about 1100-1200^{0}C temperature, the porogens drive off the samples by making the block porous.

1.4 Bone Fracture and Healing

In the skeletal system, bone is the major load-bearing tissue. The mineralized and organic matrix of bone is made up of many different types of cells, such as osteoblasts, osteoclasts, osteoprogenitor cells, and mature osteoclasts, which are all embedded in this matrix. Bones and matrix are formed by osteoblasts and osteoclasts, whereas bone resorption occurs through osteoclasts. A large portion of the bones are composed of type I collagen, which is responsible for strength and tensile properties. A proteoglycan is one of the proteins that contributes to compression strength, in addition to other proteins as well. Several matrix proteins are involved in the formation of bone and matrix, including osteocalcin, osteonectin, and osteopontin. In the process of differentiation and growth of bone cells, cytokines, and growth factors play a crucial role. The inorganic constituent is made of hydroxyapatite which provides compressive strength. Whenever the force is given upon a bone beyond its elastic limit, a fracture is caused. Bone fractures may happen under traumatic (injuries and accidents) or non-traumatic (osteoporosis, cancer) conditions. After fracturing the bones, the healing process starts. There are intrinsic and extrinsic factors that affect the healing process. One of the factors associated with bone loss is the location of the fracture, the quality of the bone, the blood supply, the health of the soft tissues, and the immobilization of the fracture. Examples of extrinsic factors: age, nutritional status, comorbid conditions, smoking, and medications can be mentioned. According to the mechanics of fracture healing, fracture healing may happen along two separate pathways in the biological environment.

- Primary healing or direct healing through internal remodeling
- Secondary healing or indirect healing through callus formation

1.4.1 Primary Healing

Primary healing involves both fracture ends being anatomically opposite, and strains are placed across the fracture site by 2%. Through compression plating rigid internal fixation may take place that gives absolute stability. Direct remodeling of the Haversian canal, lamellar bone, and blood vessels occurred. Upon fracture, both ends of the osteons cutting cones are formed. There may be osteoclasts at the leading end of the cutting cones that can absorb bone along the fracture line to form longitudinal hollows that are later filled with bone by osteoblasts. The haversian system is therefore restored by axially integrating the bony union. Upon the re-establishment of haversian systems, osteoblastic precursors penetrate

blood vessels and cause neovascularization. So, a bone fracture healing instead of periosteal callus formation happened.

1.4.2 Secondary Healing

There is relative stability in secondary healing. Strain between the fracture sites is 2-10%. There is an intra-membranous ossification process as well as an endochondral ossification process that occurs through callus formation in embryologic bone development. Several types of bone fixation and stability provide bone fixation and relative stability, including casting, external fixators, intramedullary nails, and bridging plates. The three different stages are:

- Inflammation
- Callus formation and re-vascularization
- Remodeling

1.4.2.1 Phase I (Inflammation, 0-7 days, post-trauma)

An inflammatory response to a fracture starts with the presence of hematomas and clots of fibrin, and the infiltrated neutrophils, macrophages, and platelets begin to produce inflammatory proteins such as tumor necrosis factor-a (TNF-a), interleukin-1 (IL-1), IL-6, and IL-8. In the fracture site, the mesenchymal cells differentiate into osteogenic cells, which result in the formation of the granulation tissue.

1.4.2.2 Phase II (Revascularization, 7-9 days and 3-4 months, post-trauma)

A soft callus or endochondral callus is formed in between the fracture ends where granulation tissues are formed. There is an increase in blood flow as a result of neovascularization of the capillaries in this area. Mesenchymal stem cells (differentiation of cell types) proliferated and migrated through the fracture gap callus and differentiated fibroblasts (responsible for wound healing by generating traction and contractile forces), replacing hematoma, and producing extracellular matrix. Soft tissues in between the gaps undergo endochondral ossification until a hard callus is formed. The chondrocytes become hypertrophic (chondrogenic differentiation to cartilage mineralization) and the extracellular matrix becomes calcified and forms woven bones.

1.4.2.3 Phase II (Remodeling, several months-years)

Osteoclasts reabsorb the bone-hard callus. Osteoblasts formed the lamellar bone [25]. Bones are shaped according to the mechanical stresses they experience (Wolf's law).

To salvation from bone injury problems, researchers investigate and generate many ways out. An external fixator is recommended to be applied following the osteotomy to stimulate bone healing at the fracture site by pulling at a controlled rate at the fracture site. In orthopedic cases, a fresh autograph was traditionally used as a bone graft material. In most cases, a second surgical site is created using a piece of tissue from the ipsilateral iliac crest. After

surgery, there are a variety of complications, including nerve damage, bleeding, a prolonged period of pain, and difficulty walking. An autograph harvest may result in a longer hospital stay and an increase in costs. In comparison with autograph surgeries, cadaveric allografts have been shown to have better advantages. Before implanting the cadaveric allograft, care must be taken, and wash the viable cell components to avoid any infections. A synthetic bone graft based on calcium hydroxyapatite, calcium sulfates, and calcium phosphate provides the same mechanical and physical stability as a natural bone and mimics the human cancellous bone [26].

REFERENCES

[1] Global, regional, and national burden of bone fractures in 204 countries and territories, 1990–2019: a systematic analysis from the Global Burden of Disease Study 2019, Volume 2, Issue 9, E580-E592, September 2021. https://doi.org/10.1016/S2666-7568(21)00172-0.

[2] Kel C Robi, Naranda Jakob, Kuhta Matevz and Vogrin Matjaz, The Physiology of Sports Injuries and Repair Processes. http://dx.doi.org/10.5772/54234.

[3] Autograft, allograft, and bone graft substitutes: clinical evidence and indications for use in the setting of orthopedic trauma surgery, Journal of Orthopaedic Trauma Publish Ahead of Print, DOI: 10.1097/BOT.0000000000001420.

[4] M. Roy, A. Bandyopadhyay, S. Bose, Chapter 6 Ceramics in Bone Grafts and Coated Implants, 2017, Pages 265-314. https://doi.org/10.1016/B978-0-12-802792-9.00006-9.

[5] Larry L. Hench. Bioceramics: From Concept to Clinic, American Ceramic Society,74 (7) 1487-510 (1991). https://doi.org/10.1111/j.1151-2916.1991.tb07132.x.

[6] Hongshi Ma, Chun Feng, Jiang Chang, 3D-printed bioceramic scaffolds: From bone tissue engineering to tumor therapy, 1742-7061 / 2018 Acta Materialia Inc. https://doi.org/10.1016/j.actbio.2018.08.026.

[7] Hushmat Gul, Bioceramics: types and clinical applications, 3, 2020, Pages 53-83. https://doi.org/10.1016/B978-0-08-102834-6.00003.

[8] Basics of hydroxyapatite structure, synthesis, properties, and clinical applications, Hamad Khalid, Interdisciplinary Research Centre in Biomedical Materials (IRCBM), COMSATS University Islamabad, Lahore Campus, Lahore, Pakistan

[9] Mucalo M. R., Hydroxyapatite (HAp) for Biomedical Applications. Woodhead Publishing; Cambridge, England: 2015.14 Animal-bone derived hydroxyapatite in biomedical applications; pp. 307-34.

[10] Amit Kumar Nayak, Hydroxyapatite Synthesis Methodologies: An Overview, International Journal of Chem Tech Research, CODEN (USA): IJCRGG ISSN: 0974-4290, Vol.2, No.2, pp 903-907, April-June 2010.

[11] M. Akram, R. Ahmed, I. Shakir, W.A.W. Ibrahim, R. Hussain, Extracting hydroxyapatite and its precursors from natural resources, J. Mater. Sci. 49 (2014)1461–1475.

[12] A.L. Bosky, Natural and Synthetic Hydroxyapatites. Biomaterials Science: an Introduction to Materials: Third Edit, Elsevier, 2013.

[13] B.D. Ratner, A.S. Hoffman, F.J. Schoen, J.E. Lemons, Biomaterials Science: an Introduction to Materials in Medicine, Elsevier Science, 2004.

[14] A. Ruksudjarit, K. Pengpat, G. Rujijanagul, T. Tunkasiri, Synthesis and characterization of Nanocrystalline hydroxyapatite from natural bovine bone, Curr. Appl. Phys. 8 (2008) 270-272.

[15] N.A.M. Barakat, M.S. Khil, A.M. Omran, F.A. Sheikh, H.Y. Kim, Extraction of pure natural hydroxyapatite from the bovine bones bio waste by three different methods. Mater. Process. Technol. 209 (2009) 3408-3415.

[16] W. Pon-On, P. Suntornsaratoon, N. Charoenphandhu, J. Thongbunchoo, N. Krishnamra, I.M. Tang, Hydroxyapatite from fish scale for potential use as bone scaffold or regenerative material, Mater. Sci. Eng. C 62 (2016) 183-189.

[17] Ajala, E., Eletta, O., Ajala, M., &Oyeniyi, S. (2018). Characterization and evaluation of chicken eggshell for use as a bio-resource. Arid Zone Journal of Engineering, Technology and Environment, 14, 26–40.

[18] E. M. Rivera, M. Araiza, W. Brostow, V. M. Castan˜ o, J.R.Dı´az- Estrada, R. Herna´ ndez, J. R. Rodrı´guez, Synthesis of hydroxyapatite from eggshells, Materials Letters 41 (1999) 128-134.

[19] D. Siva Rama Krishna, A. Siddharthan, S. K. Seshadri, T. S. Sampath Kumar, An over route for the synthesis of nanocrystalline hydroxyapatite from eggshell waste, Journal of Materials Science Materials in Medicine 18 (2007) 1735-1743.

[20] Xiangmei Liu, H.C. Man, Laser fabrication of Ag-HA nanocomposites on Ti6Al4V implant for enhancing bioactivity and antibacterial capability, Mater. Sci. Eng. C 70 (2017) 1-8.

[21]. I.R. Gibson, W. Bonfield, Novel synthesis and characterization of an AB-type carbonate-substituted hydroxyapatite, J. Biomed. Mater. Res. 59 (2002) 697-70.

[22] Zinc containing hydroxyapatite ceramics to promote osteoblastic cell activity, Y. Sogo, A. Ito, K. Fukasawa, T. Sakurai and N. Ichinose, Materials Science and Technology September 2004 Vol. 20.

[23] E. Wintermantel, J. Mayer, K.L. Blum, P. Eckert, P. Luscher, M. Mathey, Biomaterials 17 (1996) 83-91.

[24] Jinchuan Wu, Changshun Ruan, Vital Role of Hydroxyapatite Particle Shape in Regulating the Porosity and Mechanical Properties of the Sintered Scaffolds. http://dx.doi.org/doi:10.1016/j.jmst.2017.01.008.

[25] Kalfas, I. H., Principles of bone healing. Neurosurgical Focus, 10 (4), 1-4, 2001.

[26] Synthetic Calcium–Phosphate Materials for Bone Grafting, Oleg Mishchenko, Anna Yanovska, Oleksii Kosinov Polymers 2023, 15(18),3822; https://doi.org/10.3390/polym15183822

2. LITERATURE SURVEY

2. Introduction

Bone and joint-related diseases are prevalent in our everyday life as reflected in the number of cases reported which is about 2 million worldwide, in the last decade [1]. To alleviate the problem, researchers investigate and find ways to sort out it. Autographs and allografts are replacement surgeries that may be applicable in this field but it has some limitations [2]. Among them are morbidity at donor sites, shortages of materials, and the risk of disease transmission. To overcome these limitations, synthetically produced materials that are similar to mammal bones are increasingly being studied and prepared in laboratories. One of them is calcium phosphate-based bio-ceramic e.g., hydroxyapatite [3]. It has wide application in the biomedical field due to its biocompatibility and osseointegration properties.

Researchers have synthesized hydroxyapatite (HAp) through various routes. A number of procedures have been presented, including the solid state reaction by Pramaniket *al*. [4], the wet chemical method and the hydrothermal synthesis by Liu *et al*. [5], and Kwon *et al*. [6], the sol-gel procedures and the mechanochemical synthesis by Yeong *et al*. [7], the electrochemical deposition and the microwave radiation by Kumar et al. [8] and Wang *et al.* [9], the combustion synthesis by Taset et al. [10]. Several trace elements have been found in synthetic calcium phosphate bioceramics, including hydroxyapatite, which does not mimic the normal bone composition[11, 12]. Literature shows that adding some dopant molecules to HAp ceramics enhances their efficacy. With a view to getting a better biocompatible bioceramic material, researchers emphasized biogenic origin as a source of calcium ions. Among them are clam cells, mollusk cells, egg shells, etc.

2.1 Synthesis of Hydroxyapatite

Bayraktar *et al*. [13] show that a homogeneous, one-phase calcium hydroxyapatite powder has successfully been prepared in a simulated body fluid solution of pH 7.4 by maintaining the temperature at 37^0C. A chemical precipitation technique is used here to prepare HAp using calcium nitrate, di-ammonium hydrogen phosphate salts, and urea. One notable point is that phase stability is sustained even at 1600^0C heating temperature for 6 h.

A novel preparation of biphasic calcium phosphate ceramics (BCP) by mixing hydroxyapatite and tri-calcium phosphate (TCP) in prescribed ratios has been done by Kumar *et al*. [14] through microwave irradiation technique. The apatite formation was confirmed by scanning electron microscopic analysis. The instant preparation of biphasic calcium phosphate would be done in the operation theatre also by maintaining proper sterilization conditions. Ansari *et al*. [15] prepared hydroxyapatite by using calcium hydroxide where the calcium-phosphorus ratio is more than 1.67. Free calcium hydroxide was formed more in the solution media and has a beneficial role of inhibition in bacterial growth.

Yanagisawa et *al.* [16] prepared compact, dense HAp at mild temperature by applying the hydrothermal technique. Three reaction parameters play crucial roles in this reaction viz temperature, pressure, and time of the reaction. The experiment was done at four different temperatures 100^0C, 150^0C, 200^0C, 250^0C. Upon increasing the temperature; density and hardness have increased, which signifies that densification occurs at higher temperatures.

Chanda et *al.* [17] also sintered the prepared HAp, TCP, and its dopant variants through the microwave sintering method. Here a uniform shrinkage and lack of cracking was observed in the uniform microstructure samples. A comparative study of both the samples sintered by

conventional and microwave processes shows that there were no major changes in bulk densities but microwave sintering consumes less time indicating an economic approach.

Santos *et al*. [18] synthesized HAp by wet chemical precipitation method by three distinguished routes designated as R1, R2, and R3. The R1 and R2 were maintained at 40^0C whereas R3 at room temperature. On alteration of reaction parameters, the crystallinity may vary. Twelve types of samples have been prepared using three different routes, namely route 1 (calcium hydroxide with phosphoric acid), route 2 (calcium hydroxide with ammonium bi-phosphate), and route 3 (calcium hydroxide with calcium hydrogen phosphate hydrate) by varying stir speed, solution adding ratio, pH, and temperature. On increasing the temperature, an additional tri-calcium phosphate (TCP) phase was formed that is beneficial to bone formation.

Researchers pay heed to getting valuable products from naturally occurring waste materials that cause environmental pollution in our daily lives. Calcium phosphate bioceramics is one of them. In order to prepare calcium-related bioceramics, a lot of calcium storage resources i.e., animal shells available naturally and easily have been focused. A calcium phosphate bioceramic, called hydroxyapatite, is derived from plant and algae sources, bone, aquatic, and mineral sources.

Different literature supports the production of HAp from animal bones especially bovine bone other than camel, horse, and porcine bone because the femoral bone of the species resembles human bone [19]. Before calcination of bone, pretreatment is a crucial step to remove the dirt or other fat or membranous materials that adhere to bones. In some literature boiling water has been used to wash the bone for 8 h [20, 21], others use acetone and chloroform solution [22, 23], or applied treatment with surfactants and alkalis for the same [24]. The researchers used a lot of different methods to get hydroxyapatite from bovine bone. Akram *et al*. [11] used the calcination process at a temperature up to 1400^0C in furnace where all organic residues are removed and pathogens are killed. Barakat *et al*. [22] used hydrothermal treatment; Hosseinzadeh *et al*. [23] [23] used 2 different temperatures for 6 hrs - 750^0C and 850^0C - in their thermal decomposition study. XRD studies showed that at 750^0C pure HAp and 850^0C combination of pure HAp and TCP was produced maintaining the stoichiometric ratio 1.5 (as TCP was produced). Ruk *et al.* [21] used both calcination and vibromilling methods. In this study, it was found that a needle shape diameter of <100nm with a calcium (Ca) phosphorus (P) ratio of 1.66. On increasing the time duration of milling, the needle shape was broken into finer and homogeneous particles.

Other mammal bones like camel bone, pig bone, and horse bone had been employed to get hydroxyapatite. Jaber *et al*. [25] used calcination and ball milling to extract HAp from camel bone at 1000^0C temperature for 3 hrs. A pure HAp with a better stoichiometry of Ca/P 1.66 was obtained from this source. Ruk *et al*. [21] used a vibromilling process which is effective for the separation and preparation of hydroxyapatite from the parent compound. Jaber et al. [25] used calcination and ball milling process which is effective for nanocrystalites preparation.

Cho *et al*. [26] noticed that osteogenicity with apatite formation in hydroxyapatite would increase if sodium ion is substituted in place of calcium ion. A study by Rahavi et al. [27] obtained nano HAp from camel and horse bone at temperatures of 700^0C for 2 hrs with Ca/P ratios of 2.036 and 2.131, respectively. Janus *et al*. (28) used both alkaline and calcination

methods for HAp preparation from pig bone at 700^0C and 1200^0C. This study gives 70-180 nm nano size range of HAp.

Researchers found other biogenic sources like fish bones and scales (aquatic or marine sources) which contain a huge percentage of calcium, phosphate and carbonate ions which are essential for HAp preparation. Pretreatment was done to remove fleshy meat and debris by simply boiling at 100^0C temperature [29, 30, 31], or rinsing with mild hydrochloric acid (0.1-1M) (32, 33, 34) to deproteinize and then washed with water. Pal *et al*. [30] worked on latecalcarifer bones at 200^0C, 400^0C, 800^0C, 1000^0C, and 1200 ^{0}C for 1 h. At higher temperatures (1200^0C) both TCP and HAp have produced a stoichiometric ratio 1.62, lower than the conventional ratio. Venkatesan *et al*. [35] prepared and compared HAp from Thunnus obesus fish bone through calcination at 900^0C using the hydrolysis method.

In the calcination method, a pure HAp with better crystallinity was produced over the hydrolysis method. Ozawa *et al*. [36] stated that the crystal particle size may be preserved in the hydrolysis method. Mondal et al. studied other approaches to synthesizing HAp from fish scale [29, 37]. They calcined fish scale in different temperatures viz, 200^0C, 400^0C, 800^0C, 1000^0C, and 1200^0C for 1 hr. They confirmed that the calcination above 1000^0C gives β-TCP. Additionally, plasma atomic emission spectroscopy (ICP-AES) with inductive coupling test showed the presence of elements like K, Sr, Na, and Mg. Panda *et al*. [32] used both calcination and alkaline methods. At 75^0C temperature, fish scales were first treated with NaOH (1N), followed by a calcium chloride dihydrate ($CaCl_2.2H_2O$) solution, and finally calcined for 1 hr at 800^0C. Pon-On *et al*. [33] used an alkaline method with a slight modification and get hydroxyapatite with a size range of width 15-19 nm, length 100 nm and calcium-phosphorus ratio 2.01.

Another approach for processing calcium phosphate bioceramics from biogenic sources i.e. cockle, calm, and eggshell gives an effective pathway for HAp synthesis. Eggshell is a huge source of calcium carbonate (about 94%) [11]. Mustaffa *et al*. [38] extracted hydroxyapatite from cockle shells by using both calcination and sol-gel methods. Properly cleaned and milled eggshell was crushed in powder and calcined at 600^0C temperature. Calcium carbonate was converted to calcium oxide, then HAp was produced through the sol-gel method. Prabu et al. [39] prepared hydroxyapatite from sea shells through the calcination and precipitation method. Here sea shell was calcined at 900^0C temperature and got calcium oxide. Phosphoric acid (0.6M) with an addition rate of 1mL/min was mixed by adjusting the pH using ammonia as a solution. A precipitate was formed, which was filtered, dried, and calcined at 250^0C, 500^0C, 750^0C, and 1000^0C for 2 hr. HAp was formed at 250^0C temperature with rod-shaped sizes of 101 nm. Though HAp formation is started at 150^0C temperature. Razali *et al*. [40] used 400^0C and 800^0C calcination temperatures to get hydroxyapatite from cockle shells through a hydrothermal process. It was noticed from XRD analysis that HAp was not completely formed from calcite at 400^0C calcination temperature whereas complete HAp was formed at 800^0C. Goloshchapov *et al.* [41] applied both calcination and precipitation methods in HAp preparation from a shell source. It was noticed that on decreasing pH from 8 to 7 the stoichiometric ratio decreases from 2.1 to 1.7.

Many researchers worked on plant parts, plant wastes, and algae for the production of HAp. Nayar *et al.* [42] synthesized HAp from papaya leaves and calendula flowers by precipitation method. Biomolecules that are present in plant extract play an important role in the produced HAp morphology. Shaltout *et al*. [43] took catha edulis, basil etc. for preparing HAp. Catha edulis and basil gave HAp at 800^0C and basil gave a small amount of calcium hydroxide. By

applying the microwave method Govindaraj *et al*. [44] prepare HAp from moringa oleifera leaves. The dried leaves were powdered and mixed in nitric acid in a specified quantity. The mixture was irradiated in a micro-oven at 50W for 2 min. EDTA and (NH4)2HPO4 were added to the powder and sonicated at 30 min. after washing, drying, and treating. The powder was again irradiated for 5 min. at 100W in a micro oven. The produced HAp is in nano size and Ca/P is 1.72.

Besides animal and plant sources, researchers extract HAp from algae. Teymouri *et al*. [45] prepared hydroxyapatite from scenedesmus species through a hydrothermal mineralization process. One notable finding was that calcium hydroxide which was added to the solution for synthetic HAp production also enhanced the crystallization of the produced HAp [46, 47, and 48].

2.2 Effects of Dopants

Since hydroxyapatite is biocompatible, osseointegrated, osteoconductive, chemically and structurally similar to natural bone, and forms a strong bond between bone and implant materials, it is widely applied in biomedical fields. HAp can be prepared in the laboratory through a number of techniques. It has been found that synthetically prepared HAp does not mimic the normal bone composition due to the absence of some trace elements. Trace elements present in some natural HAp mimic the apatite produced from human bone and are essential to bone regeneration and the formation of bone. It is an excellent choice, but because of its unavoidable mechanical properties, such as brittleness, low fracture toughness, and low tensile strength, its use in biomedical applications is limited [49].

Kalita *et al*. [50] prepared nano-size HAp ranging 2–10 nm sizes and it was doped with magnesium and zinc powder at a low temperature through sol-gel processes. Incorporation of this dopant increases the hardness and compressive strength compared to pure HAp. Biodegradation studies through stimulated body fluid solution showed a decline in resorption and surface hardness degradation for doped samples.

Mardziaha et *al*. [51] incorporated zinc in the HAp lattice structure at 5, 10 and 15 mole % through wet chemical processes. They chose zinc as it promotes osteoblastic (MG63) cell responses compared to pure HAp. It has been found that on increasing the concentration of zinc in HAp, the lattice structure was distorted and a globular distinct particle was formed with a secondary β TCP phase and which is beneficial for controlling the degradation rate.

Safarzadeh et *al.* [52] worked on the multi-ion effect in carbonated hydroxyapatite (CHA) structure. There are four ingredients in prescribed CHA powder which are magnesium nitrate hexahydrate, TEOS, zinc nitrate hexahydrate, and copper (II) nitrate trihydrate, in proportions of 0.72, 0.05, 0.0039, and 0.003 wt. respectively. The structure incorporates the multi-ions Mg, Si, Zn, and Cu. FTIR and XRD results confirmed the presence of these ions and their phase stability.

Sharma *et al*. [53] successfully prepared titanium substituted HAp for betterment in respect of increased mechanical strength and biological responses. The XRD, FTIR, SEM,E-DAX study confirmed the doping substitution into the lattice. In an in-vitro study, Huang et al. [54] showed that titanium (0.8 and 1.6 wt. %) doped HAp inhibited grain growth while maintaining densification. Increasing surface grain boundaries per unit length increases

surface activity. Following the immersion of the sample in SBF solution for 3 days, it became evident that an apatite crystal had formed.

The antimicrobial activity of copper (II) substituted hydroxyapatite had been showed by Stani et *al*. [55] in wet processes. These properties will be useful as bone implant coating material and in treating skin diseases. Miao *et al*. [56] showed an idea of preparing zinc-doped fluoridated HAp film on metallic prostheses that increases the longevity of the implants. Different ratios of zinc precursors were added to the solution for the production of five different types of films maintaining the Ca/P ratio 1.67. Zinc doping lowers crystallinity and promotes the formation of apatite from the SBF solution.

Mro´z *et al*. [57] prepared and compared the characterization of different coating materials: hydroxyapatite, hydroxyapatite with magnesium precursors and tricalcium phosphate on Ti6Al4V substrates. TCP and HAp layers were more amorphous whereas the Mg layer was polycrystalline. Again Kolmas *et al.* [58] incorporated carbonate and magnesium ion in synthetically prepared hydroxyapatite. Three samples HAp, Mg-HAp and Mg-carbonated HAp were prepared. The ratio of the Ca/P for the three samples was maintained at 1.642, 1.583 and 1.561 respectively. The apatite crystal sizes are of 84, 47 and 22 nm, whereas the order of crystallinity: is HAp > Mg-HAp >> Mg-CHAp. Mroz et al. [59] investigated the biocompatibility and mechanical stability of magnesium-doped hydroxyapatite layers on titanium substrates using pulsed lasers. It had been noted that magnesium ion incorporation in HAp increases the cell adhesion with proliferation rate as compared to pure hydroxyapatite. Aina et *al*. [60] reported that the co-substitution of magnesium and strontium in the HAp structure by precipitation method stabilizes the magnesium level. Here HAp with β-TCP phases was formed that had a beneficial effect on osteogenicity. Tan *et al*. [61] prepared MgO-doped HAp with a nanocrystalline range. It has been found that the addition of MgO enhances fracture toughness and suppresses grain growth with good densification and phase stabilization properties. Again Uysal et *al*. [62] studied the co-doping effect on hydroxyapatite by using Zinc and fluorine ions through the precipitation method. The microhardness of the prepared doped samples was increased over pure HAp. Nie et *al*. [63] prepared TiO_2-doped hydroxyapatite with β-TCP phase through a microwave sintering process. Here modulus of elasticity and fracture toughness of HAp were increased by adding various weight percentages of TiO_2.

Porosity plays a vital role in scaffold fabrication. Mixing spherical and rod-shaped HAp decreases porosity and thus enhances the compressive strength of the final product [64]. Chai *et al* [65] incorporated vancomycin, ciprofloxacin, and gentamicin in porous scaffold to avoid pre-operation infection. Hue et al. (66) studied and demonstrated the effect of porosity on scaffold compressive strength. Tampieri *et al*. [67] prepared different graded porous HAp scaffolds by impregnating sponges in HAp solution in varying concentrations. After drying and sintering the sample at 1250^0C temperature porosity was measured through the mercury porosimetry method and experimented with in animals. This study gives the idea that interconnected pores play a crucial role in bone formation. In order to avoid sintering at high temperatures, Tadic et al. [68] used polyvinyl alcohol fibers and sodium chloride to form pores. The porogens are highly water soluble and they are processed to leave the sample after forming interconnected pores. Syazwan *et al*. [69] prepared 3D carbonated porous HAp scaffolds by using five different sintering aids namely sodium, magnesium, calcium, potassium hydroxide and potassium carbonate by using polyurethane foam replication method and sintered at 800^0C. It had been noted that potassium carbonate-based porous scaffolds were more effective densified material along with better biocompatibility and bio

activeness in comparison to other ones. Xingping *et al.* [70] prepared HAp-Titanium composite porous scaffolds by using ammonium bicarbonate (NH_4HCO_3) as a pore-forming material. The amount of ammonium bicarbonate in the scaffold can be changed to regulate its porosity and compressive strength. When 40% NH_4HCO_3 was added then porosity and compressive strength became 67±0.6% and 19±0.5MPa which matches with the value of human spongy bones. SBF studies demonstrated apatite formation and growth on the composite surfaces. Manivanna *et al.* [71] included beeswax-chitosan in the zinc and hydroxyapatite to develop a porous biocomposites for tissue regeneration. The adhesion test confirmed that the said composite porous material could propagate cell growth. Ren *et al*. [72] studied whether there is an enhancement of osteogenicity in making groove channels throughout the porous block. It had been observed that implantation in heterotopic and orthotopic sides in beagle dogs, the osteogenicity is increased in grooved HAp than in normal HAp scaffold. Lett *et al.* [73] reported that the application of binders plays a significant role in designing porous load-bearing HAp blocks. A hydrothermal method was used to synthesize the porous HAp scaffolds, using calcium nitrate and di-ammonium hydrogen phosphate as precursors. The scaffolds were prepared by using the polyurethane sponge method and as binders cellulose, polyvinyl alcohol, and starch were used. Binder cellulose showed the maximum density value 0.944 gm/cm^3 with 50% porosity whereas starch showed 75% porosity with 0.63 gm/cm^3 density.

2.3 In-vitro Biological Performance

When an implant material is set in a living body for a long duration, there is a chance to harm the surrounding body tissues if metallic degraded particles are formed due to corrosion and/ or wear processes may damage the tissues of the host and cause inflammation. A difference in tensile strength and elastic modulus between the host bone and implant material leads to a stress-shielding effect that causes the bone density to deteriorate. So the properties of biomaterials would be such that they can be mechanically strong enough to withhold the body pressure and biocompatible with host bone. To check the materials' physical and mechanical properties and their effect on living bodies different in-vitro analyses have been performed. It is important to choose a biomaterial based on its specific biomedical applications in order to ensure long-term effectiveness and rejection-free use [74]. The primary requirement for any material to be implanted is that it should be anti-inflammatory, anti-toxic and anti-allergenic. It must also be biocompatible, bioactive, bioinert, biofunctional and sterilizable [75, 76]. Before implantation inside a living body, developed material must be investigated for its physio-mechanical nature.

Lala *et al*. [77] prepared eggshell-derived HAp maintaining different aging times of 12, 24, 36 and 48 hrs. The apatite formation was tested through SBF studies of the samples. A 12-hour aged sample compared to 24-hour, 36-hour, and 48 hour aged samples gives the better result and the MTT assay result shows 90% cell viability.
The in-vitro antibacterial and cytocompatibility test of silver-doped HAp coating [78] had been assessed by using the CDC (The Centre for Disease Control) biofilm reactor where the samples were placed. On counting the number of living cells, bacteria upon the samples and their efficacy were measured. On increasing the concentration of silver, more bacteria would die but cytocompatibility decreases as a higher concentration of silver reduces the intracellular adenosine tri-phosphate and causes cell death.

Chitosan with silica nanocomposite in hydroxyapatite [79] was prepared by co-precipitation method by maintaining tetraethoxysilane with chitosan ratios 1, 5, 10, and 15 and 20% v/v respectively. In-vitro biomineralization studies were performed using pellets and soaking them in SBF solution for 7 days. A globular-shaped calcium phosphate apatite layer formed which was confirmed through SEM studies. Cell attachment and proliferation test was performed by using rat osteoblast-like UMR-106 cells. It has been found that forming osteoblast cells and mineralized nodule numbers were enhanced between 14 and 21 days.

In order to synthesize bone graft materials in major bone defects, researchers develop a porous biomimetic nanocomposite scaffold of gelatin and HAp. Human endometrial stem cells differentiate into osteoblast-like cells that embed themselves within the pores of the implant and hold it to the host tissues [80]. Various in-vitro studies were conducted here, including MTT assays, cell adhesion and proliferation on scaffolds, and ALP activity. MTT assay demonstrated that the scaffold would maintain the cytocompatibility and cell adhesion tests showed that cells adhered and penetrated the scaffold pores. The surface of the scaffold is attached to the cultured cells.

Munajjed *et al.* [81] successfully synthesized a biomimetic collagen-HAp scaffold by using the SBF immersion process. Biological analysis of the control scaffold (only collagen) and SBF-treated samples were seeded on MC3T3-E1 osteoblast cells. It had been noticed that SBF-treated scaffolds got more stiffness compared to only collagen-modified scaffolds. Kikuchi *et al.* [82] prepared and observed osseointegration of bone graft scaffold material made of hydroxyapatite and collagen. Here a more bioactive nano-range self-organized composite same as bone apatite had been formed. In-vivo study of the beagle's tibia portion was performed and had been noticed that the composite fitted fracture portion almost filled with new bone within eight weeks after created defect. New bone formation with haversian canal and soft non-calcified tissues were observed which were directly bonded to each other. An in-vitro study of hydroxyapatite with titanium composites in SBF solution was investigated [83]. In this experiment, a layer of apatite was formed on the surface of the bone after a four-week interval of immersion in an SBF solution. At the initial period i.e., up to seven days calcium oxides were entered into the solution, and calcium ion concentration was increased.

2.4 Animal Experimentation Study

After preparing the desired specimens, their applicability to living bodies should be assayed. Different literature depicted the effects of sample material substitution during specific time intervals. Nandi *et al*. [84] prepared and studied the efficacy of porous, nano-hydroxyapatite on a goat's body (a created bony defected area in the diaphysis of radius). Calcium nitrate tetrahydrate was mixed with di-ammonium hydrogen orthophosphate to prepare HAp. Urea and glycine were utilized as fuel precursors. The solution was heated at 700^0C. In order to make porous HAP, combustible organic materials such as polyvinyl alcohol and naphthalene were added and pressed (100MPa) to get uniform densification. Twelve randomly selected goat samples were taken and divided into two groups: group I where no samples were implanted and group II where samples were implanted. Local inflammatory reaction, radiological, histological, and fluorochrome labeling studies were done after 21, 30, 60, and 90 days/3 months postoperatively. Up to 90^{th} days, no inflammatory reactions on surrounding tissues were found. Radiography showed that after 90 days, the bony defects were completely healed in group II animals. Histological study reported a complete haversian canal with ossification blood vessels were produced and a remarkable amount of bone formation is

evident in group II animals based on fluorescence test results. The study showed that porous HAp material produces osseointegration without causing any systemic toxicity.

Kundu *et al*. [85] studied the efficacy of porous ocular HAp implants on six healthy adult male mongrel dogs. The prostheses accustomed to the implant surrounding tissue, not hampered the lower lid movement and freely move in the socket. The tailored ocular implant made from HAp is economical and satisfactory for industrial use.

Dupoirieux *et al*. [86] employed powdered eggshells on the defects that were created on different body sites and observed the biocompatibility of eggshell powder. Salah *et al*. [87] experimented with powdered eggshells as a pulp capping material on thirty number of 2.5 kg New Zealand male rabbits. Comparative analysis has also been done with calcium hydroxide powder applied directly to the upper right incisor. Eggshell-filled areas showed less inflammation (4-week interval) and better fibrosis and bridge formation.

In three different animals, Ripamonti et al. [88] implanted 20mm-long, 7mm-diameter porous HAp rods intramuscularly in rectus abdominis sites to investigate the osteoinductive property of porous HAp. After 90 days postoperatively, bone regeneration was found in a porous HAp scaffold pretreated with BMP (bone morphogenetic protein).

Jin *et al*. [89] prepared HAp, chitosan-alginate composite as chitosan and alginate are cationic and anionic biopolymers and suitable for bone tissue replacement. Animal experimentation of HAp chitosan-alginate implantation after 8 weeks showed better bone-forming abilities than chitosan-alginate composite. Dey *et al*. [90] tested the rate of healing artificially created defects in tibia portions of New Zealand white rabbits using uncoated SS316L intramedullary pins against pure HAp-βTCP coated pins. After observing the results of the fluorochrome, histological study, it was confirmed that the coated pin gave enhanced alkaline phosphatase up to 15^{th} days postoperatively. A well-developed haversian canal with peripherally osteoblastic cells was formed. Here micro plasma technique was used as it could give stability in long bone fractures. Okada *et al*. [91] did an in-vivo comparative study to see the bio effectiveness between βTCP-PDLGA composite with only granular βTCP materials. The composite material uniformly filled the defect area without causing more inflammation with bone resorption. In a study conducted on 20 rats, Ding et al. [92] assessed the efficacy of nano-hydroxyapatite in promoting osteoblastic differentiation in suture-derived stem cells (SUSC) and osseointegration in sagittal sutures. Nano HAp concentrations of 0, 25, 50, and 100 g/ml were dipped into isolated SUSCs. It was noticed that 25 µg/ml concentrated SUSC gives better osteoblastic gene expression and the healing gap was reduced readily compared to other concentrated materials.

References

[1] Volume 2, issue 9, e580-592, September 2021 https://doi.org/10.1016/S2666-7568 (21) 00172-0 Global, regional, and national burden of bone fractures in 204 countries and territories, 1990–2019: a systematic analysis from the Global Burden of Disease Study 2019.

[2] Autograft, allograft, and bone graft substitutes: clinical evidence and indications for use in the setting of orthopaedic trauma surgery, Journal of Orthopaedic Trauma Publish Ahead of Print, DOI: 10.1097/BOT.0000000000001420.

[3] The mechanism of biomineralization of bone-like apatite on synthetic hydroxyapatite: an in vitro assessment, Hyun-Min Kim, Teruyuki Himeno, J. R. Soc. Interface (2004) 1, 17–22, DOI: 10.1098/rsif.2004.0003.

[4] Pramanik, S., Agawal, A. K., Rai, K. N. and Garg, A. 2007. Development of high-strength hydroxyapatite by solid-state-sintering process. Ceramic International. 33: 419-426.

[5] H.S. Liu, T.S. Chin, L.S.Lai, S.Y.Chiu, K.H.Chung, C.S.Chang, M.T.Lui Hydroxyapatite synthesized by a simplified hydrothermal method, CeramicsInternational Volume 23, Issue 1, Pages 19-25,1997.

[6] Kwon S, Jun Y, Hong S and Kim H, Synthesis and dissolution behavior of β-TCP and HA/β-TCP composite powders J. Eur. Ceram. Soc. 23 1039–45 23 909–14, 2003.

[7] Yeong, K. C. B., Wang, J. and Ng, S. C. Mechanochemical synthesis of nanocrystalline hydroxyapatite from CaO and CaHPO4. Biomaterials.22:2705-2712.2001.

[8] Kumar, T. S. S., Manjubala, I. & Gunasekaran, J. Synthesis of carbonated calcium phosphate ceramic using microwave irradiation, Biomaterials. 21: 1623-1629. 2000.

[9] Xinlong Wang, Hongsong Fan, Yumei Xiao, Xingdong Zhang, Fabrication and characterization of porous hydroxyapatite/β-tricalciumphosphate ceramics by microwave sintering, Materials Letters 60, 455–458,2006.

[10] Tas, A.C., Combustion synthesis of calcium phosphate bioceramic powders. Journal of the European Ceramic Society. 20: 2389-2394. 2000.

[11] M. Akram, R. Ahmed, I. Shakir, W.A.W. Ibrahim, R. Hussain, Extracting hydroxyapatite and its precursors from natural resources, J. Mater. Sci. 49 (2014)1461–1475.

[12] D. Milovac, T.C. Gamboa-martínez, M. Ivankovic, G. Gallego, H. Ivankovic, PCL coated hydroxyapatite scaffold derived from cuttlefish bone: in vitro cell culture studies, Mater. Sci. Eng. C 42 (2014) 264–272.

[13] Defne Bayraktar and A. CuÈ neyt Tas, Chemical Preparation of Carbonated Calcium Hydroxyapatite Powders at 37^0C in Urea-containing Synthetic Body Fluids, Journal of the European Ceramic Society 19 (1999) 2573±2579.

[14] T.S. Sampath Kumar, I. Manjubala, J. Gunasekaran, Synthesis of carbonated calcium phosphate ceramics using microwave irradiation, Biomaterials 21 (2000) 1623-1629.

[15] Mojtaba Ansari, Seyed Morteza Naghib,Fathollah Moztarzadeh,Amir Salati,Synthesis and characterization of Hydroxyapatite calcium hydroxide for dental composites, Ceramics – Sili káty 55 (2) 123-126 (2011).

[16] Kazumichi Yanagisawaa, Jae-Hyen Kima, Hydrothermal Sintering under Mild Temperature Conditions: Preparation of Calcium-deficient Hydroxyapatite Compacts.

[17] Abhijit Chanda , Sudip Dasgupta, Microwave sintering of calcium phosphate ceramics, Materials Science and Engineering C 29 (2009) 1144–1149.

[18] Maria Helena Santos, Marise de Oliveira, Synthesis Control and Characterization of Hydroxyapatite Prepared by Wet Precipitation Process, Material Research, Vol 7,No 4,625-630, 2004.

[19] M.K. Herliansyah, D.A. Nasution, M. Hamdi, A. Ide-Ektessabi, M.W. Wildan,A.E. Tontowi, Preparation and characterization of natural hydroxyapatite: a comparative study of bovine bone hydroxyapatite and hydroxyapatite from calcite,Mater. Sci. Forum 561–565 (2007) 1441–1444.

[20] M.R. Ayatollahi, M.Y. Yahya, H.A. Shirazi, S.A. Hassan, Mechanical and tribological properties of hydroxyapatite nanoparticles extracted from natural bovine bone and the bone cement developed by nano-sized bovine hydroxyapatite filler, Ceram. Int. 41 (2015) 10818–10827.

[21] A. Ruksudjarit, K. Pengpat, G. Rujijanagul, T. Tunkasiri, Synthesis and characterization of nanocrystalline hydroxyapatite from natural bovine bone, Curr. Appl. Phys. 8 (2008) 270–272

[22] N.A.M. Barakat, M.S. Khil, A.M. Omran, F.A. Sheikh, H.Y. Kim, Extraction of pure natural hydroxyapatite from the bovine bones bio waste by three different methods, J. Mater. Process. Technol. 209 (2009) 3408–3415.

[23] E. Hosseinzadeh, M. Davarpanah, N.H. Nemati, S.A. Tavakoli, Fabrication of a hard tissue replacement using natural hydroxyapatite derived from bovine bones by thermal decomposition method, International Journal of Organ Transplantation Medicine 5 (2014) 23–31.

[24] R.-X. Sun, Y. Lv, Y.-R. Niu, X.-H. Zhao, D.-S. Cao, J. Tang, X.-C. Sun, K.-Z. Chen, Physicochemical and biological properties of bovine-derived porous hydroxyapatite/ collagen composite and its hydroxyapatite powders, Ceram. Int. 43 (2017) 16792–16798

[25] H.L. Jaber, A.S. Hammood, N. Parvin, Synthesis and characterization of hydroxyapatite powder from natural Camelus bone, J. Aust. Ceram. Soc. 54 (2018)1–10.

[26] J.S. Cho, S. Um, D.S. Yoo, Y. Chung, S.H. Chung, J. Lee, S. Rhee, Enhanced osteoconductivity of sodium- substituted hydroxyapatite by system instability, J. Biomed. Mater. Res. B Appl. Biomater. 102B (2013) 1046–1062.

[27] S.S. Rahavi, O. Ghaderi, A. Monshi, M.H. Fathi, A comparative study on physicochemical properties of hydroxyapatite powders derived from natural and synthetic sources, Russ. J. Non-Ferrous Metals 58 (2017) 276–286.

[28] A.M. Janus, M. Faryna, K. Haberko, A. Rakowska, T. Panz, Chemical and microstructural characterization of natural hydroxyapatite derived from pig bones, Microchimica Acta 161 (2008) 349–353.

[29] S. Paul, A. Pal, A.R. Choudhury, S. Bodhak, V.K. Balla, A. Sinha, M. Das, Effect of trace elements on the sintering effect of fish scale derived hydroxyapatite and its bioactivity, Ceram. Int. 43 (2017) 15678–15684.

[30] A. Pal, S. Paul, A.R. Choudhury, V.K. Balla, M. Das, A. Sinha, Synthesis of hydroxyapatite from Latescalcarifer fish bone for biomedical applications, Mater. Lett. (2017) 89–92.

[31] B.R. Sunil, M. Jagannatham, Producing hydroxyapatite from fish bones by heat treatment, Mater. Lett. 185(2016) 411–414.

[32] N.N. Panda, K. Pramanik, L.B. Sukla, Extraction and characterization of biocompatible hydroxyapatite from fresh water fish scales for tissue engineering scaffold, Bioproc. Biosyst. Eng. 37 (2014) 433–440.

[33] W. Pon-On, P. Suntornsaratoon, N. Charoenphandhu, J. Thongbunchoo, N. Krishnamra, I.M. Tang, Hydroxyapatite from fish scale for potential use as bone scaffold or regenerative material, Mater. Sci. Eng. C62 (2016) 183–189.

[34] S. Kongsri, K. Janpradit, K. Buapa, S. Techawongstien, S. Chanthai, Nanocrystalline hydroxyapatite from fish scale waste: preparation, characterization and application for selenium adsorption in aqueous solution, Chem. Eng. J. 215–216 (2013)522–532.

[35] J. Venkatesan, Z.J. Qian, B. Ryu, N.V. Thomas, S.K. Kim, A comparative study of thermal calcination and an alkaline hydrolysis method in the isolation of hydroxyapatite from Thunnus obesus bone, Biomed. Mater. 6(2011) 1–12.

[36] M. Ozawa, S. Suzuki, Microstructural development of natural hydroxyapatite originated from fish-bone waste through heat treatment, J. Am. Ceram. Soc. 85(2004) 1315–1317.

[37] B. Mondal, S. Mondal, A. Mondal, N. Mandal, Fish scale derived hydroxyapatite scaffold for bone tissue engineering, Mater. Char. 121 (2016) 112–124.

[38] R. Mustaffa, M.R. Mohd Yusof, Y. Abdullah, A novelty of synthetic hydroxyapatite from cockle shell and characterization, Adv. Mater. Res. 1087 (2015) 429–433

[39] S. Santhosh, S.B. Prabu, Thermal stability of nano hydroxyapatite synthesized from sea shells through wet chemical synthesis, Mater. Lett. 97 (2013) 121–124.

[40] N.A.I. Mohamad Razali, S. Pramanik, N.A. Abu Osman, Z. Radzi, B. Pingguan-Murphy, Conversion of calcite from cockle shells to bioactive nanorod hydroxyapatite for biomedical applications, J. Ceram. Process. Res. 17 (2016)699–706.

[41] D.L. Goloshchapov, V.M. Kashkarov, N.A. Rumyantseva, P.V. Seredin, A.S. Lenshin,B.L. Agapov, E.P.Domashevskaya, Synthesis of nanocrystalline hydroxyapatite by precipitation using hen's eggshell, Ceram. Int.39 (2013) 4539–4549.

[42] S. Nayar, A. Guha, Waste utilization for the controlled synthesis of nanosized hydroxyapatite, Mater. Sci. Eng. volume 29 (2009) 1326–1329.

[43] A.A. Shaltout, M.A. Allam, M.A. Moharram, FTIR spectroscopic, thermal and XRD characterization of hydroxyapatite from new natural sources, Spectrochim. Acta Mol. Biomol. Spectrosc. 83 (2011) 56–60.

[44] D. Govindaraj, M. Rajan, Synthesis and spectral characterization of novel nanohydroxyapatite from Moringaoleifera leaves, Mater. Today: Proceedings 3 (2016)2394–2398.

[45] A. Teymouri, B.J. Stuart, S. Kumar, Hydroxyapatite and dittmarite precipitation from algae hydrolysate, Algal Res. 29 (2018) 202–211.

[46] K. Tsuru, M. Maruta, S. Matsuya, K. Ishikawa, Effects of the method of apatite seed crystals addition on setting reaction of α-tricalcium phosphate based apatite cement, J. Mater. Sci. Mater. Med. 26 (2015) 1–8.

[47] Y. Wang, L. Liu, S. Guo, Characterization of biodegradable and cytocompatible Nano hydroxyapatite/polycaprolactone porous scaffolds in degradation in vitro, Polym. Degrad. Stabil. 95 (2010) 207–213.

[48] N.A. Oladoja, I.A. Ololade, A.O. Adesina, R.O.A. Adelagun, Y.M. Sani, Appraisal of gastropod shell as calcium ion source for phosphate removal and recovery in calcium phosphate minerals crystallization procedure, Chem. Eng. Res. Des. 91(2013) 810–818.

[49] T. J. Webster, E. A. Massa-Schlueter, J.L. Smith, E.B. Slamovich, Biomaterials 25 (2004) 2111–2121.

[50] Nanocrystalline hydroxyapatite doped with magnesium and zinc: Synthesis and characterization, Samar J. Kalita, Himesh A. Bhatt, Materials Science and Engineering C 27 (2007) 837–848.

[51] Effect of zinc ions on the structural characteristics of hydroxyapatite Bioceramics, C.M. Mardziah, S. Ramesh, https://doi.org/10.1016/j.ceramint.2020.02.192, Ceramics International.

[52] Effect of multi-ions doping on the properties of carbonated hydroxyapatite bioceramic, Marjan Safarzadeh, S. Ramesh, https: //doi.org /10.1016 /j.ceramint. 2018 .11.003, Ceramics International

[53] Synthesis and characterization of pure and titania doped Hydroxyapatite, Anushikaa, Prakhar Sharmaa, Alok Trivedia, Howa Begam, Materials Today: Proceedings 16 (2019) 302–307.

[54] Development and characterization of titanium-containing hydroxyapatite for medical applications, J. Huang, S.M. Best, Acta Biomaterialia 6 (2010) 241–249.

[55] Synthesis, characterization and antimicrobial activity of copper and zinc-doped hydroxyapatite nanopowders, Vojislav Stani´ca, Suzana Dimitrijevi, Applied Surface Science 256 (2010) 6083–6089, doi:10.1016/j.apsusc.2010.03.124.

[56] Sol–gel preparation of Zn-doped fluoridated hydroxyapatite films, Shundong Miaoa, Wenjian Weng, Surface &Coatings Technology 198 (2005) 223– 226.

[57] Characterization of calcium phosphate coatings doped with Mg, deposited by pulsed laser deposition technique using ArF excimer laser, W. Mro´z a, M. Jedyn´ski, Micron 40 (2009) 140–142.

[58] Incorporation of carbonate and magnesium ions into synthetic hydroxyapatite: The effect on physicochemical properties, Joanna Kolmas, Andrzej Jaklewicz, Journal of Molecular Structure 987 (2011) 40–50.

[59] Structural studies of magnesium doped hydroxyapatite coatings after osteoblast culture, W. Mroz a, A. Bombalska , S. Burdyn´ ska, Journal of Molecular Structure 977 (2010) 145–152,doi:10.1016/j.molstruc.2010.05.025.

[60] Magnesium- and strontium-co-substituted hydroxyapatite: the effects of doped-ions on the structure and chemico-physical properties, Valentina Aina, Gigliola Lusvardi, Basil Annaz, Iain R. Gibson, J Mater Sci: Mater Med (2012) 23:2867–2879 DOI 10.1007/s10856-012-4767-3.

[61] Sintering and mechanical properties of MgO-doped nanocrystalline hydroxyapatite C.Y. Tana, A.Yaghoubia, S.Ramesha, Ceramics International 39(2013)8979–8983, http://dx.doi.org/10.1016/j.ceramint.2013.04.098.

[62] Co-doping of hydroxyapatite with zinc and fluoride improves mechanical and biological properties of hydroxyapatite, Idil Uysala, FerideSevercana,b, Aysen Tezcanera, MaterialsInternational24(2014)340–349, http:// dx.doi. org/10. 1016 /j.pnsc.2014.06.004.

[63] Effect of TiO2 doping on densification and mechanical properties of hydroxyapatite by microwave sintering, Jun Feng Nie, Jian Zhou, Xiaoguang Huang, https:// doi.org/ 10.1016/j.ceramint.2019.04.007.

[64] Vital Role of Hydroxyapatite Particle Shape in Regulating the Porosity and Mechanical Properties of the Sintered Scaffolds, Jinchuan Wu1, Changshun Ruan, http://dx.doi.org/doi:10.1016/j.jmst.2017.01.008.

[65] Antibacterial activation of hydroxyapatite (HA) with controlled porosity by different antibiotics, F. Chai a, J.-C.Hornez b, N. Blanchemain, Biomolecular Engineering 24 (2007) 510–514, doi:10.1016/j.bioeng.2007.08.001.

[66] Influence of porosity on the mechanical resistance of hydroxyapatite ceramics under compressive stress, J.C. Le Huec", T. Schaeverbeke", *Biomoteriols 16* (1995) 113-118, 1995 Elsevier Science Limited.

[67] Porosity-graded hydroxyapatite ceramics to replace natural bone, A. Tampieri, G. Celotti, S. Sprio, Biomaterials 22 (2001) 1365-1370.

[68] A novel method to produce hydroxyapatite objects with interconnecting porosity that avoids sintering,D.Tadica, F. Beckmann, Biomaterials 25 (2004) 3335–3340.

[69] Effectiveness of various sintering aids on the densification and *in vitro* properties of carbonated hydroxyapatite porous scaffolds produced by foam replication technique,

Muhammad Syazwan M.N. a, Ahmad-Fauzi M.N.Materials Today Communications 27 (2021) 102395.

[70] Preparation and performance of hydroxyapatite/Ti porous biocomposite scaffolds, Fan Xingping, Ceramics International, https://doi.org/10.1016/j.ceramint.2019.05.178.

[71] Novel beeswax-chitosan/Zinc-hydroxyapatite biocomposite porous scaffolds: Preparation and biological evaluation, K. Manivannan, G. Jaganathan, Journal of Science: Advanced Materials and Devices 6 (2021) 197-201.

[72] Enhancement of Osteogenesis Using a Novel Porous Hydroxyapatite Scaffold in *Vivo* and *Vitro*, Xiaohua Rena,Qiang Tuob, Kun Tian, *Ceramics International*, https://doi.org/10.1016/j.ceramint.2018.08.249.

[73] Porous hydroxyapatite scaffolds for orthopedic and dental applications - the role of binders, J. Anita Letta, M.Sundareswaria, K. Ravichandran, Materials Today: Proceedings 3 (2016) 1672–1677.

[74] Chen, Q., Thouas, G.A.: Metallic implant biomaterials. Mat. Sci. Eng. R. 87, 1–57 (2015).

[75] Bauer, S., Schmuki, P., Von Der Mark, K., Park, J.: Engineering biocompatible implant surfaces Part I: materials and surfaces. Prog. Mater Sci. 58, 261–326, 2013.

[76] Domanska, A., Boczkowska, A: Biodegradable polyurethanes from crystalline prepolymers. Polym. Degrad. Stab. 108, 175–181, 2014.

[77] Physico-chemical and biological behaviour of eggshell bio-waste derived nano-hydroxyapatite matured at different aging time , Sumit Das Lala, Emon Barua, Payel Deb, Materials Today Communications 27 (2021) 1024-43, https://doi.org/10.1016/j.mtcomm.2021.102443.

[78] Mechanical, In vitro Antimicrobial, and Biological Properties of Plasma-Sprayed Silver-Doped Hydroxyapatite Coating, Mangal Roy, Gary A. Fielding, Haluk Beyenal, Amit Bandyopadhyay, 2012 American Chemical Society, dx. doi.org/10.1021/am201610q ACS Appl. Mater. Interfaces 2012, 4, 1341−1349.

[79] In vitro study of the SBF and osteoblast-like cells on hydroxyapatite/chitosan–silica nanocomposite Prapaporn Jongwattanapisan, Narattaphol Charoenphandhu, Materials Science and Engineering C xxx (2010) xxx–xxx, doi:10.1016/j.msec.2010.09.009.

[80] In vitro evaluation of biomimetic nanocomposite scaffold using endometrialstem cell derived osteoblast-likecells Mahmoud Azamia, Jafar Aia, Somayeh Ebrahimi-Barough, Tissue and Cell xxx (2013) xxx– xxx, http://dx.doi.org/10.1016/j.tice.2013.05.002.

[81] Development of a Biomimetic Collagen-Hydroxyapatite Scaffold for Bone Tissue Engineering Using a SBF Immersion Technique, Amir A. Al-Munajjed,1,2 Niamh A. Plunkett,1,2 John P. Gleeson, Published online 29 January 2009 in Wiley Inter Science (www.interscience.wiley.com). DOI: 10.1002/jbm.b.31320.

[82] Self-organization mechanism in a bone-like hydroxyapatite/collagen nanocomposite synthesized in vitro and its biological reaction in vivo, Masanori Kikuchi, Soichiro Itoh, Shizuko Ichinose, Biomaterials 22 (2001) 1705-1711.

[83] In vitro studies of plasma-sprayed hydroxyapatite/Ti-6Al-4V composite coatings in simulated body fluid (SBF)Y.W. Gua, K.A. Khora,, P. Cheang, Biomaterials 24 (2003) 1603–1611, doi:10.1016/S0142-9612(02)00573-2.

[84] Evaluation of new porous tri-calcium phosphate ceramic as bone substitute in goat model, Samit K. Nandi ,Samir K. Ghosh, Biswanath Kundu, Small Ruminant Research 75 (2008) 144–153,doi:10.1016/j.smallrumres.2007.09.006.

[85] Fabrication and characterization of porous hydroxyapatite ocular implant followed by an *in vivo* study in dogs, B Kundu, M K Sinha, M K Mitra and D Basu, Bull. Mater. Sci., Vol. 27, No. 2, April 2004, pp.133–140. © Indian Academy of Sciences.

[86] Powdered eggshell: a pilot study on a new bone substitute for use in maxillofacial surgery, Laurent Dupoirieux, Didier Pourquier, Frangois Souyris, Journal of cranio-maxillo-facial surgery(1995)23,187-194.

[87] Evaluation of eggshell powder as an experimental direct pulp capping material Mohamed Salah, Mohamed M. Kataia, Engy M. Kataia, Future Dental Journal xxx (xxxx) xxx–xxx, https://doi.org/10.1016/j.fdj.2018.05.008.

[88] Osteoinduction in porous hydroxyapatite implanted in heterotopic sites of different animal models, UgoRipamonti, *Biomoteriols* 17 (1996) 31-35, 1995 Elsevier Science Limited.

[89] In vivo evaluation of porous hydroxyapatite/chitosan–alginate composite scaffolds for bone tissue engineering, Hyeong-Ho Jin a, Dong-Hyun Kima, Tae-Wan Kima, International Journal of Biological Macromolecules 51(2012) 1079– 1085, http://dx.doi.org/10.1016/j.ijbiomac.2012.08.027.

[90] Evaluation of hydroxyapatite and b-tri calcium phosphate microplasma spray coated pin intra-medullary for bone repair in a rabbit model, Arjun Dey, Samit Kumar Nandi, Biswanath Kundu, Ceramics International 37 (2011) 1377–1391, doi:10.1016/j.ceramint.2011.01.005

[91] Performance of two bone substitutes of novel cotton-like β-TCP/PDLGA and granular β-TCP on bone regeneration in the femoral bone defect of the Beagle dogs, Yasuaki Okadaa, Yoshiaki Yamanakaa, Kunitaka Menukia, Bone Reports 13 (2020) 100718, https://doi.org/10.1016/j.bonr.2020.100718.

[92] Hydroxyapatite Nanoparticles Facilitate Osteoblast Differentiation and Bone Formation Within Sagittal Suture during expansion in Rats, Wei Liang Pengbing Ding, Drug Design, Development and Therapy 2021:15 905– 917.

3. SCOPE OF THE WORK

To overcome autografting and allografting surgery in traumatic patients, several research works have been done to develop hydroxyapatite an important inorganic mineral constituent in bone and teeth that take part in osseointegration and ossification. Researchers investigated and used some alternative sources to make hydroxyapatite besides chemical reagents. In our research hydroxyapatite scaffold was prepared by using both chemical reagent and eggshell calcined powder and then observed their efficacy and evaluated their different properties through a comparative assessment study on implanting the samples in animal bone.

To reduce the environmental threats caused by eggshell waste, it is beneficial for mankind to convert or recycle this waste into wealth. Every day million tons of eggshells are gathered in our surroundings like restaurants, canteens, household sites, etc. After collecting and preparing hydroxyapatite from this waste the shell cost would be less in comparison to using laboratory-grade chemical reagent (Let us collect 200 gm of eggshell waste at no price then boil it with water and the total processing cost =reagent cost Rs.65+electricity 30+ResiduaryRs.10. We get 150 gm of powder in approx. Rs.105, whereas in synthetic Hap powder, it is Rs.245/100gm, Indiamart product) Further being a biological source material many trace elements are present on it that are essential for our body. Some researchers studied upon enhancing mechanical stability by adding some dopant ions. There has not been extensive research on zinc, magnesium, and titanium-based hydroxyapatite in animal models, although these ions are reported to improve cell-material interactions. In our study, dopant ions were added into hydroxyapatite obtained from both sources and observed their impact on the animal body.

Therefore, the identified scopes of the research are mentioned below:

- Application of eggshell as an alternative raw material in hydroxyapatite synthesis
- Application of different Osseo-inducing trace metals as a dopant in hydroxyapatite crystals
- Application of these dopant/HAp composites in the animal body

Objectives:

- To prepare Pure HAp, Eggshell HAp, and their doped verities and to study their physical, mechanical, and invitro performance analysis.
- To conduct a dedicated experiment/animal trial on a site-specific area and observe the implanted materials' effect on living body.
- A comparative analysis between a synthetic source and bio-sourced HAp has been done to observe the efficacy of the bio-sourced product.

4. MATERIALS & METHOD

4.1 Physical Characterization

4.1.1 Preparation of Biogenic and Synthetic HAp

The biogenic HAp power was prepared through the calcination of eggshell (denoted as Eggshell HAp) and synthetic HAp (denoted as Pure HAp) from laboratory-grade calcium hydroxide following wet chemical precipitation techniques. The eggshells collected from the canteen were boiled and washed with clean water to remove the contaminants. Dry eggshells are crushed into fine pieces and then calcined in a muffle furnace at 800^0C for 2 hrs. The required amount of calcined dry powder was mixed with distilled water in a beaker and was done in steps with a spatula. The mixing was done through a magnetic stirrer with a hot plate (REMI India) for 30 min at 80^0C. The stoichiometric amount of orthophosphoric acid (0.6M) was added to the beaker very slowly from a stop cock fitted flask with a duration of about 45 min. Continuous stirring by a magnetic stirrer was done to get a homogeneous mixer. In a cool, dark place, the mixture was kept aside for 24 hrs to settle down the precipitate, then filtered. In a hot-air oven, the filtered precipitate was dried for 48 hrs at 40^0C in Petri dishes. After drying the precipitate, it was calcined for 2 hrs at 80^0 C. The obtained Egg shell HAp was ball-milled to get fine particles. Similarly, Pure HAp was prepared from laboratory-grade calcium hydroxide.

.

4.1.2 Preparation of Doped Hydroxyapatite

For preparing the doped variants (zinc, titanium, and magnesium) of both Egg shell HAp and Pure HAp, required quantities of zinc oxide (ZnO, 99% pure), titanium oxide (TiO_2,99% pure), and magnesium oxide (MgO, $6H_2O$, 98% pure) was mixed to the calcined eggshell powder or calcium hydroxide powder before addition to the acid solution. Here 3% and 5% doped variants of both Eggshell HAp and Pure HAp had been prepared. After forming the doped samples in solution, it was kept aside for aging and then filtrate precipitated using Buckner funnel. A hot-air oven was used to dry the filtrate mass at 80^0C in Petri dishes. After drying, the sample was calcined at 800^0C using a muffle furnace at a speed of 5^0C/min.

4.1.3 Powder Compaction

The pure HAp, Eggshell HAp, and their doped samples were hard pressed uniaxially in steel moulds with a diameter of 12.50 mm (12.5 mm internal diameter). A hydraulic press machine developed by PEECO (PEECO Pvt Ltd, NO.-3/PR-2/HP-1/07-08) was used to apply a 2-ton pressing pressure for a period of 2 min. The pellet samples' green density was measured and then sintered at 950^0C and 1050^0C in the furnace for 2 hrs.

4.1.4 Sintering of Dense Ceramics

A muffle furnace was used to sinter the green pellets at 950^0C and 1050^0C for 2 hrs at a constant 50C/min rate. Some sintered samples were crushed and sieved to get a uniform particle size. To investigate the phase composition of sintered samples and their crystallinity, the X-ray diffraction (XRD) method was employed. An analysis of FTIR analysis was

performed to determine the functional groups. SEM study of sintered samples was done to check surface morphology and microstructure.

4.1.5 Green and Sintered Density

The mass-to-volume ratio of the prepared HAp samples has been measured in order to determine the density of the green and sintered samples. In this study, the mass of pellets was measured by means of a weighting machine (iScale-i-02), and the diameter (mm), radius (mm), and thickness (mm) of all samples were measured by means of a digital Vernier caliper.

Density = M/V, Volume = $\pi r^2 h$

4.1.6 Percentage of Diametric, Linear and Volumetric Shrinkage

After sintering the pellets the volume was changed due to shrinkage. The initial dimensions of the green samples were recorded and after sintering at 950^0C and 1050^0C the dimensions were again recorded and the percentage change in dimension was calculated. Suppose X_1 was the initial diameter and X_2 was after sintering diameter. Then the changes of diameter were X_1- X_2 and the percentage of changes was {X1- X_2/ X_1} x100.

4.1.7 Average Grain and Pore Size

Using Perfect Screen Ruler Software, the samples were measured for their pore size and grain size. For this measurement, five SEM pictures at the same magnification were captured from each sample.

4.1.8 Porosity Measurement

Porosity plays a crucial role in implantable bioceramic fields as tissue is regenerated throughout it. It is either interconnected or closed. In order to measure apparent porosity, dry compact samples were weighed (Wd), reweighed when immersed in water (WS), and then reweighed again after removal from water (WW).

Apparent Porosity, $\phi = \frac{W_w - W_d}{W_w - W_s} X100$

Where, Wd = wt. of dry sample.

Ws = wt. of the sample immersed in water.

W_W = weight of the sample after removal from water.

4.1.9 Lattice Parameter Study

It is a physical dimension and gives the geometry of the unit cell in the crystal lattice. In general, there are three lattice constants named a, b, c, and three lattice angles α, β, *and* γ. In the case of a hexagonal lattice, two sides are equal so, a = b. In the case of a cubic crystal, the three sides are equal. Since HAp has hexagonal lattice parameters (an axis and c axis) they are calculated using the Unit Cell Plane spacing relationship [1].

$$\frac{1}{d^2}=\frac{4}{3}\left(\frac{h^2+hk+k^2}{a^2}\right)+\frac{l^2}{c^2}$$

Where, d is the distance between the next adjacent planes according to the conventional set of Miller Indices (h, k, l). The unit cell volume (V) is calculated by the relation $V=0.866\ a^2c$ [2] and particle size of the powders by XRD images. By using the Scherrer's equation below, the particle size can be calculated:

$$W_{FWHM} = \frac{k\lambda}{D Cos\theta}.\frac{180}{\pi} \qquad \text{Or} \qquad D = \frac{k\lambda}{W Cos\theta}.\frac{180}{\pi}$$

Where, W_{FWHM} = full width as a half maximum of the peak (in degrees 2Θ) calculated automatically by the XRD, D = grain size, K = constant generally equated as 0.94, and λ = radiation wavelength.

4.1.10 X-ray Diffraction (XRD) Analysis

XRD methods provide information about a material's crystallographic structure, chemical composition, and physical properties without destroying it**.** The generated collimated X-rays fall on the materials and the diffracted beams are processed and counted. The different materials produce varying diffraction patterns due to their crystal arrangement and different phases. It is necessary to compare XRD measurements taken on several crystalline samples with the standard database of the International Center for Diffraction Data (ICDD) in order to determine phase identification. In XRD analysis, the peak plays a crucial role in phase identification and material characterization. The width of the peak indicates average crystallite size. The sharp peak indicates larger crystallites whereas the broader peak indicates smaller crystallites.

The calcined powder was subjected to an XRD analysis for all samples, namely, hydroxyapatite manufactured from chemical reagents and eggshell sources as well as their doped derivatives. Calcined (800^0C) powders were crushed into fine powders. An X-ray diffractometer (Model-Mini Flex, Rigaku Co., Tokyo, Japan) was used for the analysis of the sample in scanning mode. The tube voltage and current were set at 30 KV and 15 mA, and a scan rate of 1 deg./min was employed. XRD patterns down to 80° were recorded with a 2θ range of 0-80°.

4.1.11 Fourier Transform Infrared Spectroscopy

The FTIR technique is the best method for IR (infrared) spectroscopy. When IR radiation falls on a sample, some of it is absorbed and the rest is transmitted. Spectrums are derived from molecular fingerprints of specimen samples. An absorption peak is a measure of the frequency of vibration between the atoms that make up a material. The infrared spectrum produced by different materials will be different since they contain different kinds of atoms. It indicates that functional groups are present within the material. Peak intensity indicates the amount of materials present in a spectrum. In the experiment FTIR was performed through Perkin- Elmer, Model No- 1615 (USA) by using KBr pallets in IR region (5000-400 cm^{-1}).

4.1.12 SEM and EDX Study

Scanning Electron Microscopy (SEM) involves focusing an electron beam on a sample's surface. The falling electrons interact with the samples and the emerging signals produce the images that carry the surface topography and chemical compositions of the sample. Sintered HAp and its dopant samples were broken and their pore dimensions measured. Several SEM images were captured from the surfaces and pore diameters were calculated using perfect screen ruler software. Statistical analysis was based on the average of five SEM images per sample. The EDX experiment was performed with a JSM-7900F Schottky Field Emission Scanning Electron Microscope.

4.2 Mechanical Characterization

4.2.1 Hardness

Vickers hardness tester was used for the measurement of hardness. In this method constant load is applied on the sample's surface making an indentation on the surface by using a diamond indenter and the depth is measured optically. A load of 1-100Kgf was applied for 10-15 seconds and an angle of 136^0 was formed between two opposite surfaces. The diagonals marked on the material surfaces after removing the loads were measured through a microscope and calculated the average value. The indentation area was calculated based on sloping surfaces. A hardness value was calculated by indenting the area over the surfaces of the materials and dividing the load applied. .

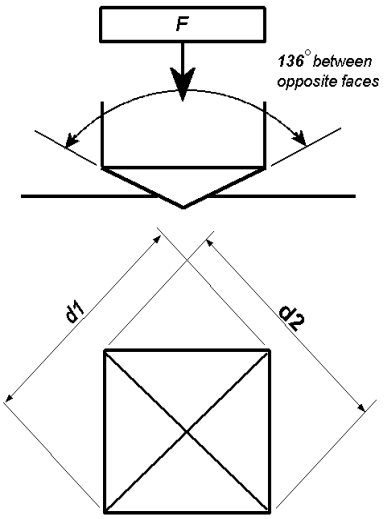

Where F is the Load in kgf

d is the Arithmetic mean of d1 and d2 in mm in the two diagonals,

Hardness measurements of this type are based on the principle that indenters make geometrically similar impressions regardless of load. Accordingly, the amount of load that

can be applied to a flat surface depends on the hardness of the material to be measured. Vickers hardness is calculated using F/A ratio, where F is applied force, A is indenting surfaces, and d is the average diagonal length. Hence, HV = Vickers hardness (kgf/mm²) is given by [3]

HV= $\frac{2FSin\frac{136^\circ}{2}}{d^2}$ HV= $1.854\frac{F}{d^2}$ approximately

4.3 Biological Characterization

Prepared compact material has to be placed in the living body. The living tissues form a layer around the material. If the materials are not biocompatible it would cause inflammation and irritation in the tissues. Hence, in-vitro and in-vivo testing should be conducted to evaluate the biological properties of prepared materials.

4.3.1 In-vitro Study

4.3.1a Bio Resorption Analysis

After implanting the bioactive biomaterial, it forms a tight and chemically stable bond with the living tissue by forming an appetite-like bonding interfaces. Our body consists of various kinds of compounds like protein, electrolytes, potassium, sodium, amino acid, etc.
According to the literature [4] SBF solution composition is closest to human blood plasma as depicted in Table 4.1.

Table 4.1: Concentration of ions for SBF and Human Blood Plasma [5]

Ion	Conc. (mmol/dm^3)	
	Simulated Body Fluid (SBF)	**Human Blood Plasma**
Na^+	142.0	142.0
K^+	5.0	5.0
Mg^{2+}	1.5	1.5
Ca^{2+}	2.5	2.5
Cl^-	147.8	103.0
HCO_3^-	4.2	27.0
HPO_4^{2-}	1.0	1.0
SO_4^{2-}	0.5	0.5

Preparation of SBF:

(a) Cleaning

Before preparing the solution all the apparatus used for it are well cleaned by using alternatively dilute hydrochloric acid, distilled water, and formaldehyde as a sterilizing agent. The bottles for preparing the SBF solution are first washed with water to remove any unwanted debris. The bottles are then immersed in a dilute solution of hydrochloric acid and left for 4-5 hrs. A sterilizing liquid was put on them and allowed to sit overnight before being washed in distilled water and then sterilized again. The bottles were wrapped in paper after they had been thoroughly washed. If necessary, the bottles are dried in a drier overnight, below 50^0C temperature.

(b) Dissolution of Chemicals

In a 1000 ml beaker (preferably polyethylene), 750 ml of distilled water is poured. The water is continuously stirred by magnetic stirring to make a homogeneous mixer and maintained the temperature at 37^0C. The chemicals are dropped one by one (1 to 8) by maintaining Table 4.2. Before the addition of the number 9 reagent precaution will be taken to add less than 1 gm of the sample so that increasing the pH would be minimized.

(c) pH Adjustment

First, a standard buffer solution was used to calibrate the pH meter. After adding all the reagents (#1 to #9) in Table 4.2 to the solution, the temperature was checked and a pH meter was used to measure pH at 37.5^0C. The pH was maintained by titrating with HCl and adjusted to 7.25. Once the pH has been adjusted, transfer the solution to a 1000 ml glass volumetric flask. After washing the beaker several times with distilled water, add the solution to the flask.

A total volume of 1000mL of the solution was added to the flask, and the flask was shaken well to adjust the volume. The solution should be approximately 20^0C. Following the cooling of the solution, add distilled water to the solution again, so that the total volume of the solution is 1000 mL, and shake the flask vigorously to ensure good mixing.

Table 4.2: Reagents for SBF (pH 7.25, 1L) [5]

Order	Reagent	Purity and company	Amount
# 1	NaCl	Assaymin.99.5%,MERCK,INDIA	7.996 g
# 2	$NaHCO_3$	Assay (after drying) min. 99.5-100.3%, MERCK, INDIA	0.350 g
# 3	KCl	Assay min.99.5%,MERCK,INDIA	0.224 g

# 4	$K_2HPO_4.3H_2O$	Assay min.99.0%,MERCK,INDIA	0.228 g
# 5	$MgCl_2.6H_2O$	Assay min. 98.0%, MERCK,INDIA	0.305 g
# 6	HCl	87.28 mL of 35% HCl is diluted to 1000 mL with a volumetric flask	40 mL
# 7	$CaCl_2$	Assay min. 95.0%, MERCK, INDIA Use after drying at 1200C for more than 12 hours	0.278 g
# 8	Na_2SO_4	Assay min. 99.0%, MERCK, INDIA	0.071 g
# 9	$(CH_2OH)_3CNH_2$	Assay (after drying) min. 99.9%, MERCK, INDIA	6.057 g
# 10	HCl	87.28 mL of 35% HCl is diluted to 1000 mL with a volumetric flask	Appropriate amount for adjusting pH

The prepared hydroxide made from two sources and their dopant variants are immersed in laboratory-graded prepared SBF solution and evaluate the dissolution characteristics of the samples. Degradation started from the sintering pellets after immersion in the SBF solution. A cleaned conical flask with a lid is taken for each sample. 100 ml of the prepared SBF solution was poured into each of the conical flasks. In each flask, one sample is allowed. The flask was then placed in an incubator at 37^0C temperature. The samples are degraded into the solution and the degraded sintered samples are taken out from the solution, dried at 80^0C, and weight is measured in three alternate days during one month. The loss of weight was calculated and evaluated with time.

4.3.1b Haemolysis Study

A critical parameter to check before using any kind of blood contact application is the hemocompatibility for orthopedic implants. In the body, implanted materials may contact blood vessels, such as capillaries, and can induce complications if they are not hemocompatible. When found non-hemocompatible during the initial evaluation, there is a need to alter the surface or redesign the product to improve the hemocompatibility. An in vitro hemocompatibility study was conducted on human blood in order to determine its compatibility. The procedure is as below:

STEP-1: A solution containing 3.8 grams of sodium citrate solution in a ratio of 10:1 is added to human blood after it has been collected. The citrated blood was then mixed with normal saline solution in a ratio of 4:5 to dilute the mixture and make it more of a diluted solution.

STEP-2: A total of seventy (70) test tubes (for 14 no. of samples*5) were filled with 10 mL of (N) saline solution for total Egg shell HAp and Pure HAP samples. The pellets from each type of HAp were immersed in one test tube. Pallets weigh about 3 grams each. As a next step, all the test tubes were incubated for 30 min at 37^0C.

STEP-3: Each of the test tubes was filled with 0.2 ml of the blood sample that had been prepared during STEP-1. It was further incubated for 60 min at 37^0°C.

STEP-4: The positive control was taken in a standard test tube with 10 ml of 0.1% Na_2CO_3 solution. A 0.2 ml part of the blood sample that was prepared in STEP-1 was added to that solution. After that, the solution was incubated for 60 min at 37^0C.

STEP-5: As a negative control, 0.2 ml of the blood sample prepared in STEP-1 was added to a normal saline solution. It was then incubated at 37^0C for 60 min.

All samples were then centrifuged at 500g for 5 min. As part of the measurement of the optical density (OD) of the supernatant liquid at 545 nm, a UV-Vis spectrophotometer was used. In order to determine the percentage of haemolysis, the following formula was used.

$$\% \text{ Haemolysis} = \frac{\text{OD (Test)} - \text{OD (Negative)}}{\text{OD (Positive)} - \text{OD (Negative)}} \times 100$$

4.3.1c MTT Assay

The assay was conducted using Murine Osteoblastic MC3T3-E1 Cells. In an environment of 95% air and 5% CO_2, cells were cultured in a medium (αMEM-Gibco) containing 10% heat-inactivated fetal bovine serum and 1% penicillin streptomycin solution. Growth of cells on confluence was achieved in a 25 mm flask with 0.5% trypsin, and then seeded onto a 24-well plate (cell density: 5.0 x 10^4 cells/cm^2). The cells were incubated for 24 hrs with pure HAp, eggshell HAp, and doped HAp samples. Adding MTT solution and mixing it for 15 min was followed by incubating for another 4 hrs. Viable cells convert MTT into formazan crystals. To dissolve crystals into a purple-colored solution, DMSO (dimethyl sulfoxide) was added after removing the media. The intensity of the purple-colored solution depends on number of crystals formed. An absorbance (OD) measurement was conducted at 545nm using spectrophotometric equipment. A triplicate experiment was conducted and the mean value was reported.

4.3.1d Bactericidal Study

The study was performed to detect any bacterial colonies growing on the samples that cause implant failure. In a conical flask, a diluted solution of nutrient agar was poured and autoclaved at 121^0C for 20 min. After cooling at 40-45^0C, the culture of Staphylococcus aureus was added to the media mixed thoroughly, and then poured into Petri dishes and solidify it. Two porcelain bits containing the sample solution having 2mg/10ml (2mg sample powder in 10ml solution) and 1mg/10ml (1mg sample powder in 10ml solution) were taken and placed in Petri dishes and incubated for 24 hrs at 35^0C. For control, oxytetracycline is taken in porcelain bits.

4.3.2 In-vivo Study

The animal clinical study was conducted following the guidelines of the Institution's Animal Ethical Committee, WBUAFS. This study was evaluated for early-stage osteogenesis & bone remodeling Invivo through a critical-size defect model in femoral condyle in New Zealand white Rabbits over 2 months.

4.3.2a Implant Preparation

After preparing the Eggshell HAp, Pure HAp, and their dopant powders, the samples were pressed at 150 MPa pressure in a hydraulic press machine. The prepared green specimens were dried at 80^0C for three days. The cylindrical shaped samples (dia. 5 mm and height 6 mm) were sintered at 950^0C for densification (holding time in the furnace is 2 hrs). Before implanting, the sintered specimens were autoclaved at 121^0C for 30 min.

4.3.2b Surgery and Implantation Procedure

The study involved 42 New Zealand white rabbits of either sex were distributed randomly into 2- groups: A. Control Group I (only defect was done and no implant was given: 6 animals were taken, three animals at each time point) and B. Test Group II. In the group II category: Pure HAp (06 samples), Eggshell HAp (06 samples), Pure HAp with 5% titanium dopant sample (06 samples), Eggshell HAp with 5% titanium dopant (06 samples), Pure HAp with 5% zinc dopant (06 samples), Eggshell HAp with 5% zinc dopant (06 samples) were implanted in the created defect sites of the animals and rate of bone healing with osteogenic activity was observed. The rabbits were kept in a humidity-controlled room with 12 hrs of light and dark cycles before surgery and sample implantation. Rabbits were kept without restriction of movement and provided with adequate water and libitum. After implantation, an assessment was carried out over 30 days and 60 days.

Xylazine hydrochloride (XYLAXIN®, Indian Immunological, and India) was injected intramuscularly at 1 mg/kg and ketamine hydrochloride (Ketalar®, Parke-Davis, India) at 25 mg/kg body weight during surgery. In all the animals, a bone defect of 5mm x 2.5mm x 3mm was created in the femoral condyle using a motorized dental drill. The implanted sites muscles, subcutaneous tissues and skins were sutured for securing the specimens. A 125 mg/kg body weight dose of cefotaxime sodium (Mapra India, India) was administered intramuscularly once a day for five days to the animals, and 0.2 ml of meloxicam (MELONEX®, Intas Pharmaceuticals, India) was administered once a day for five days to each animal. Povidone iodine with antibiotic ointment was given daily for dressing of the defected sites. There was a similar pattern observed in the studies conducted by Kaushik et. al [6] and Samanta et.al [7].

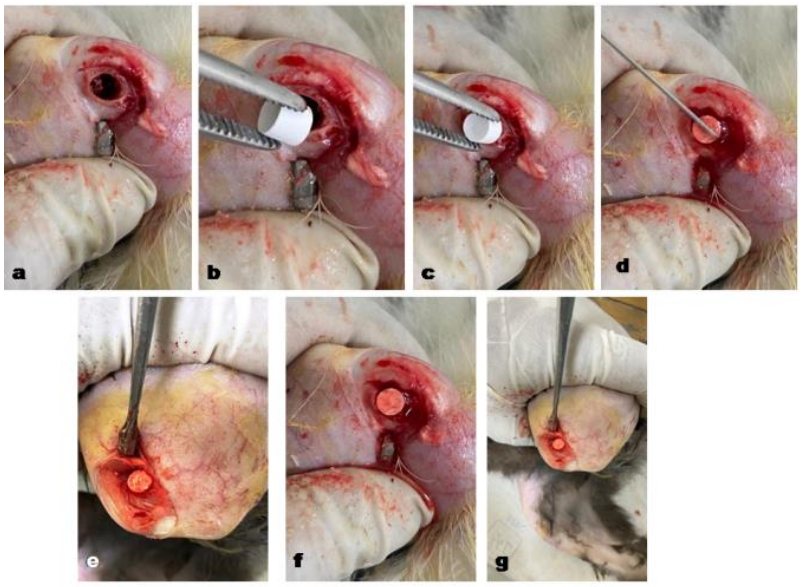

Fig 4.1: Some pictures of Surgery and Implantation procedure

4.3.2c Local Inflammatory Reaction and Wound Healing

Over 2 months after surgery, local inflammatory reactions and associated signs were observed, including swellings, sarcoma formation, hematomas, lameness, weight-bearing, oedema, and fracture repair capability.

4.3.2d Radiological Examination

The implant status, host tissue reaction, and bone formation were observed and recorded through Radiographs.

4.3.2e Histological Study

The surrounding bone with implants was taken out surgically from the sites after 1 and 2 months of implantation. The specimens were cut into 3-4 mm thin samples by hacksaw. All slices were cleaned thoroughly in saline solution and then immersed in formalin (10%) solution for 7 days. The decalcification was performed in Gooding and Stewart solution and then sliced into 4 µm and stained with haematoxylin solution. The cellular responses were studied under a microscope.

4.3.2f SEM of the Implants

A 5% glutaraldehyde phosphate solution was used to fix the samples, followed by a 30 min wash in a phosphate buffer solution. Samples were fixed in 5% glutaraldehyde phosphate solution and then washed in phosphate buffer solution for 30 min. The dehydration was done using a graded alcohol solution and then dried with hexamethyldisilazane. All samples were coated with gold by ion sputtering techniques. SEM examinations were carried out for all resin-mounted sample surfaces.

4.3.2g Oxytetracycline Labelling Study

Fluorochrome (oxytetracycline dihydrate) 50 mg/kg body mass was introduced into the implant sides. The implanted portions of bones were taken and cut transversely into 2-3 mm thickness with a hacksaw. The un-decalcified ground sections were grounded to 20 µm using sand papers under moderate pressure. The detailed bone structure within the ground sections was examined microscopically using ultraviolet light and observed the amount of tetracycline labeling and source of new bone formation.

REFERENCES

[1] J. H. Kim, S. H. Kim, H. K. Kim, T. Akaike, and S. C. Kim, “Synthesis and characterization of hydroxyapatite crystals: A review study on the analytical methods,” J. Biomed. Mater. Res.,
vol. 62, no. 4, pp. 600–612, 2002, doi: 10.1002/jbm.10280.

[2] B D Cullity, Elements of diffraction quasi-optics, Second., No. 1. London-Amstrerdam-Don Mills,Ontario-Sydney: Addison-Wesley Publishing Company Inc, 197.

[3] ASTM E384-99 A. Standard test method for microindentation hardness of materials. 1984

[4] T. Kokubo, H. Kushitani, S. Sakka, T. Kitsugi, and T. Yamamuro, “Solutions able to reproduce in vivo surface-structure changes in bioactive glass-ceramic W3,” J. Biomed. Mater. Res., vol. 24, no. 6, pp. 721–734, 1990, doi: 10.1002/jbm.820240607.

[5] A. Oyane, H.-M. Kim, T. Furuya, T. Kokubo, T. Miyazaki and T. Nakamura, "Preparation and assessment of revised simulated body fluid", *J. Biomed. Mater. Res.*, 65A, 188-195 (2003).

[6] Kaushik Sarkar, Vinod Kumar, K. Bavya Devi, Anomalous in Vitro and in Vivo Degradation of Magnesium Phosphate Bioceramics: Role of Zinc Addition, DOI: 10.1021/acsbiomaterials.9b00422 ACS Biomater. Sci. Eng. 2019, 5, 5097−5106.

[7] Sujan Krishna Samanta, K. Bavya Devi, Piyali Das, Metallic ion doped tri-calcium phosphate ceramics: Effect of dynamic loading on in vivo bone regeneration, journal-of-the-mechanical-behavior-of-biomedical-materials, Volume 96, August 2019, Pages 227-235.

5. RESULT & DISCUSSION

5. Physical Characterization of Pure HAp, Eggshell HAp and their Doped Variants

5.1.1 X-ray Diffraction Data

The obtained powder samples of Pure HAp, Eggshell HAp and their 3% and 5% dopant variants (Zn, Ti, Mg) were calcined at 800^0C temperature and analyzed the phase analysis of these calcined powder were examined through x-ray diffractometry in 2θ range. The calcined Pure HAp and Eggshell HAp samples showed various peaks with high intensity corresponding to various planes i.e.(0 0 2), (2 1 1), (3 0 0), (2 0 2), (2 1 2), (2 2 2), (2 1 3) which matches with the standard card number JCPD (09-0432) for hydroxyapatite. A sharp peak at 2θ range of ~32.07 similar to (2 1 1) confirmed hydroxyapatite crystals. The presence of this peak indicates calcinations at 800^0C resulted in hydroxyapatite crystals.

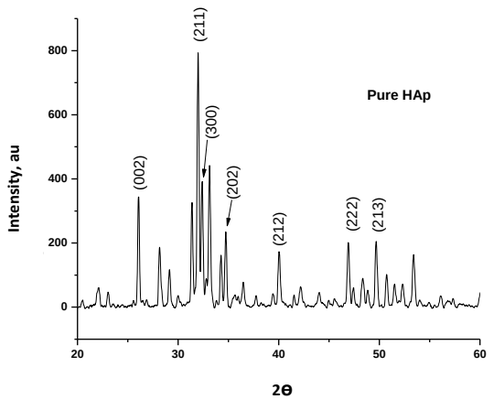

Figure 5.1: XRD pattern of Pure HAp

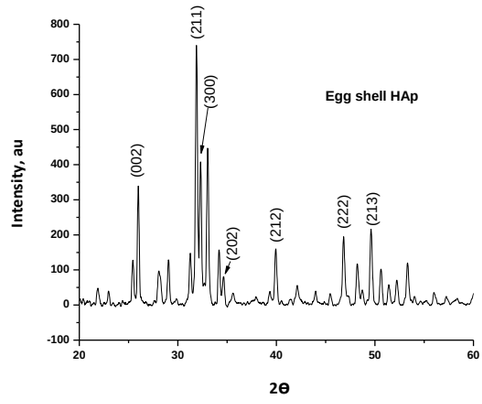

Figure 5.2: XRD pattern of Egg shell HAp

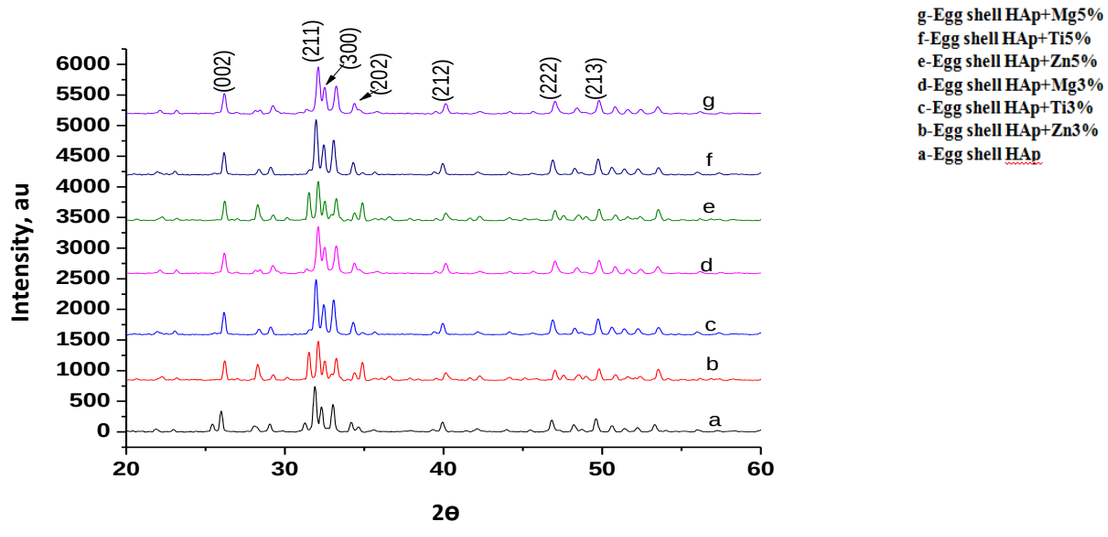

Figure 5.3: XRD pattern of Eggshell HAp and its dopants

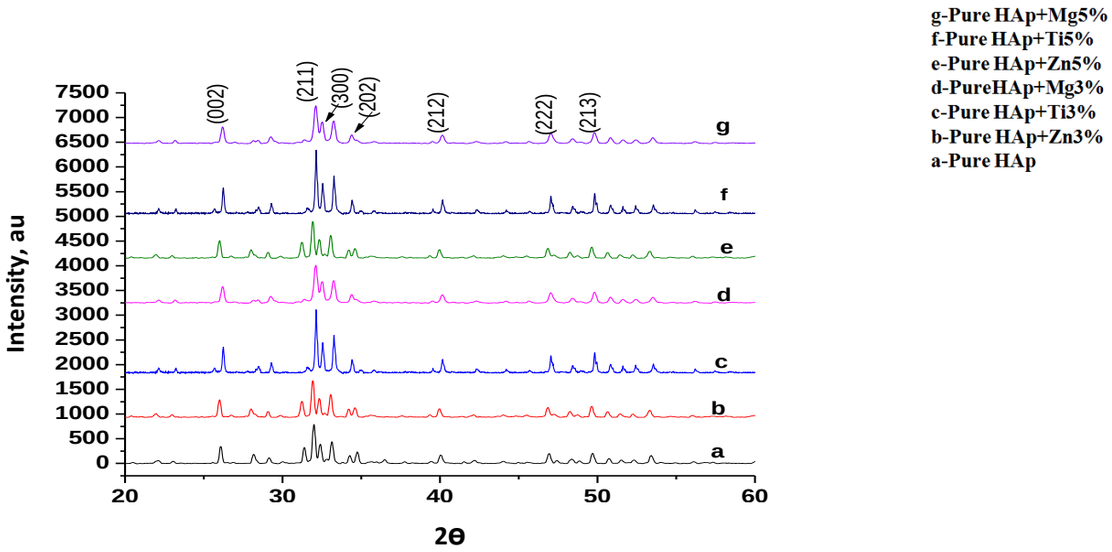

Figure 5.4: XRD pattern of Pure HAp and its dopants

The HAp prepared from egg cell powder produced peaks that matched standard card no JCPD (09-0432). The 3% and 5% Zn, Ti, and Mg verities had the same intensity peaks with a little bit of shifting due to the substitution of calcium ions by zinc, titanium, and magnesium ions. A comparative analysis with laboratory-grade hydroxyapatite (Pure HAp) and its dopants signifies that the experimentally prepared eggshell HAp and their derivatives carry almost the same crystalline structure as reflected in the results.

5.1.2 Lattice Parameter Study

Incorporating different dopant ions resulted in minor changes in the lattice parameters. In all cases, both the 'a' and 'c' axis values decreased systematically, shown in below Table1. One of the possible reasons for this may be due to the smaller atomic radius of some of the dopants, such as zinc (134 pm), magnesium (160 pm), and titanium (147 pm), compared to calcium (197 pm). In the results, calcium ion was substituted by dopants, resulting in a reduction in cell size.

In the lattice parameter study, the percentage of crystallinity is decreasing in doped variants compared to Pure HAp and Eggshell HAp. In Eggshell HAp, % crystallinity is less due to the presence of a number of trace elements.

Table 5.1 Result of Lattice Parameters

Sl. No	Composition	a axis (Å)	c axis (Å)	Unit cell volume (Å3)	Crystallite size (Å)	% Crystallinity
1	Pure HAp	9.4230±.0.097	6.841 ±0.120	533.93±22.02	3.6286±12.67	93.81± 3.82
2	Egg shell HAp	9.416±0.11	6.787±0.17	521.05±18.29	3.5556±9.84	84.81±5.76
3	Pure HAp + Zn 5%	9.221±.0.077	6.693 ±0.142	508.78±22.54	3.3681±11.57	82.41± 4.12
4	Egg shell HAp + Zn 5%	9.215±0.31	6.671 ±0.320	487.05±18.29	3.3291±14.77	84.01±5.76
5	Pure HAp + Ti 5%	9.28±0.34	6.731±0.21	501.91±16.29	3.4121±8.02	82.47±6.82
6	Egg Shell HAp + Ti 5%	9.22±0.23	6.71±0.37	493.97±19.16	3.3912±11.12	88.46±4.02
7	Pure HAp + Mg 5%	9.383±.0.086	6.791 ±0.110	517.83±26.12	3.5475±22.61	80.54± 3.94
8	Egg Shell HAp + Mg 5%	9.326±0.19	6.741 ±0.020	509.05±16.19	3.4581±10.42	81.61±5.06

5.1.3 FTIR Analysis

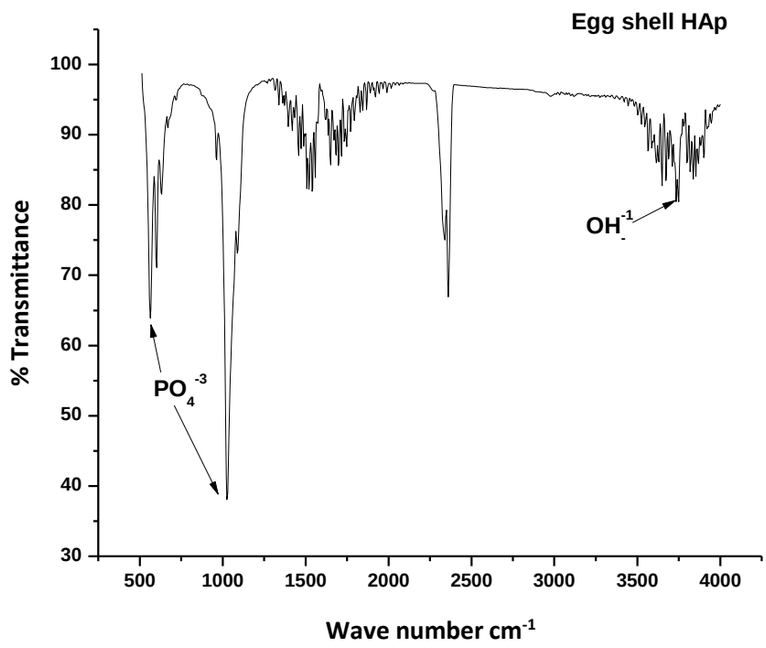

Figure 5.5: FTIR spectra of Eggshell HAp

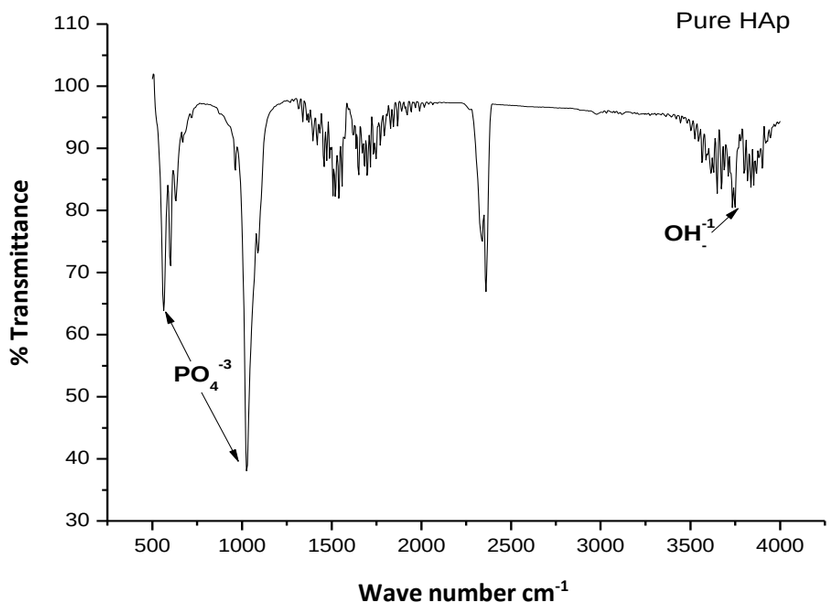

Figure 5.6: FTIR spectra of Pure HAp

In Fig 5 & 6 we got a FTIR plot of Egg shell HAp and Pure HAp sample. At 570 &1023 the peak signifies the presence of phosphate ion whereas at 3752, a stretching band of hydroxyl ion are present. A sharp peak at 2357 is due to the presence of some unreacted carbonate ion.

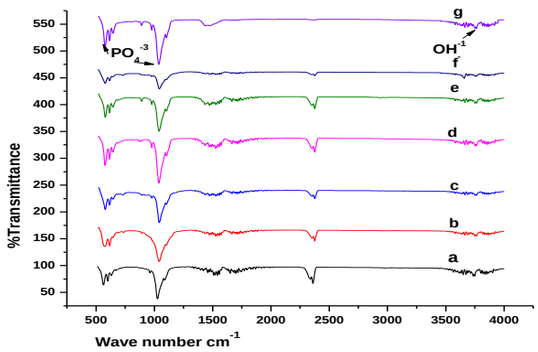

Figure 5.7: FTIR spectra of Egg shell HAp along with its dopants

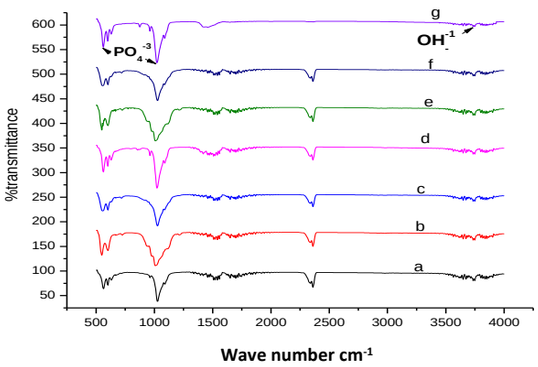

Figure 5.8: FTIR spectra of Pure HAp along with its dopants

5.1.4 Green Density of Egg shell HAp, Pure HAp and their Dopants

Green density did not differ significantly between samples of different compositions, indicating similar bulk volumes. Result of this measurement is presented in table 5.2 and table 5.3.

Table 5.2 Green density of Egg shell HAp and their derivatives

Sl. No.	Composition	Green Density
1	Egg shell HAp	1.546 ± 0.011402
2	Egg shell HAp + Zn 3%	1.602 ± 0.008367
3	Egg shell HAp + Ti 3%	1.562 ± 0.020494
4	Egg shell HAp + Mg 3%	1.504 ± 0.020736
5	Egg shell HAp + Zn 5%	1.628 ± 0.013038
6	Egg shell HAp + Ti 5%	1.596 ± 0.011402
7	Egg shell HAp + Mg 5%	1.526 ± 0.020618

Table 5.3 Green density of Pure HAp and their derivatives

Sl. No.	Composition	Green Density
1	Pure HAp	1.53 ± 0.022361
2	Pure HAp + Zn 3%	1.6 ± 0.015811
3	Pure HAp + Ti 3%	1.564 ± 0.016733
4	Pure HAp + Mg 3%	1.462 ± 0.031145
5	Pure HAp + Zn 5%	1.644 ± 0.023022
6	Pure HAp + Ti 5%	1.602 ± 0.019235
7	Pure HAp + Mg 5%	1.494 ± 0.021909

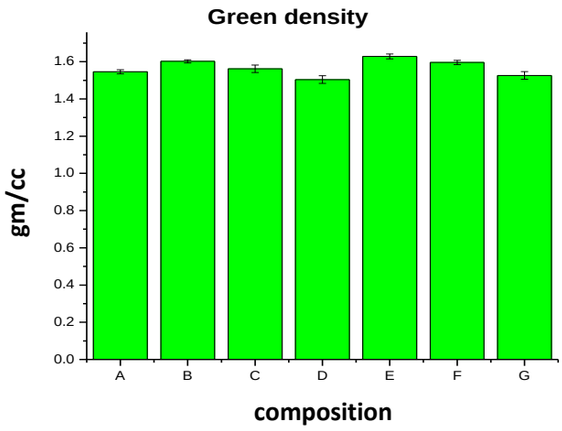

(A) Eggshell HAp
(B) Eggshell HAp+Zn 3%
(C) Egg shell HAp+Ti 3%
(D) Egg shell HAp+Mg 3%
(E) Eggshell HAp+Zn 5%
(F) Egg shell HAp+Ti 5%
(G) Eggshell HAp+Mg 5%

Figure 5.9: The average green density of (A) Eggshell HAp, (B) Eggshell HAp + Zn 3%, (C) Eggshell HAp + Ti 3%, (D) Eggshell HAp + Mg 3%, (E) Eggshell HAp + Zn 5%, (F) Eggshell HAp + Ti 5%, (G) Eggshell HAp + Mg 5%.

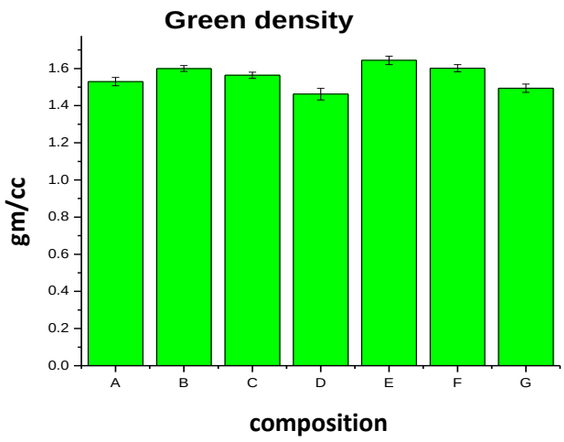

(A)Pure HAp
(B) Pure HAp+Zn 3%
(C) Pure HAp+Ti 3%
(D) Pure HAp+Mg 3%
(E) Pure HAp+Zn 5%
(F) Pure HAp+Ti 5%
(G) Pure HAp+Mg 5%

Figure 5.10: The average green density of (A) Pure HAp (B) Pure HAp + Zn 3% (C) Pure HAp + Ti 3% (D) Pure HAp + Mg3% (E) Pure HAp + Zn 5% (F) Pure HAp + Ti 5% G) Pure HAp + Mg 5%.

The above said plot in figure 5.9 & 5.10 depicted that the green density of pure HAp, Eggshell HAp, and their dopants are nearly the same or equal.

5.1.5 Sintered Density and Percentage of Diametric, Linear and Volumetric Shrinkage at Different Temperatures

After the prepared HAp and their dopants, it is pressed to form pellets and green density is measured. The diameters of the pellets are 10±0.03 mm and the thickness is 6±0.03 mm. After sintering at 950^0C &1050^0C, there was shrinkage of diameter and length. Tables 5.6 & 5.7 illustrate this. Diametric and volumetric shrinkages are measured through a digital Vernier scale. The average sintering density of Pure HAp and Eggshell HAp at 950^0C are 2.97gm/cc and 2.94gm/cc whereas at 1050^0C it is 3.01gm/cc & 3.04gm/cc respectively. The result showed that (Table 5.4 &5.5) density increased with increasing sintering temperature from 950^0C to 1050^0C, but there were no major changes happened. The percentage of diametric, linear, and volumetric shrinkage at different temperatures is shown below. It has been noted that the Sintering density is almost double the green density (reflected in Table 5.2, Table 5.3, Table 5.4, and Table 5.5).

Table5.4: Sintered density data of Eggshell HAp and their dopants at different temperatures

Sl. No.	Compositions	At 950^0C	At 1050^0C
1	Eggshell HAp	2.94 ± 0.0115	3.04 ± 0.0145
2	Eggshell HAp + Zn 3%	3.03 ± 0.0153	3.07 ± 0.0173
3	Egg shell HAp + Ti 3%	2.97 ± 0.0378	3.03 ± 0.0207
4	Egg shell HAp + Mg 3%	2.81 ± 0.010	2.89 ± 0.014
5	Eggshell HAp + Zn 5%	3.13 ± 0.0361	3.18 ± 0.0261
6	Egg shell HAp + Ti 5%	3.06 ± 0.0252	3.12 ± 0.0152
7	Egg shell HAp + Mg 5%	2.87 ±0 .02	2.94 ± 0.018

Table 5.5: Sintered density data of Pure HAp and their dopants at different temperature

Sl. No.	Compositions	At 950^0C	At 1050^0C
1	Pure HAp	2.97 ± 0.015	3.01 ± 0.021
2	Pure HAp + Zn 3%	3.06 ± 0.021	3.09 ± 0.019
3	Pure HAp + Ti 3%	3.02 ± 0.016	3.06 ± 0.017
4	Pure HAp + Mg 3%	2.83 ± 0.025	2.89 ± 0.022
5	Pure HAp + Zn 5%	3.14 ± 0.020	3.19 ± 0.023
6	Pure HAp + Ti 5%	3.07 ± 0.021	3.10 ± 0.025
7	Pure HAp + Mg 5%	2.88 ± 0.010	2.92 ± 0.016

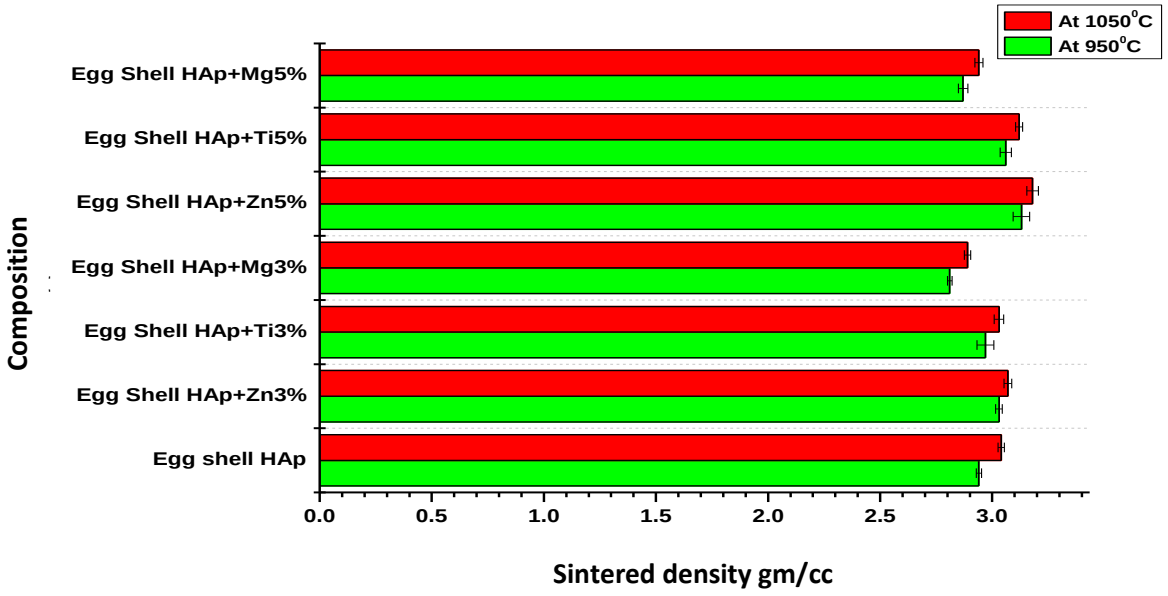

Figure 5.11: Representation of Sintered density of Eggshell HAp and their dopants at two different temperatures

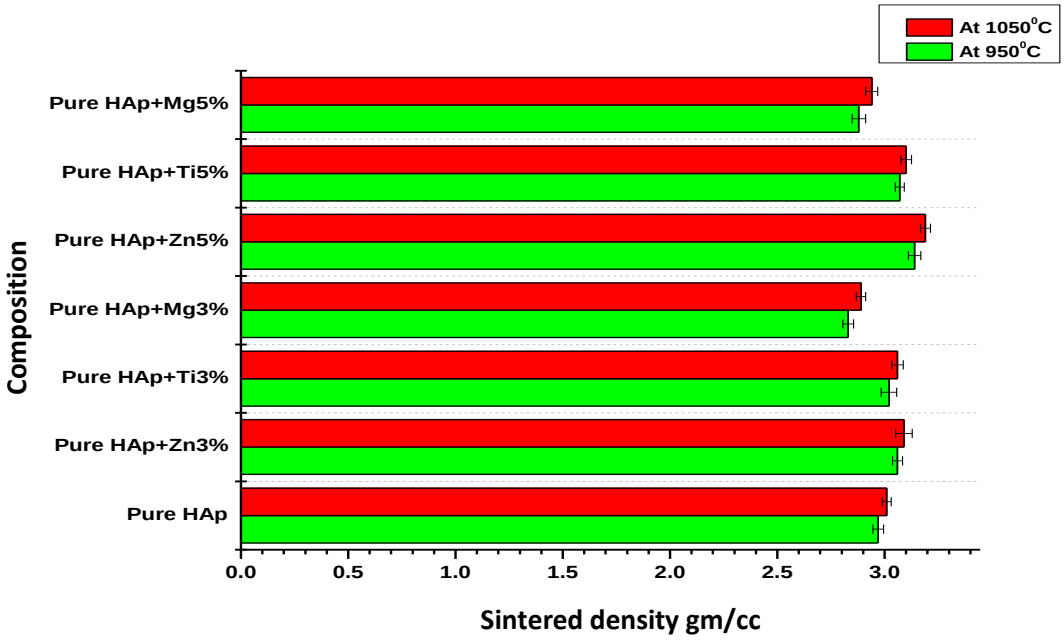

Figure 5.12: Representation of Sintered density of Pure HAp and their dopants at two different temperatures

The 5% zinc-doped Pure HAp and Eggshell HAp show the maximum density at 1050^0C. From Tables 5.4 & 5.5 it has been seen that magnesium-doped samples have lower density whereas titanium-doped samples show a moderate value

Major observations:

- ❖ It was observed from the XRD plot that pure hydroxyapatite phases were developed in both Pure HAp and Eggshell HAp samples.
- ❖ The dopant ions substitution had been noticed through lattice parameter study.
- ❖ The presence of a functional group was confirmed through the FTIR study.
- ❖ The sintering density was almost doubled to the green density.
- ❖ On increasing the sintering temperature, density was increased (Table 5.4 &Table 5.5)
- ❖ All types of shrinkage happened in all the samples (Table 5.6).

Table 5.6: Percentage of diametric, linear, and volumetric shrinkage of eggshells and their dopants at different temperatures

Compositions	%Diametric shrinkage		% Linear Shrinkage		% Volumetric Shrinkage	
	950^0C	1050^0C	950^0C	1050^0C	950^0C	1050^0C
Egg shell HAp	19.31	19.42	21.12	21.30	48.83	49.05
Eggshell HAp + Zn 3%	19.42	19.56	21.25	21.38	49.05	49.4
Egg shell HAp + Ti 3%	19.30	19.45	21.02	21.22	47.92	48.22
Egg shell HAp + Mg 3%	19.33	19.47	21.23	21.36	48.96	49.09
Eggshell HAp + Zn 5%	19.38	19.52	21.43	21.58	49.25	49.45
Egg shell HAp + Ti 5%	19.26	19.36	20.95	21.06	47.63	47.78
Egg shell HAp + Mg 5%	19.28	19.39	20.78	20.91	48.87	48.98

Table 5.7: Percentage of diametric, linear and volumetric shrinkage of pure HAp and their dopants at different temperatures

Compositions	% Diametric shrinkage		% Linear Shrinkage		% Volumetric Shrinkage	
	950^0C	1050^0C	950^0C	1050^0C	950^0C	1050^0C
Pure HAp	19.28	19.36	21.02	21.16	48.67	48.78
Pure HAp + Zn 3%	19.36	19.45	21.17	21.29	48.92	49.31
Pure HAp + Ti 3%	19.22	19.31	20.96	21.08	47.81	47.92
Pure HAp + Mg 3%	19.28	19.37	21.18	21.26	48.87	49.02
Pure HAp + Zn 5%	19.35	19.46	21.33	21.45	49.15	49.28
Pure HAp + Ti 5%	19.22	19.34	20.82	21.05	47.54	47.69
Pure HAp + Mg 5%	19.23	19.39	20.62	20.76	48.61	48.81

5 .1.6 Apparent Porosity at Different Temperatures

Porosity plays a significant role in scaffold engineering. A minimum percentage of porosity is needed for cell growth during tissue regeneration. The properties of the scaffold would be such that it can withhold the body pressure along with its inherent characteristics. It is reported that a pore size greater than 150µm in a scaffold is essential for osteoconduction. Bone tissues pass through the pores causing the mechanical fixation of the implant to the body.

Table 5.8. Apparent porosity of Eggshell HAp and their dopants at different temperatures

Sl. No.	Compositions	At 950^0C (%)	At 1050^0C (%)
1	Eggshell HAp	30.48 ± 1.72	19.41 ± 1.21
2	Eggshell HAp + Zn 3%	37.13 ± 0.96	27.34 ± 1.12
3	Egg shell HAp + Ti 3%	34.90 ± 1.06	24.81 ± 0.85
4	Egg shell HAp + Mg 3%	31.90 ± 1.20	23.87 ± 0.95
5	Eggshell HAp + Zn 5%	34.95 ± 0.94	24.55 ± 0.68
6	Egg shell HAp + Ti 5%	32.57 ± 1.02	23.05 ± 0.52
7	Egg shell HAp + Mg 5%	32.64 ± 0.65	22.54 ± 0.61

Table 5.9: Apparent porosity of Pure HAp and their dopants at different temperatures

Sl. No.	Compositions	At 950^0C (%)	At 1050^0C (%)
1	Pure HAp	22.02 ± 1.66	17.52 ± 0.75
2	Pure HAp + Zn 3%	25.91 ± 1.94	20.93 ± 1.89
3	Pure HAp +Ti 3%	24.31 ± 2.48	18.27 ± 0.83
4	Pure HAp + Mg 3%	23.22 ± 0.73	18.01 ± 0.92
5	Pure HAp + Zn 5%	23.36 ± 2.13	20.42 ± 0.78
6	Pure HAp + Ti 5%	21.05 ± 2.94	17.57 ± 1.01
7	Pure HAp + Mg5%	21.67 ± 1.18	16.53 ± 1.28

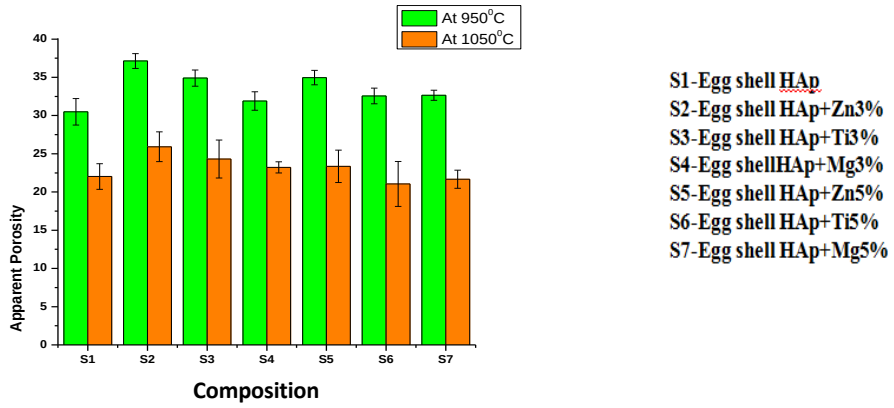

Figure 5.13: Bar diagram of apparent porosity of Eggshell HAp and their dopants at different temperatures (950^0C & 1050^0C)

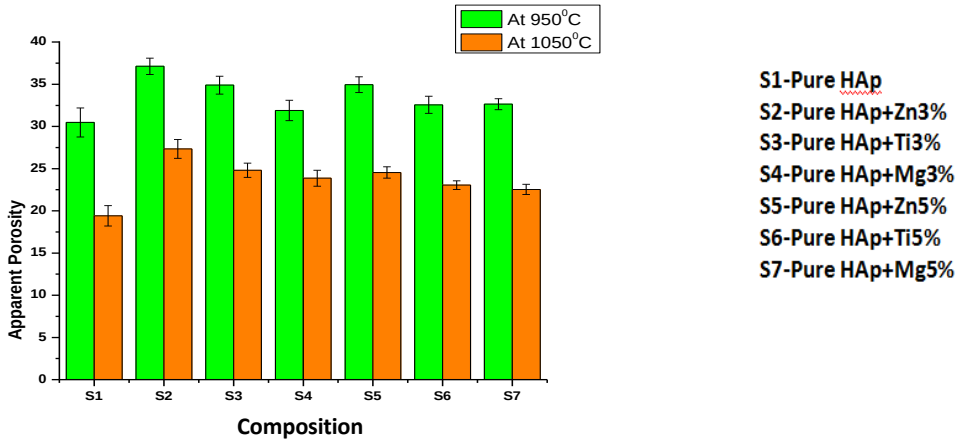

Figure 5.14: Bar diagram of apparent porosity of Pure HAp and their dopants at different temperatures (950^0C &1050^0C)

From Figures 5.13 and 5.14 it is observed that porosity is lesser at 1050°C than 950°C. From Tables 5.8 &5.9 it is observed that Egg cell HAp has more porosity than pure HAp for all its varieties. Further, it can be said that all the 5% doped variants are showing lesser porosity than their own 3% doped variants.

5.1.7 Grain Size and Pore Size

By using Perfect Screen Ruler software, the grain size and pore size are measured. Here five random SEM images of the samples are taken.

Table5.10. Grain Size, pore size of Eggshell HAp and their dopants at different temperatures

Sl. No.	Compositions	Grain Size (µm)	Pore Size (µm)
1	Eggshell HAp	569 ± 3.05	158 ± 1.15
2	Eggshell HAp + Zn 3%	539 ± 2.52	157 ± 3.0
3	Egg shell HAp + Ti 3%	552 ± 5.0	169 ± 2.08
4	Egg shell HAp + Mg 3%	555 ± 4.04	180 ± 1.52
5	Eggshell HAp + Zn 5%	547 ± 6.0	170 ± 4.04
6	Egg shell HAp + Ti 5%	565 ± 4.0	168 ± 3.51
7	Egg shell HAp + Mg 5%	568 ± 3.51	192 ± 2.08

Table 5.11. Grain size, pore size of Pure HAp and their dopants at different temperatures

Sl. No.	Compositions	Grain Size (µm)	Pore Size (µm)
1	Pure HAp	572 ± 5.51	152 ± 3.6
2	Pure HAp + Zn 3%	545 ± 4.51	154 ± 2.0
3	Pure HAp + Ti 3%	555 ± 3.61	164 ± 3.51
4	Pure HAp + Mg 3%	558 ± 2.52	174 ± 4.16
5	Pure HAp + Zn 5%	549 ± 2.0	175 ± 2.64
6	Pure HAp + Ti 5%	565 ± 3.51	158 ± 3.6
7	Pure HAp + Mg 5%	569 ± 2.51	187± 2.51

Grain size and pore size measurement an important parameter in porous scaffold materials as these are responsible for osteoconduction, cell migration, and cell-cell interaction. In our study, it is observed from tables 5.10&5.11 that Pure HAp and Eggshell HAp have the largest grain sizes 572 µm and 569 µm. The 3 % Zn doped pure HAp and Eggshell HAp samples show the smallest grain size 545 µm and539 µm.

5.1.8 SEM-EDX Study

A standard SEM image of each sample is shown in Fig.5.15 and Fig.5.16. The figures confirm that nodular pores are present in enough quantity in the samples to support bony ingrowth throughout. The presence of pores gives the structural integrity of the scaffolds. Elemental analysis through E-DAX studies reflected in figures 5.17 &5.18 provide the presence of trace elements zinc, titanium, and magnesium ions. In Figure 5.17 elemental analysis of Eggshell Hap and with its 3% and 5% zinc, titanium, and magnesium dopants are reflected.

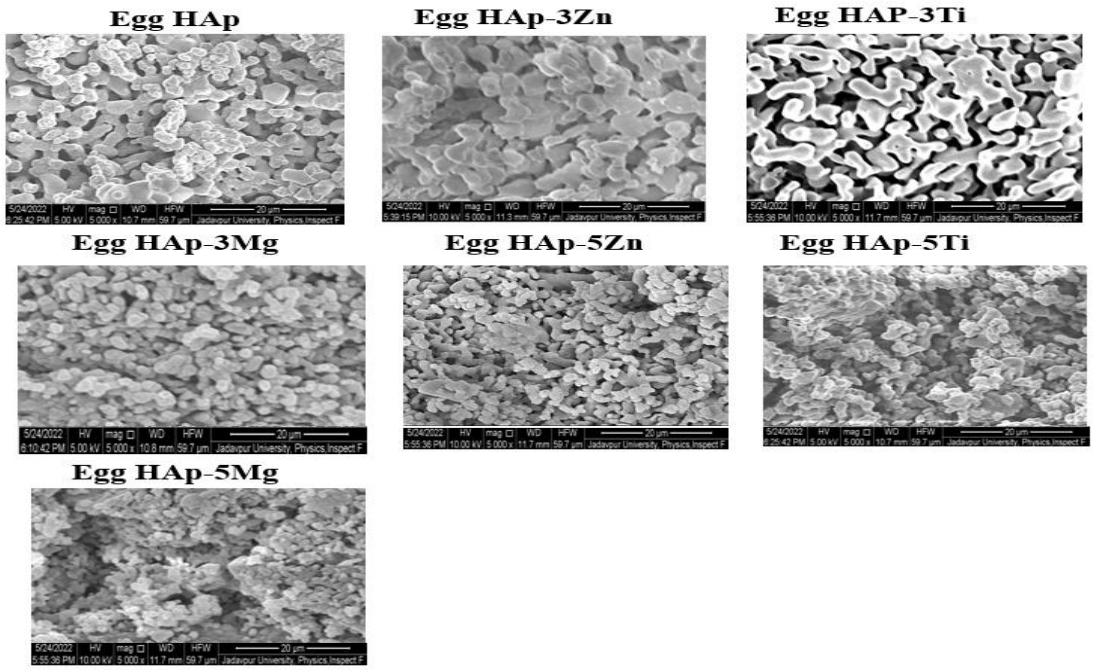

Figure 5.15: SEM images of Eggshell HAp and their dopants in 3% and 5% variation

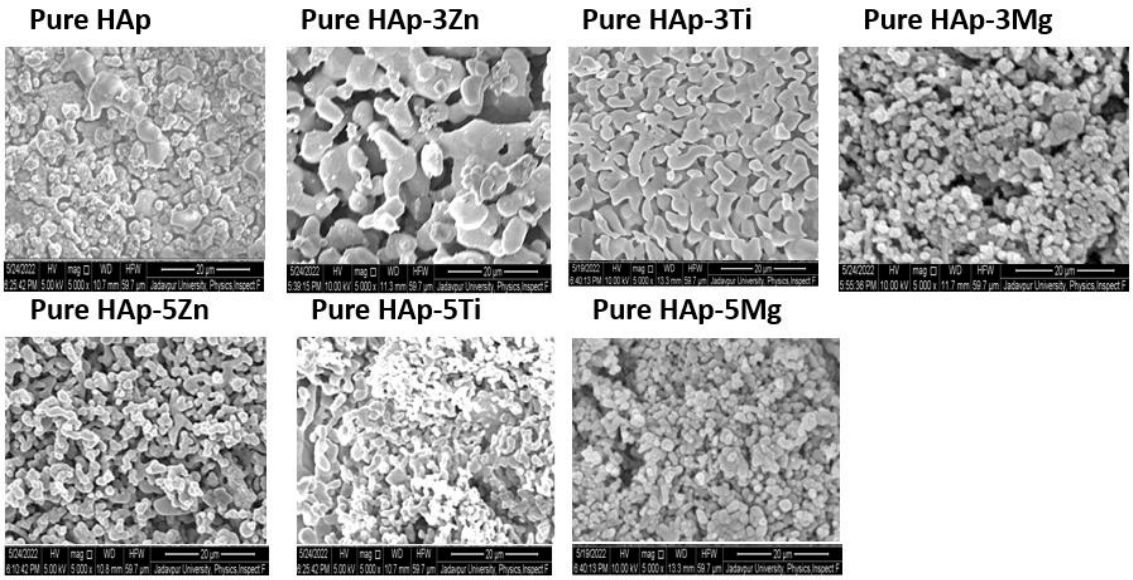

Figure5.16: SEM images of Pure HAp and their dopants in 3% and 5% variation

5.1.9 E-DAX analysis

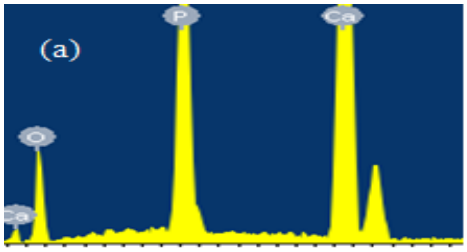

Element	Weight%	Atomic%
O K	37.42	57.69
P K	21.04	16.75
Ca K	41.54	25.56
Totals	100	

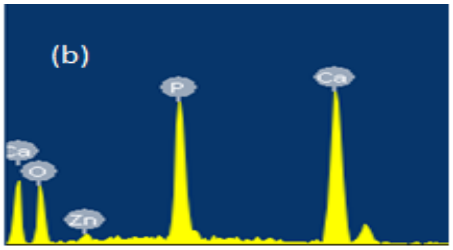

Element	Weight%	Atomic%
O K	49.8	69.49
P K	18.03	13
Ca K	30.32	16.89
Zn K	1.84	0.63

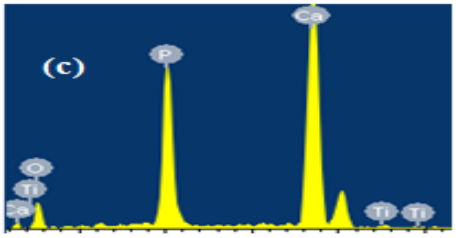

Element	Weight%	Atomic%
O K	31.68	51.76
P K	19.56	16.51
Ca K	48.09	31.37
Ti K	0.67	0.37

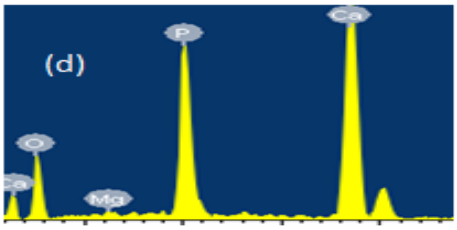

Element	Weight%	Atomic%
O K	47.15	66.95
Mg K	0.65	0.6
P K	17.13	12.56
Ca K	35.08	19.88

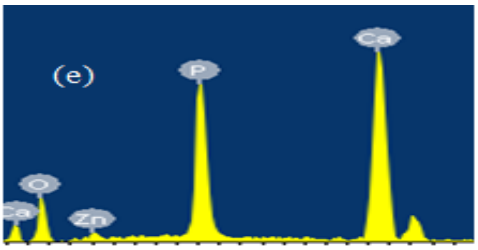

Element	Weight%	Atomic%
O K	40.8	61.63
P K	19.98	15.59
Ca K	35.45	21.38
Zn K	3.77	1.39

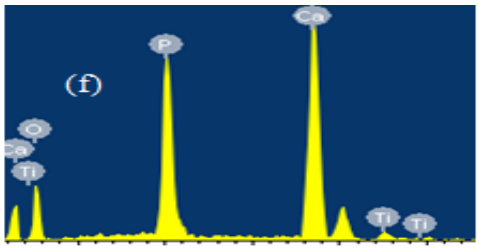

Element	Weight%	Atomic%
O K	46.18	66.24
P K	18.37	13.61
Ca K	33.82	19.37
Ti K	1.63	0.78

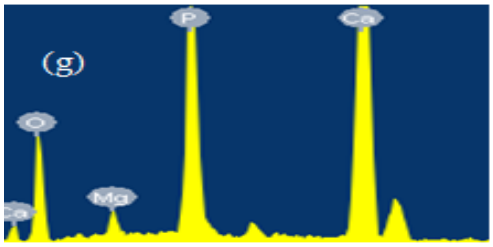

Element	Weight%	Atomic%
O K	48.08	67.56
Mg K	1.78	1.65
P K	16.16	11.73
Ca K	33.98	19.06

Figure 5.17: EDS pattern of Eggshell HAp and their dopants sintered at 1050°C (a) Eggshell HAp (b) Eggshell HAp + Zn 3%(c) Eggshell HAp +Ti 3% (d) Eggshell HAp + Mg3% (e) Eggshell HAp + Zn 5% (f) Egg shell HAp +Ti 5%(g) Egg shell HAp + Mg 5%

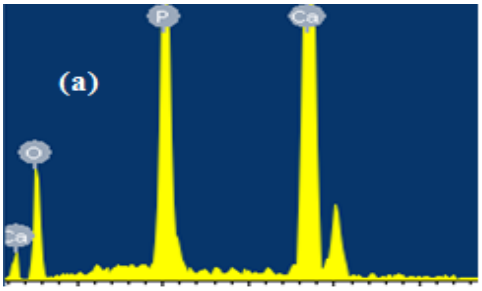

Element	Weight%	Atomic%
O K	41.6	61.84
P K	20.11	15.44
Ca K	38.3	22.72
Totals	100	

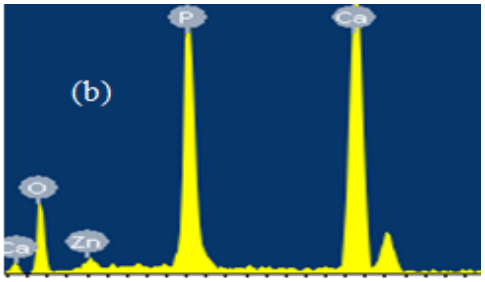

Element	Weight%	Atomic%
O K	42.59	63.1
P K	19.3	14.77
Ca K	36.32	21.48
Zn K	1.79	0.65

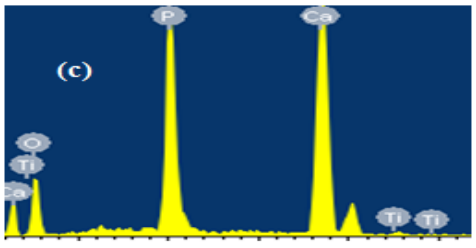

Element	Weight%	Atomic%
O K	43.71	63.86
P K	19.72	14.88
Ca K	35.97	20.98
Ti K	0.59	0.29

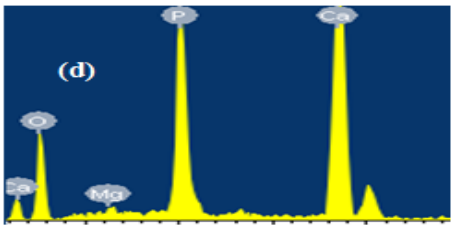

Element	Weight%	Atomic%
O K	49.57	69.04
Mg K	0.63	0.58
P K	16.42	11.82
Ca K	33.38	18.56

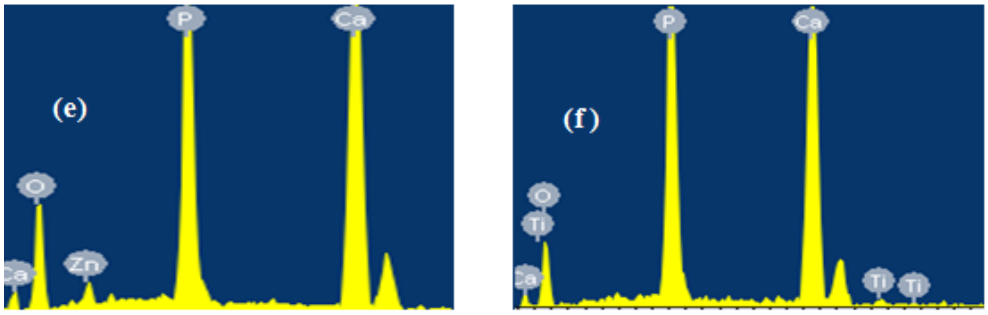

Element	Weight%	Atomic%
O K	42.98	63.68
P K	19.48	14.91
Ca K	34.06	20.15
Zn K	3.48	1.26

Element	Weight%	Atomic%
O K	38	57.97
P K	24.41	19.23
Ca K	36.75	22.38
Ti K	0.84	0.43

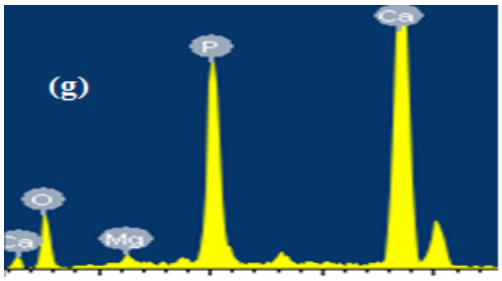

Element	Weight%	Atomic%
O K	39.14	59.55
Mg K	0.86	0.86
P K	17.69	13.9
Ca K	42.31	25.69

Figure 5.18: EDS pattern of pure HAp and their dopants sintered at 1050°C (a) Pure HAp(b) Pure HAp + Zn 3% (c) Pure HAp + Ti 3% d) Pure HAp + Mg3% (e) Pure HAp + Zn 5%(f) Pure HAp + Ti 5% (g) Pure HAp + Mg 5%

5.2 Mechanical Characterization of Eggshell HAp, Pure HAp, and their Doped Variants

It is observed from the data shown in tables 5.12 &5.13, that the hardness figure of the prepared samples at 1050^0C temperature. The hardness value increases with the addition of dopant elements due to the densification properties. It may be due to the transformation of calcium carbonate into calcium oxide and the presence of trace elements that eggshell components have increased in hardness.

Table 5.12. The hardness value of Eggshell HAp and their dopants at different temperatures

Sl. No.	Composition	Hardness (GPa)
1	Eggshell HAp	3.71 ± 0.020
2	Eggshell HAp + Zn 3%	3.92 ± 0.031
3	Egg shell HAp + Ti 3%	3.98 ± 0.036

4	Egg shell HAp + Mg 3%	3.84 ± 0.021
5	Eggshell HAp + Zn 5%	3.97 ± 0.010
6	Egg shell HAp + Ti 5%	4.0 5± 0.040
7	Egg shell HAp + Mg 5%	3.91 ± 0.066

Table 5.13. The hardness value of Pure HAp and their dopants at different temperatures

Sl. No.	Composition	Hardness (GPa)
1	Pure HAp	3.64 ± 0.030
2	Pure HAp + Zn 3%	3.78 ± 0.031
3	Pure HAp + Ti 3%	3.83 ± 0.015
4	Pure HAp + Mg 3%	3.67 ± 0.017
5	Pure HAp + Zn 5%	3.86 ± 0.025
6	Pure HAp + Ti 5%	3.94 ± 0.03
7	Pure HAp + Mg 5%	3.74 ± 0.021

In the case of 5% Ti-doped Pure HAp and 5% Ti-doped Egg shell HAp, the hardness values were displayed as 3.94 GPa and 4.05 GPa, respectively. It may be due to the higher densification of the ceramic by Titanium ions in the compositions. The hardness of all doped compositions is higher than pure value.

5.3 Biological Characterization of Eggshell HAp, Pure HAp, and their Doped Variants

5.3.1 SBF Study

Apatite layer formation above the sintered pellets after 7 days was noticed through scanning electron microscopy. Porous apatite layer formation was started after 7 days. On the 30th day, the apatite was denser as compared to the previous one. Apatite layer thickness and size were increased with increasing immersion times.

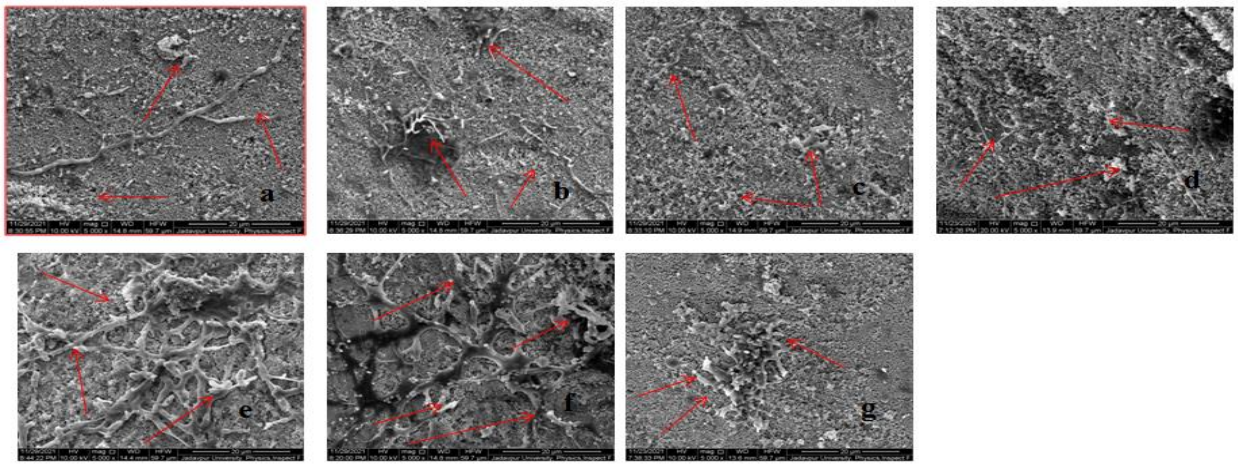

Figure 5.19: SBF apatite images of pure HAp and their dopants (a) Pure HAp (b) Pure HAp + Zn 3% (c) Pure HAp + Ti 3% d) Pure HAp + Mg3% (e) Pure HAp + Zn 5% (f) Pure HAp + Ti 5% (g) Pure HAp + Mg 5%.

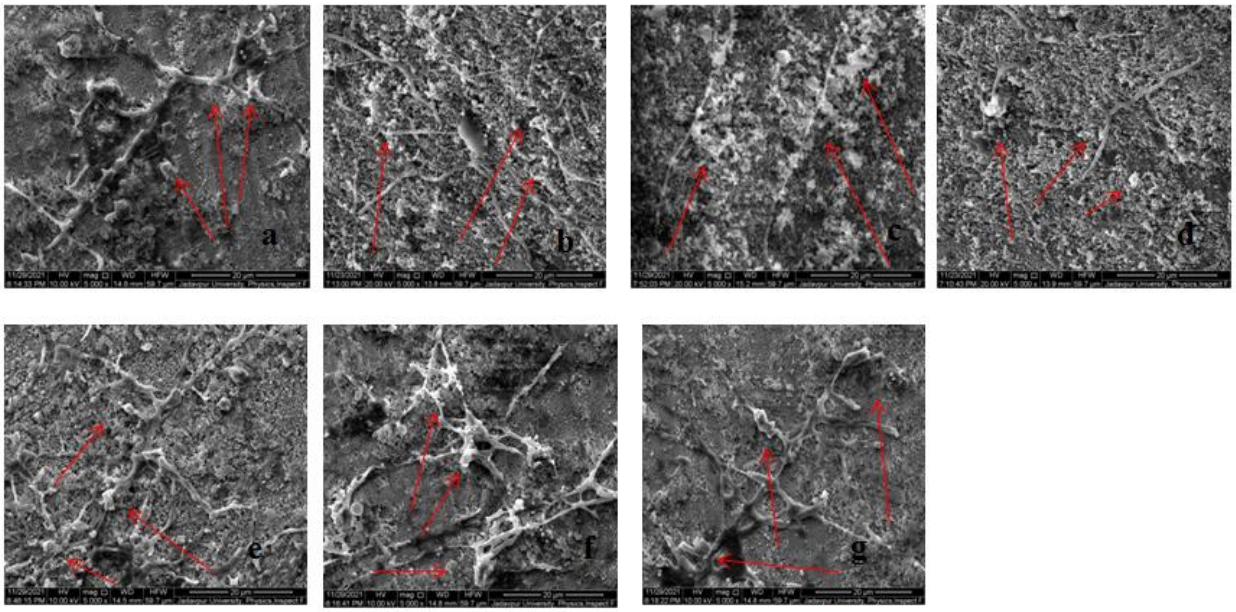

Figure 5.20: SBF apatite images of Eggshell HAp and their dopants (a) Eggshell HAp (b) Eggshell HAp + Zn 3% (c) Eggshell HAp + Ti 3% d) Eggshell HAp + Mg 3% (e) Eggshell HAp + Zn 5% (f) Eggshell HAp + Ti 5% (g) Eggshell HAp + Mg 5%.

5.3.2 Weight Degradation

In the SBF solution, the pellets lose their weight. The weight degradation study was done every 3 days for one month. After 3 days, pellets were removed from the solution, dried, and weighed in order to determine their weight. Following are the percentages of weight degradation shown in Figures 21 and 22. The rate of degradation is faster up to the 12-15 days, after that the rate becomes slower probably because of apatite layer formation above the pellets.

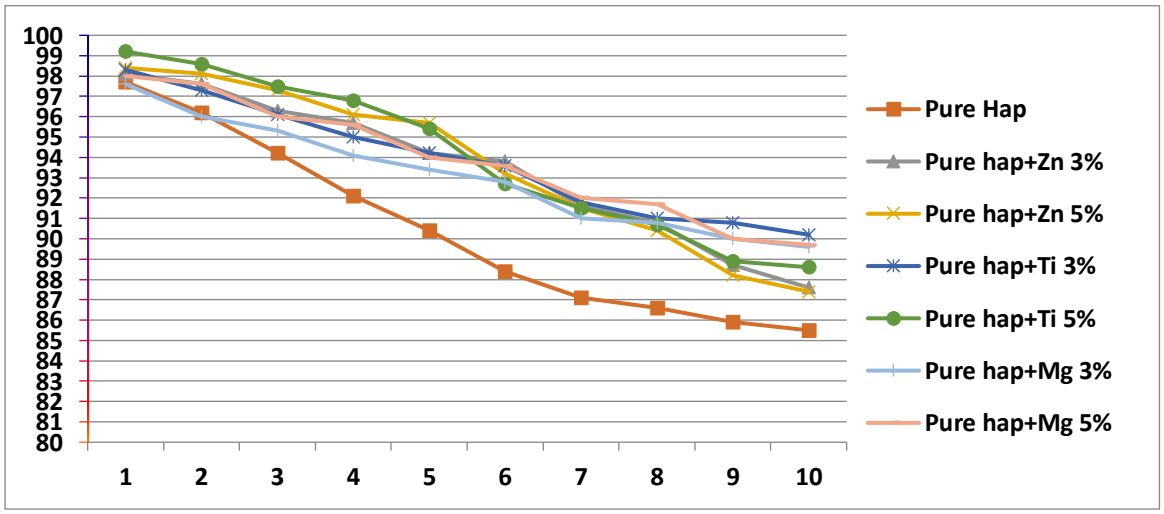

Figure 5.21 Plot of percentage weight degradation in SBF with days (Pure HAp & its dopants)

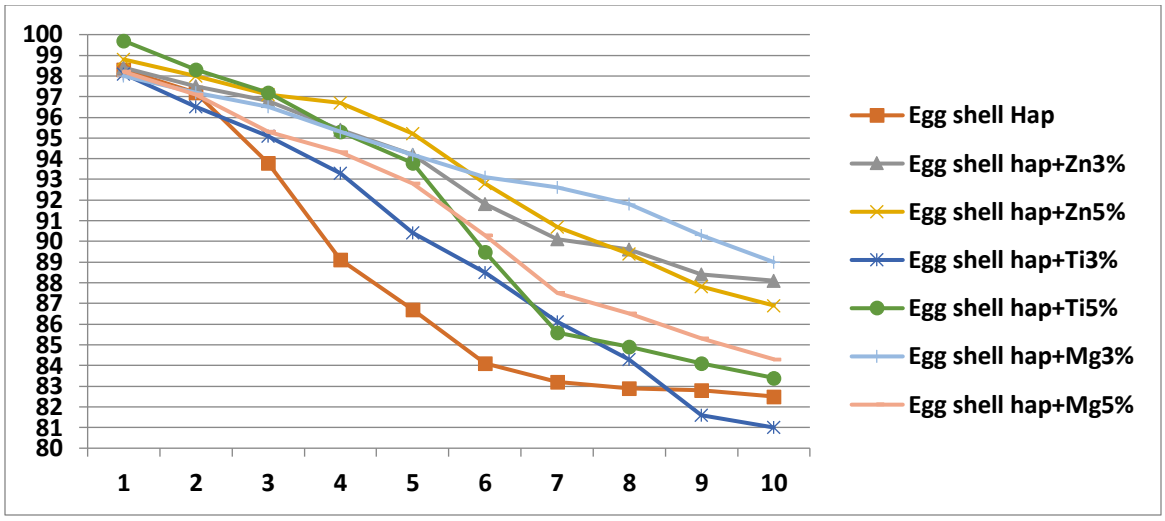

Figure 5.22 Plot of percentage weight degradation in SBF with days (Eggshell HAp & its dopants)

5.3.3 Percentage Transmittance of SBF

After dissolving the pellets in SBF solution the rate of degradation is higher and more particles of the pellets leaching out into the solution and the percentage of transmittance is gradually changing up to 12-15 days. After that the change is stable.

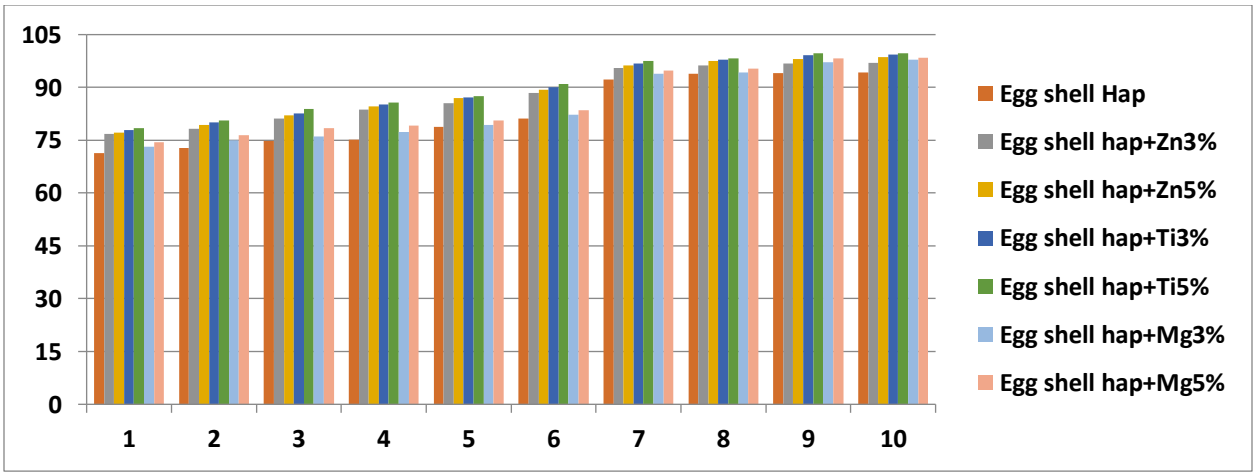

Figure 5.23 Plot of transmittance percentage of Eggshell HAp and its dopants of SBF solution

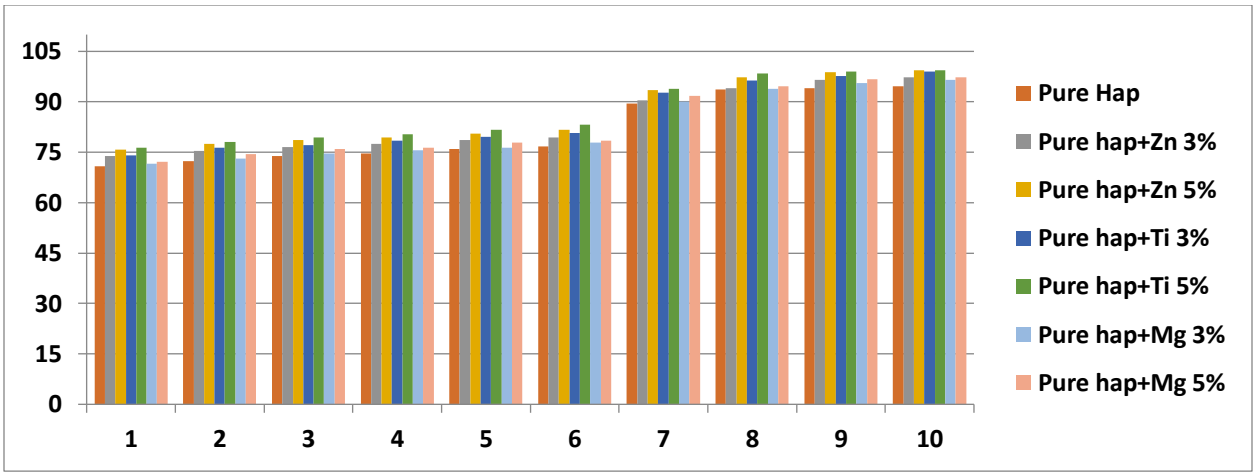

Figure 5.24 Plot of transmittance percentage of Pure HAp and its dopants of SBF solution

5.3.4 Haemolysis Study

As per the ASTM standards, a hemocompatibility test was done. An average OD was determined for each composition by analyzing five pellets (of three observations).

Table 5.14 Haemolysis observation data for Eggshell HAp and their dopants

Sl. No.	Composition	Wavelength (nm)	Avg. O.D. of Test sample	O.D. (+) ve control	O.D. (-) ve control	% Hemolysis
1	Eggshell HAp	545	0.067	0.47	0.059	1.98
2	Eggshell HAp + Zn 3%		0.071			2.90
3	Egg shell HAp + Ti 3%		0.072			3.17
4	Egg shell HAp + Mg 3%		0.074			3.68
5	Eggshell HAp + Zn 5%		0.069			2.49
6	Egg shell HAp + Ti 5%		0.068			2.19
7	Egg shell HAp + Mg 5%		0.073			3.42

Table5.15 Haemolysis observation data for Pure HAp and their dopants

Sl. No.	Composition	Wavelength (nm)	Avg. O.D. of Test sample	O.D. (+) ve control	O.D. (-) ve control	% Hemolysis
1	Pure HAp	545	0.071	0.46	0.061	2.50
2	Pure HAp + Zn 3%		0.074			3.25
3	Pure HAp + Ti 3%		0.072			2.75
4	Pure HAp + Mg 3%		0.078			4.26
5	Pure HAp + Zn 5%		0.075			3.50
6	Pure HAp+Ti 5%		0.073			3.00
7	Pure HAp+Mg 5%		0.075			3.50

Five such different data sets were prepared for five pellets and from there the average hemolysis data is presented in the following tables.

Table 5.16 Data for haemolysis analysis of Eggshell HAp and their dopants

Sl. No.	Composition	% Hemolysis
1	Eggshell HAp	1.98 ± 0.036
2	Eggshell HAp + Zn 3%	2.90 ± 0.030
3	Egg shell HAp + Ti 3%	3.17 ± 0.050
4	Egg shell HAp + Mg 3%	3.68 ± 0.040
5	Eggshell HAp + Zn 5%	2.49 ± 0.055
6	Egg shell HAp + Ti 5%	2.19 ± 0.041
7	Egg shell HAp + Mg 5%	3.42 ± 0.026

Table 5.17 Data for haemolysis analysis of Pure HAp and their dopants

Sl. No.	Composition	% Hemolysis
1	Pure HAp	2.82 ± 0.20
2	Pure HAp + Zn 3%	3.43 ± 0.34
3	Pure HAp + Ti 3%	2.97 ± 0.21
4	Pure HAp + Mg 3%	4.10 ± 0.43
5	Pure HAp + Zn 5%	3.50 ± 0.46
6	Pure HAp + Ti 5%	3.15 ± 0.20
7	Pure HAp + Mg 5%	3.74 ± 0.38

All the samples have a percentage of hemocompatibility less than 5%. So according to the ASTM guidelines, all samples are highly hemocompatible. Among the different compositions Pure HAp and Eggshell HAp have shown the maximum hemocompatibility. The 5% dopant variants show a better result than 3%variants due to the haemocomtable nature of the trace elements.

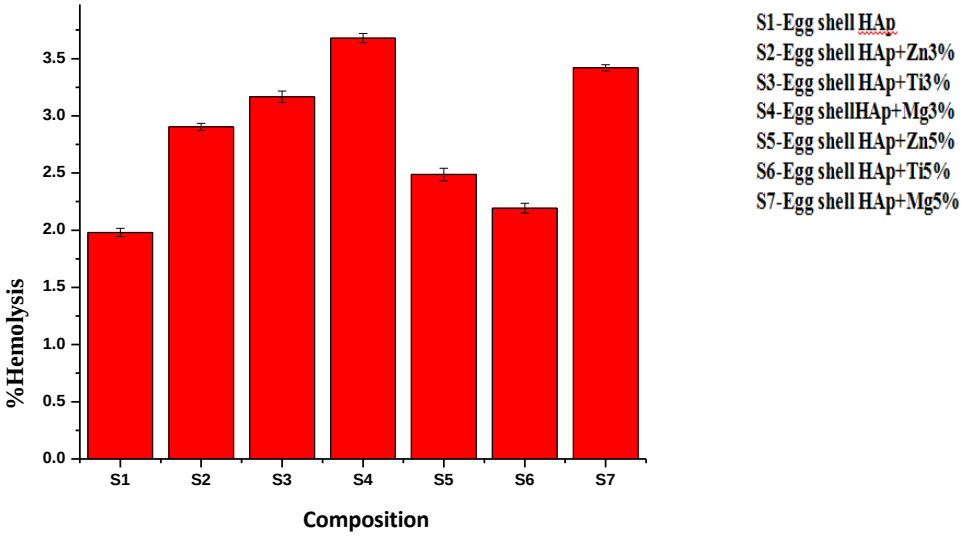

Fig:5.25 Bar diagram of % Hemolysis of eggshell HAp and their dopant

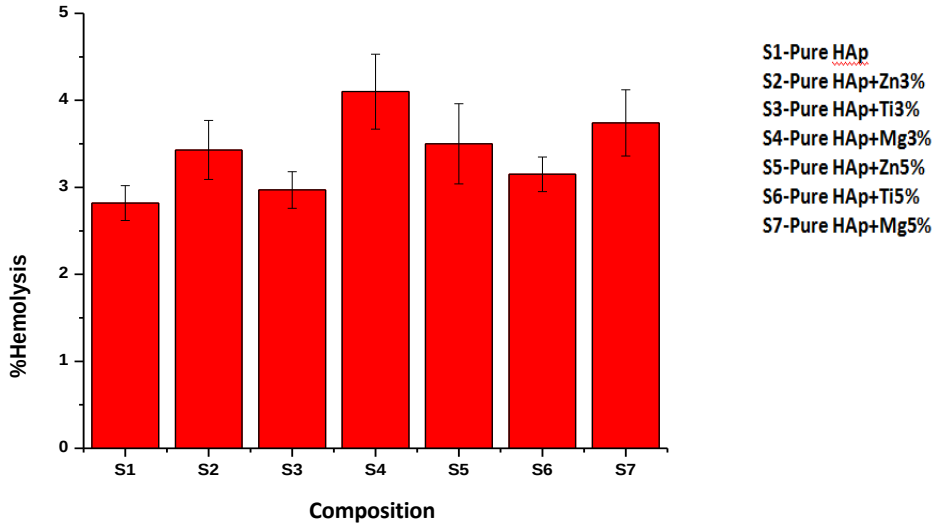

Fig: 5.26 Bar diagram of % hemolysis of Pure HAp and their dopants

5.3.5 MTT Assay

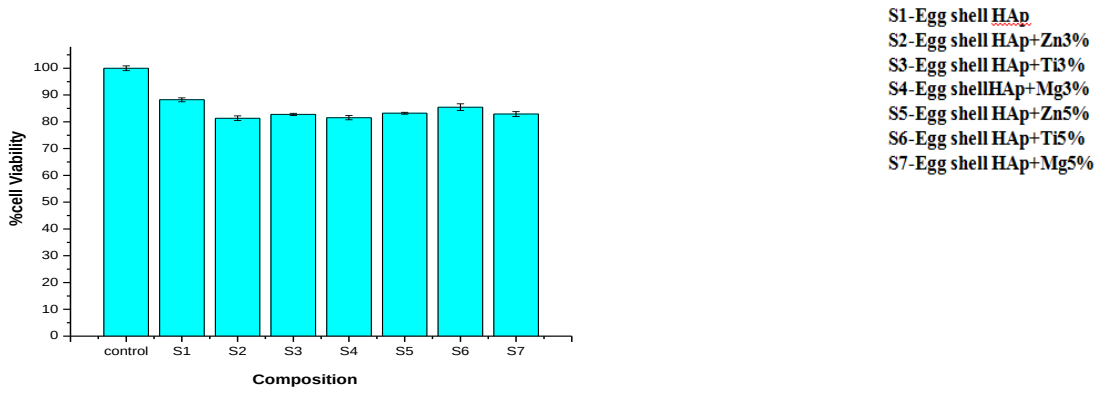

Figure 5.27: % cell viability of Eggshell HAp and their dopants as observed in MTT assay

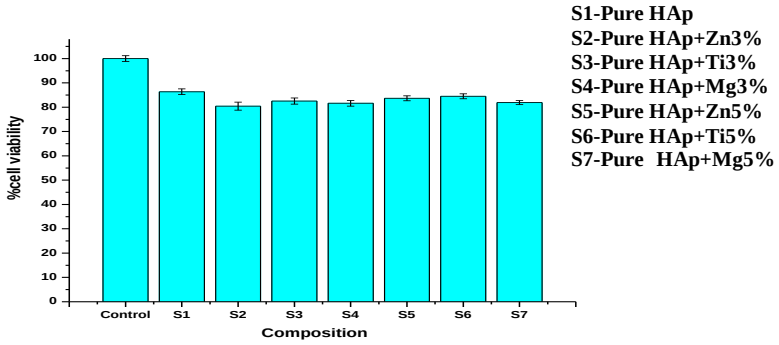

Figure 5.28: % cell viability of Pure HAp and their dopants as observed in MTT assay

The viability of all samples is greater than 80%. It can be concluded that all of the samples tested are non-cytotoxic.

5.3.6 Anti bactericidal Study

The antimicrobial activity of a material is determined by its ability to inhibit microbial growth. A photograph of the examined Petri dish can be found in Figure 29 and Figure 30.

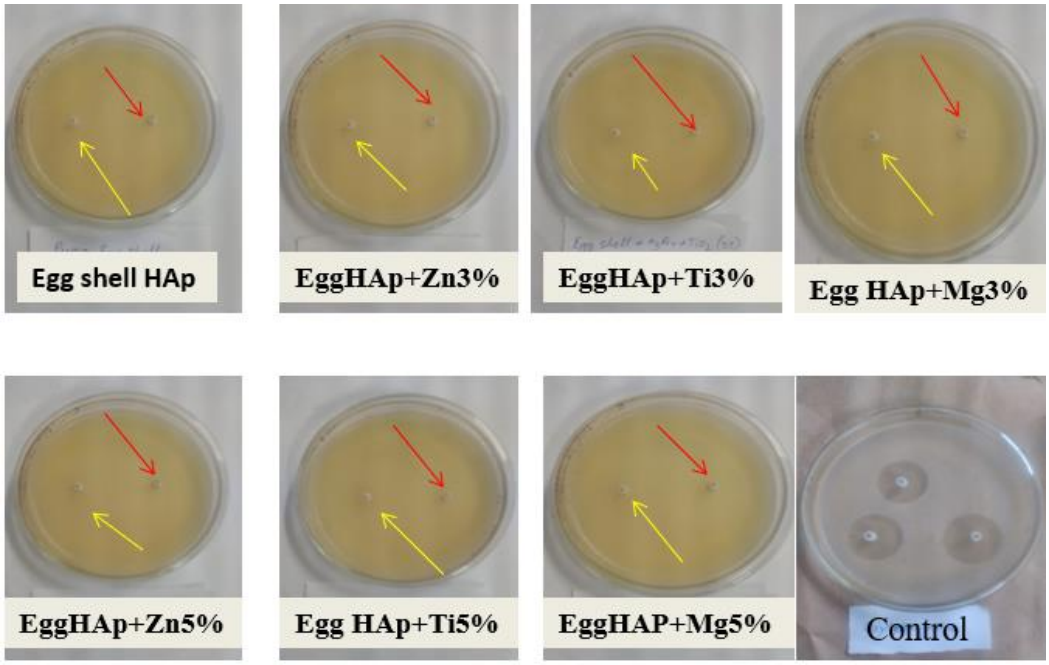

Red and yellow arrow indicate the porcelain bit of having 2mg/10 ml &1 mg/10ml of composition respectively

Fig.5.29: Petri dishes showing no zone of inhibition of Eggshell HAp and their dopants

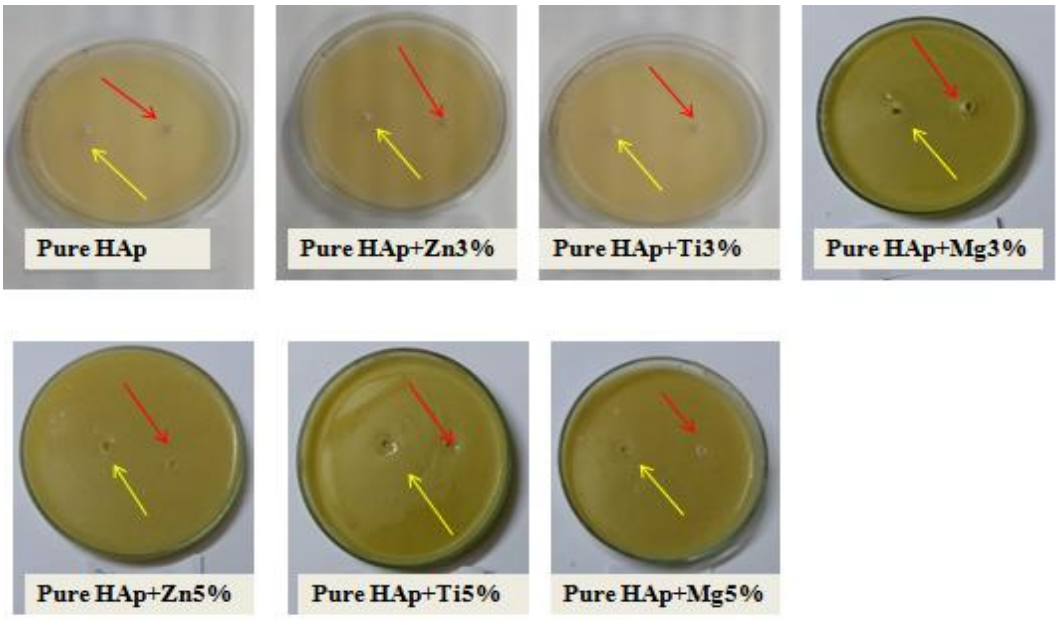

Fig 5.30: Petri dishes showing no zone of inhibition of Pure HAp and their dopants

In any Petri dish after 24 hours, neither concentration exhibited any inhibition zone. As a result, Pure HAp and Eggshell HAp and its dopants lack any bactericidal properties at these concentrations (1 mg/10 ml & 2 mg/10 ml). The control sample shows zone of inhibition abound the bits.

Major observations:

- ❖ On increasing the sintering temperature, porosity was decreased.
- ❖ All doped samples had more hardness value than pure samples.
- ❖ Uniform microstructure and interconnected pores were observed from SEM analysis.
- ❖ The presence of dopants was confirmed through E-DAX study.
- ❖ Apatite layer formation above the sintering pellets was confirmed through SBF study
- ❖ Greater amount of apatite layers was seen on titanium substituted samples.
- ❖ All the samples are hemocompatible.
- ❖ MTT assay and bactericidal study showed the nontoxic nature of all samples.

5.4 In-Vivo Analysis of Pure Hydroxyapatite and Eggshell Hydroxyapatite

A comparative analysis between the synthetic (Pure Hydroxyapatite) and biogenic (Eggshell) source-made hydroxyapatite has been done to observe the efficacy of the eggshell-used HAp pellets. A number of physical characterization studies had been done upon both Pure HAp, and Eggshell HAp and their 3% & 5% Zinc, titanium, and magnesium variants. In our study, we took 5% doped variants as this variant gave better physical properties (porosity, SBF analysis) than the 3% variant. The animal experimentation study was done by following the guidelines of the ethical committee and due to the restriction of using animal samples we have done only 5% zinc and titanium doped variants. We chose only zinc and titanium variants as these gave more apatites (reflected in figures 5.19 &5.20) compared to magnesium dopants.

For group I (control) defect was created, not placing any sample, and for group II (test), the created defective portion was placed with pure HAp, Eggshell HAp, and 5% zinc and titanium composite of both verities. The healing effect was studied at the starting day (0 days), the 30^{th} days post-operatively, and the 60^{th} days postoperatively.

5.4.1 Local Inflammatory Reactions and Wound Healing

In both group I and group II animals, no such inflammatory effects were observed 60 days after the sample pellets were implanted. No adverse side effects such as marked hematoma or oedema were seen. So the implants were clinically stable. The implant did not elicit a foreign body response or toxic response, thereby confirming its suitability as an alternative bone graft.

5.4.2 Radiological Observations

Group I (Control Study): On 0 days the radiograph exhibited a rectangular diaphyseal bone defect on the femoral condyle portion. The defect is still visible after a one-month interval with decreasing

the size of the defect. After two months the radiograph showed that the gap was reduced but not totally filled up.

Group II: Here Pure HAp, Eggshell HAp, Pure HAp with 5% zinc dopant, Pure HAp with 5% titanium dopant, Eggshell HAp with 5% zinc dopant, and Eggshell HAp with5% titanium dopant are implanted into the bony defect area.

At starting '0' days all the biomaterials are within the cortical line. Defect margins are seen to be regular without any radiographic bony damage during defect creation In all of the groups, there is a minimum and uniform amount of soft tissue reactions. The bony structures of the rest of the body are normal, and the joint spaces are normal as well.

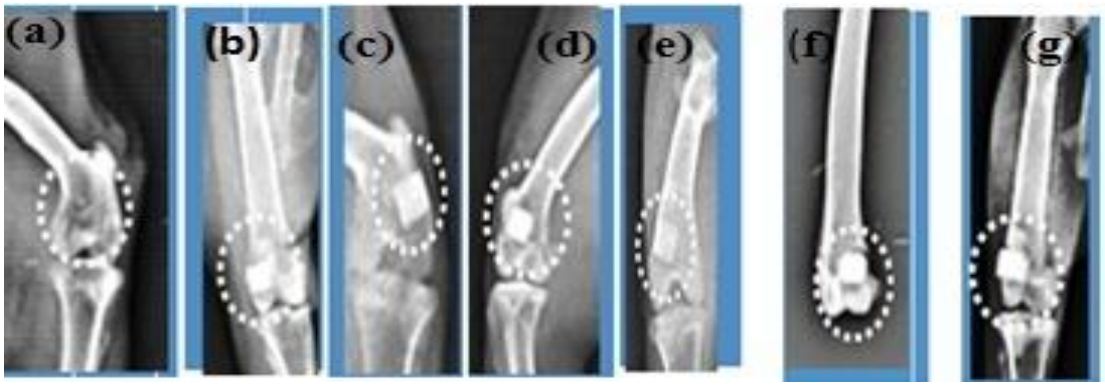

Figure 5.31: Radiographs of the '0' day (a) Control (b) Pure HAp (c) Eggshell HAp (d) Zn doped Pure HAp (e) Zn doped Egg shell HAp (f) Ti-doped Pure HAp (g) Ti-doped Egg Shell HAp

After 1 month interval, in the pure HAp group severe bone tissue reaction is radiographically visible. There is a slight degeneration of the rectangular implant in this group to a somewhat rounder one. Neither epiphyseal abnormalities metaphyseal abnormalities nor diaphyseal abnormalities were observed. In eggshell HAp, the implant is degraded to a greater extent. In Zn-doped pure HAp groups, the created defect is still evident but in Zn-doped eggshell HAp group, the defect is healed satisfactorily. In Zn-doped eggshell HAp, the size of the implantation is condensed as compared with 0 days reflecting partial degradation of the implant. It has been observed that the osteophytic changes are more pronounced in the Ti-doped pure HAp group and that the defects reflecting discontinuity of the cortical margin are more apparent. Isolated eggshell HAp with Ti-doped glass was shown to have rectangular implants, each with varying degrees of loss of marginalization at every border of the implant. It is evident that in this group, optimum healing has been achieved with no radiographic diaphyseal defect, along with the minimum amount of callus development. Osteophytic changes are visualized in all the groups.

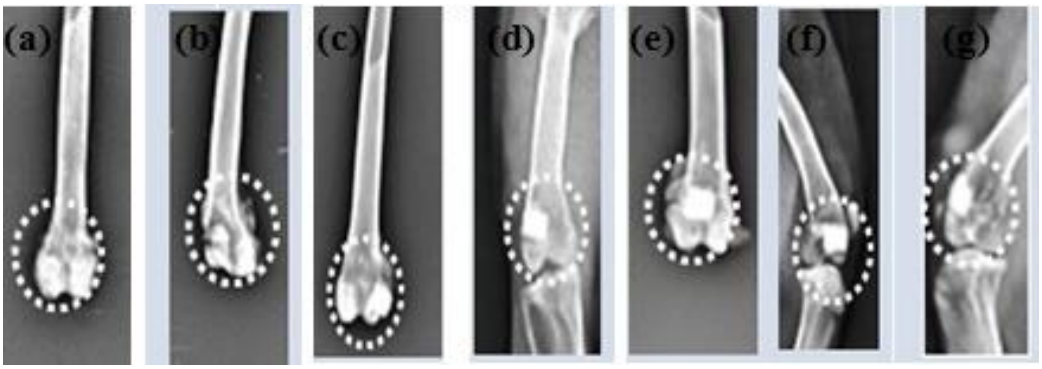

Figure 5.32: Radiographs of the '30' day (a) Control (b) Pure HAp (c) Eggshell HAp (d) Zn doped Pure HAp (e) Zn doped Egg shell HAp (f) Ti-doped Pure HAp (g) Ti-doped Egg Shell HAp

After a 2-month interval, in Pure HAp and Eggshell HAp groups, the cortical discontinuity is radiographically evident even for 2 months along with the visible implant. But in, Zn doped Egg shell HAp, the bony defect is healed completely along with further degradation of implanted materials. In this group, there is no gap between host tissue and bone itself. The implant-bone interface is not clearly evident indicating good acceptance of the implant material by bone tissue. In Ti-doped Pure HAp, still implant is still visible along with continued host-implant interface reaction. The created bone defect is also visible in this group. It has been observed that the implant is nearly degraded with the establishment of cortical continuity with Ti-doped Egg shell HAp. In radiographic examination, there were no obvious defects to be observed. It appears that the bone density of this group, as compared with the day 1 group, is normal. The uptake of implants by the bone tissue in this group is satisfactory.

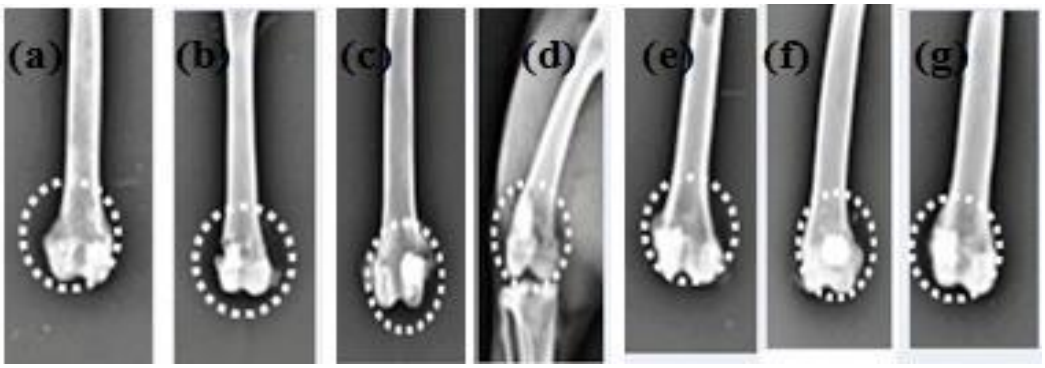

Figure 5.33: Radiographs of the '60' day (a) Control (b) Pure HAp (c) Eggshell HAp (d) Zn doped Pure HAp (e) Zn doped Egg shell HAp (f) Ti-doped Pure HAp (g) Ti-doped Egg Shell HAp

5.4.3 Histological study

Group I (Control): It was evident from the histological section that was stained with hematoxylin and eosin (H&E) at 1 month that the control sample had inadequate haversian canals, with fewer sinusoidal spaces and less osteoblast proliferation than the experimental sample. At the 2-month time point, control sections showed a greater number of haversian canals with the presence of osteoblast. The medullary cavity had few RBCs with mononuclear cells. It contained less amount of fibrin and osteocytes. Angiogenesis invasion was normal.

Group II: The histological images of the Pure HAp after a one-month interval showed that there were few or no haversian canals, with moderate amounts of red blood cells (RBCs), mononuclear cells, osteoblasts, and fibrinous threads present. On the other hand, Eggshell HAp sections showed a higher number of haversian canals as well as more mononuclear cells, RBCs, and scanty osteocytes. HAp section of the Ti-doped Eggshell at the same time point revealed a large Haversian canal located centrally that contained angiogenic vessels, mononuclear cells, osteoblasts, and a small number of osteocytes. In the Zn-doped HAp and Eggshell samples, there were proliferating osteocytes, mononuclear cells, abundant RBCs, and fibrinous cells in the medullary cavity, which showed that the healing process had started, as evidenced by the presence of proliferating osteoblasts.

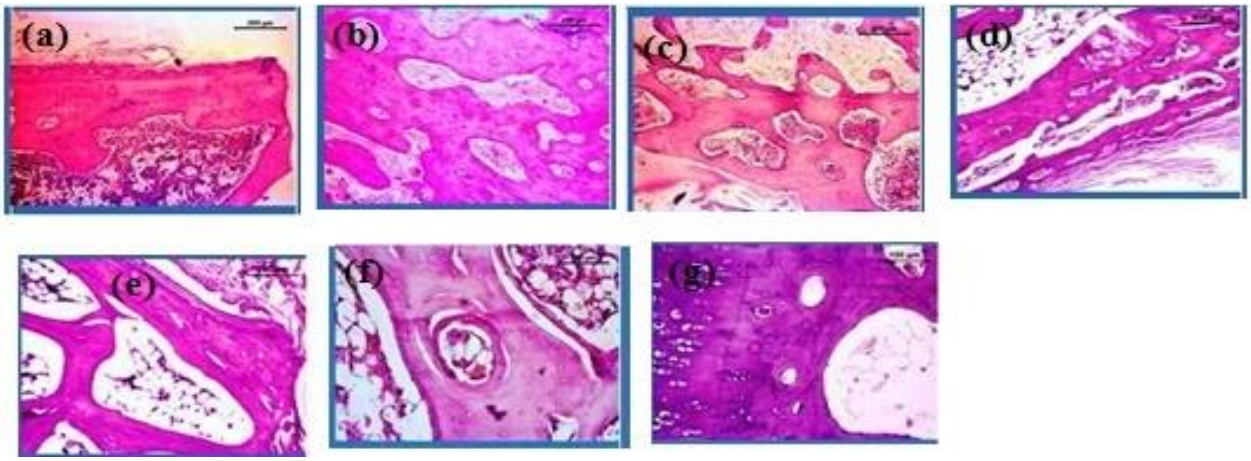

Figure 5.34: Histological section of the bone of control & Gr. II animal after 1 M: (a) Control (b) Pure HAp (c) Eggshell HAp (d) Zn doped Pure HAp (e) Zn doped Egg shell HAp (f) Ti-doped Pure HAp (g) Ti-doped Egg Shell HAp

Compared to control sections, control sections showed a greater number of Haversian canals with osteoblasts present at the 2-month time point. Pure HAp sections were found to have larger haversian canals with a higher number of osteoblasts and few osteoclasts, while the sections that had Pure HAp sections had smaller haversian canals. It was found that both Eggshell HAp and Ti-doped Pure HAp sections had abundant haversian canals with the presence of osteoblasts, and osteoclasts, and with a reasonable amount of angiogenesis. HAp microphotographs of Ti-doped Eggshells revealed abundant osteoblasts, osteoclasts with Haversian canals, and signs of angiogenesis as a result of the Doped Eggshells. In Zn-doped Pure HAp sections, the bony structure consisted of Haversian canals, sinusoidal spaces, abundant mononuclear cells, and osteoblasts. The Zn-doped Egg shell HAp showed the presence of abundant osteoblast and osteoclast cells.

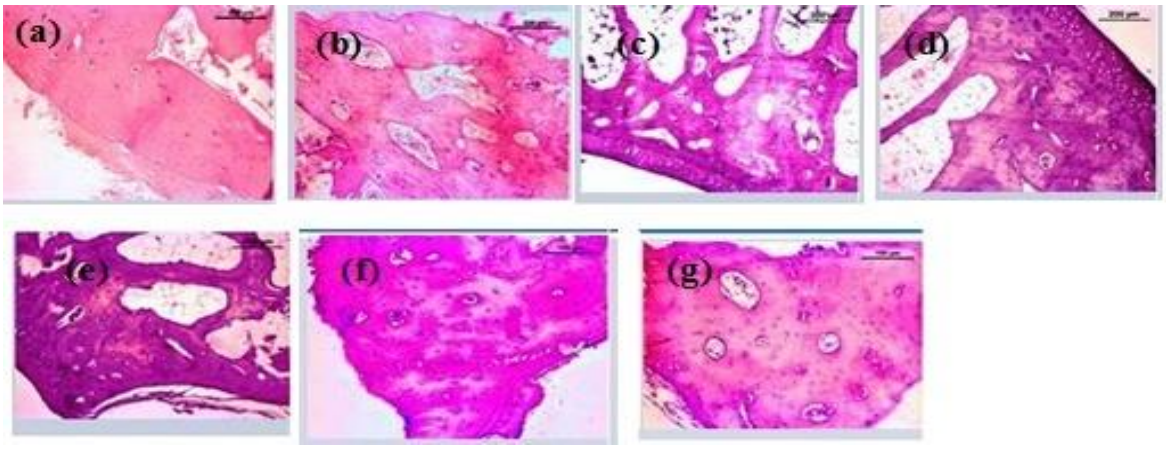

Figure 5.35: Histological section of the bone of control & Gr. II animal after 2 M: (a) Control (b) Pure HAp (c) Eggshell HAp (d) Zn doped Pure HAp (e) Zn doped Egg shell HAp (f) Ti-doped Pure HAp (g) Ti-doped Egg Shell HAp

5.4.4 Oxytetracycline Labelling Study

A characteristic bright gold-yellow fluorescence was observed in oxytetracycline-labeled new bone, while sea green fluorescence was observed in the host bone. In each group, the implanted bone specimens were harvested at 1 and 2 months. The pictures of both specimens are given in below Figure 36.

Group I (Control): The control sample showed a slight bone development (15.50 x 1.88 mm) at 1 month, and by 2 months, the value jumped up to 26.47 x 1.9 mm.

Group II: It was observed that the image of the control group at one month demonstrated a small amount of minute golden yellow fluorescence in the central part (15.50 x 1.88%) of the image against a backdrop of green deep sea colour. There was a very small area of yellow fluorescence in the pure HAp image that could be seen in the central area, which appeared to indicate to some extent a newer bone formation (21.41 ± 2.10%). In the Eggshell HAp image, there is a compressible area of golden yellow fluorescence which represents superior new osseous tissue formation (25.60 ± 1.9%) whereas, in the Zn-doped Eggshell HAp image, there is a greater amount of new bone formation (36.35% ± 1.8%) 10%. The amount and intensity of bright golden yellow fluorescence colour were observed to be substantially higher in Ti-doped pure HAp samples compared to Ti-doped eggshell HAp samples, respectively (33.69 ± 2.06%) and (37.50 ± 2.17%) in the background by sea green colored host tissue at the same time point.

At 2 months, all groups displayed significant improvements in new bone formation compared with the previous time point. Compared to the control sample, the 2-month image of the control sample showed more golden yellow fluorescence of newly formed osseous tissue (26.47 ± 1.98%). Compared to their base value, the golden yellow fluorescence observed in the central zone (31.47

± 1.86%) in the pure HAp group at this time point demonstrated improved bone formation when compared to the base group. Eggshell HAp image showed fluorescence of newly formed osseous tissue (43.30 X 0.84%) in more areas, indicating active bone regeneration. This study reported the presence of golden yellow fluorescence in the Ti-doped Pure HAp bone section, indicating that the section was showing much more osseous activity than the other sections (54.41 ± 1.93 %). Zn-doped Egg shell HAp displays more intense golden yellow fluorescence around new osseous tissue formation (58.52 ± 2.06%) compared to Zn-doped Pure HAp samples. It was evident that abundant plaques of golden yellow appeared in Ti-doped Egg shell HAp samples with a deep green sea-coloured host tissue (59.31 ± 1.89%).

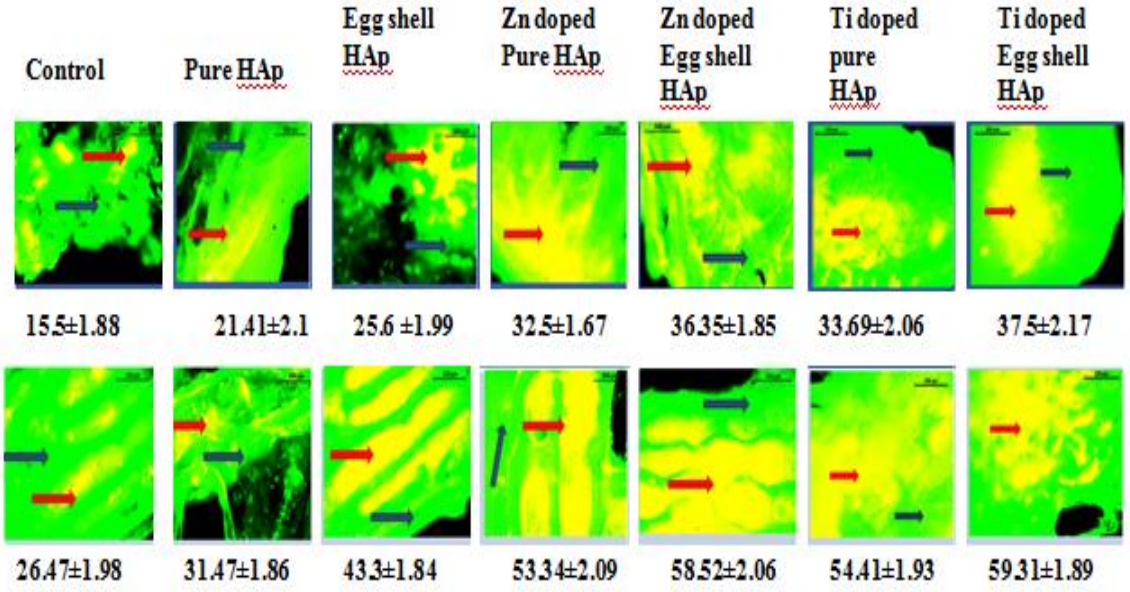

Figure 5.36: Oxytetracycline labeling study at the defected site of Control, Group II animals after 1 and 2 months of installation. The yellow portions depict new bone formation

Table 5.18: Oxytetracycline labeling study result of % new bone formation in 1 & 2 months

Sl. No.	Composition	1 month	SD (±)	2 months	SD (±)
1	Control	15.5	1.88	26.47	1.98
2	Pure HAp	21.41	2.1	31.47	1.86
3	Egg shell HAp	25.6	1.99	43.3	1.84
4	Zn doped Pure HAp	32.5	1.67	53.34	2.09
5	Zn doped Egg shell HAp	36.35	1.85	58.52	2.06
6	Ti- doped Pure HAp	33.69	2.06	54.41	1.93
7	Ti-doped Egg Shell HAp	37.5	2.17	59.31	1.89

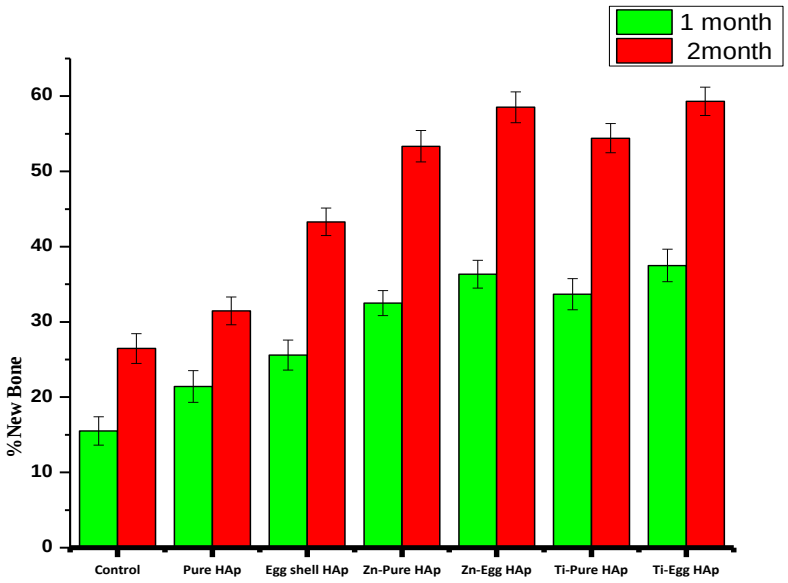

Figure 5.37: Bar diagram showing % new bone formation in 1 and 2 Months

5.4.5 SEM Images of Bone Implant Interface Study

The SEM images of control and Group II animals' bone-implant-interfaces (BII) of Pure HAp, Eggshell HAp, Pure HAp with 5% zinc dopant, pure HAp with5% titanium dopant, Eggshell HAp with 5% zinc dopant, Eggshell HAp with 5% titanium dopant ceramics have been analyzed using SEM, images are displayed in Figure 38.

Control: The SEM images of the defect site show that the gap is quite visible in 1 month and after 2 months, a minor portion has been covered.

Group II: After 1 month of implantation, the Pure HAp and Eggshell HAp samples showed some irregular bone tissue arrangement. The samples exhibit binding abilities to the old bone with the implant. The bridging gap was found less in 5% Zn-doped and 5% Ti-doped varieties in comparison to pure samples. At the end of 2-month intervals, Ti-doped Egg shell HAp and Zn-doped Egg shell HAp implants showed firmly bonded to the host tissue with the filling of the entire gap.

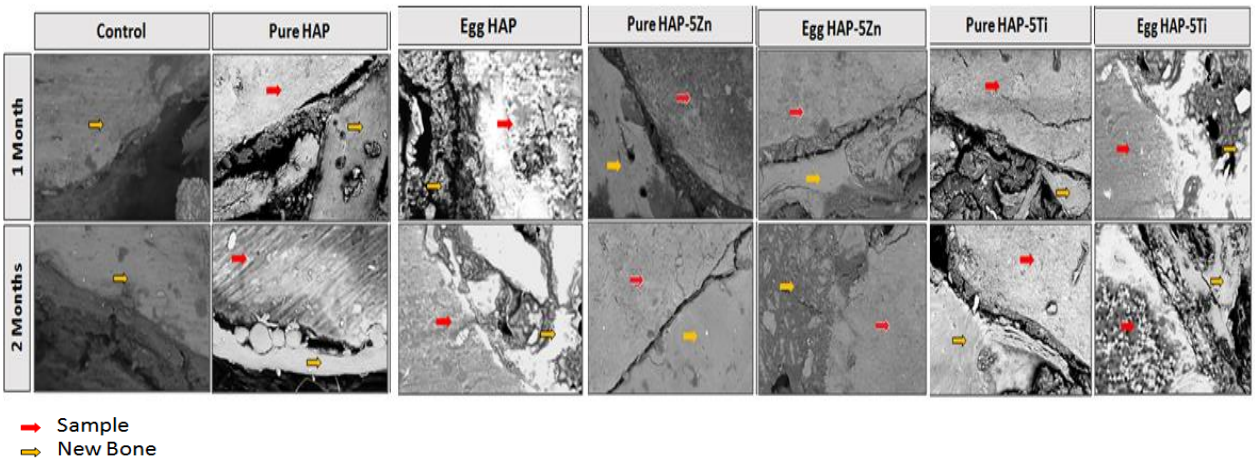

Figure 5.38: SEM images of all groups of bone-implant interface after 1 month & 2 months (Scale bar =100µm)

Major Observations:

- ❖ No inflammatory reactions were seen on the implanted materials. All the materials were clinically stable to the bone.
- ❖ Radiological studies revealed faster healing in HAp and its doped variants compared to control samples.
- ❖ Histological studies showed a very prompt and better proliferation of images in group II animals.
- ❖ The bonding of implants to the host bone was better in doped variants compared to the control one.
- ❖ An oxytetracycline labelling study showed that eggshell-doped varieties formed more new bones than pure eggs.
- ❖ In group II animals Ti doped Egg shell HAp samples exhibited a higher percentage of bone formation.

In our experiment, it was found that eggshell-substituted implant materials rendered better results. The same findings were concluded in the work [1], where eggshell powder was used to cap pulp directly to improve biological responses. In another study [2], a gelatin methacrylate-eggshell-derived calcium phosphate composite scaffold was found to be bioactive, biocompatible, and biodegradable. Kattimani et al. [3] produced nano-hydroxyapatite by using a waste eggshell and noticed a trabecular bone pattern with increased bone density in the mandibular zone. In order to improve the efficacy of synthetically prepared hydroxyapatite i.e. enhancing the mechanical characteristics and bioactivity different dopant ions are added [4]. In our study, 5% Zn doped and 5%Ti doped samples of both varieties were prepared. An in vivo study was done by implanting the scaffold materials on a rabbit's femoral condyle junction. Radiographic studies show that in Zn-doped Egg shell HAp and Ti-doped Egg shell HAp, the bony defect healed completely. It has

been found that the femoral-diaphyseal tissues with fracture healing produce a large number of proteins, such as TGF-β1, osteocalcin, albumin, and other proteins [5]. Zinc increases the production of these proteins, which are essential for fracture bone repair. As fracture healing occurs, zinc stimulates DNA synthesis in the femoral-diaphyseal tissues. The mineral zinc stimulates osteoblastic bone formation in fracture healing by stimulating mineralization in bone tissues. Murine osteoblastic cell viability and proliferation rate are increased in zinc-doped eggshell HAp. Zinc is present on the calcification site i.e. osteons calcified cartilages increase bone mineralization as alkaline phosphatase co-factor [6]. In addition to providing inorganic phosphate from pyrophosphates and phosphomonoesters, it hydrolyses pyrophosphate (mineralization inhibitor) for the synthesis of hydroxyapatite [7]. It was found that % of bone formation in Zn-doped Egg shell HAp was 58.52 ± 2.06 whereas in Zn-doped Pure HAp it was 53.34 ± 2.09.

Titanium is used as a dopant as it exhibits a strong affinity to biological substances [8]. Several literatures showed that the application of titanium and HAp/Titania thin film improved the mechanical properties and is a choice of material in bone injury and implant fixation [9-11]. Titanium is not only used as an implant material, but is also used as an ossification inducer in dental surgery and prostheses to enhance corrosion resistance, low elastic modulus, and mechanical properties, as well as overall biocompatibility [12-15]. Again, other studies showed that titanium-induced bioactive glass exhibited an enhanced osteoblastic proliferation rate in calvarial defect sites in rabbits [16]. Fernandes et al. [17] studied that TiO_2 nanoparticles were added to dense bovine hydroxyapatite and were found to improve osteoblast mineralization activity in humans. Moreover, TiO_2 /HAp coatings may be bioactive due to the presence of hydroxyl groups on their surface, which promote calcium and phosphate precipitation and improve osteoblastic cell interactions [18].

REFERENCES

[1] Salah, M.; Kataia, M. M.; Kataia, E. M.; El Din, E. A.; Essa, M. E., Evaluation of Eggshell Powder as an Experimental Direct Pulp Capping Material. Futur. Dent. J.2018, 4 (2), 160–164. https://doi.org/10.1016/j.fdj.2018.05.008.

[2] Ahmed, J. M.; Hamad, S. A., In Vitro and In Vivo Evaluation of Osteoconductive Properties of Novel GelMa/Eggshell-Derived Calcium Phosphate Composite Scaffold. Eur. J. Mol. Clin. Med. 2020, 7 (2), 1–19.

[3] Kattimani, V.; Lingamaneni, K. P.; Yalamanchili, S.; Mupparapu, M. Use of Eggshell-Derived Nano-Hydroxyapatite as Novel Bone Graft Substitute - A Randomized Controlled Clinical Study. J. Biomater. Appl.2019, 34 (4), 597–614. https://doi.org/10.1177/0885328219863311

[4] Bhattacharjee, P.; Begam, H.; Chanda, A.; Nandi, S. K., Animal Trial on Zinc Doped Hydroxyapatite: A Case Study. J. Asian Ceram. Soc.2014, 2 (1), 44–51. https://doi.org/10.1016/j.jascer.2014.01.005.

[5] Igarashi A, Yamaguchi M., Increase in bone protein components with healing rat fractures: Enhancement by zinc treatment. Int J Mol Med 4:615-620, 1999.

[6] Igarashi A, Yamaguchi M, Increase in bone growth factors with healing rat fractures: The enhancing effect of zinc. Int J Mol Med 8: 433-438, 2001.

[7] Starcher, B.; Kratzer, F.H., Effect of Zinc on Bone Alkaline Phosphatase in Turkey Poults. J. Nutr. 1963, 79, 18–22, doi:10.1093/jn/79.1.18.

[8] Tsuruoka, A.; Isobe, T.; Matsushita, S.; Wakamura, M.; Nakajima, A., Comparison of Photocatalytic Activity and Surface Friction Force Variation on Ti-Doped Hydroxyapatite and Anatase under UV Illumination. J. Photochem. Photobiol. A Chem.2015, 311, 160–165. https://doi.org/10.1016/j.jphotochem.2015.07.001.

[9] Anushika; Sharma, P.; Trivedi, A.; Begam, H., Synthesis and Characterization of Pure and Titania Doped Hydroxyapatite. Mater. Today Proc. 2019, 16, 302–307. https://doi.org/10.1016/j.matpr.2019.05.094.

[10] Aufa, A. N.; Hassan, M. Z.; Ismail, Z.; Harun, N.; Ren, J.; Sadali, M. F., Surface Enhancement of Ti-6Al-4V Fabricated by Selective Laser Melting on Bone-like Apatite Formation. J. Mater. Res. Technol. 2022, 19, 4018–4030. https://doi.org/10.1016/j.jmrt.2022.06.135.

[11] Yao Ding, Bailong Tao, Ruichen Ma, Xin Zhao, Peng Liu, K. C., Surface Modification of Titanium Implant for Repairing/Improving Microenvironment of Bone Injury and Promoting Osseointegration, Journal of Materials Science & Technology. Journal of Materials Science & Technology, 2022. https://doi.org/https://doi.org/10.1016/j.jmst.2022.09.044.

[12] Geetha, M.; Singh, A. K.; Asokamani, R.; Gogia, A. K. Ti Based Biomaterials, the Ultimate Choice for Orthopaedic Implants - A Review. Prog. Mater. Sci.2009, 54 (3), 397–425. https://doi.org/10.1016/j.pmatsci.2008.06.004.

[13] Mahyudin, F.; Hermawan, H., Biomaterials and Medical Devices. Adv. Struct. Mater.2016, 161–181. https://doi.org/10.1007/978-3-319-14845-8.

[14] Pal, S., Design of Artificial Human Joints & Organs. Des. Artif. Hum. Joints Organs 2014, 9781461462, 1-419. https://doi.org/10.1007/978-1-4614-6255-2.

[15] Meng, E.; Sheybani, R., Insight: Implantable Medical Devices. Lab Chip2014, 14 (17), 3233-3240. https://doi.org/10.1039/c4lc00127c.

[16] Lee, J. E.; Bark, C. W.; Van Quy, H.; Seo, S. J.; Lim, J. H.; Kang, S. A.; Lee, Y.; Lee, J. M.; Suh, J. Y.; Kim, Y. G., Effects of Enhanced Hydrophilic Titanium Dioxide-Coated Hydroxyapatite on Bone Regeneration in Rabbit Calvarial Defects. Int. J. Mol. Sci.2018, 19 (11), 1-13. https://doi.org/10.3390/ijms19113640.

[17] Fernandes, P. H. M.; Bordini, E. A. F.; Cassiano, F. B.; de Azevedo-Silva, L. J.; Ferrairo, B. M.; Lisboa-Filho, P. N.; Fortulan, C. A.; Soares Dos Passos, D. G.; Borges, A. F. S., TiO_2 Nanoparticles Added to Dense Bovine Hydroxyapatite Bioceramics Increase Human Osteoblast Mineralization Activity. Dent. Mater. 2022, 38 (11), e275-e283. https://doi.org/10.1016/j.dental.2022.08.007.

[18] Ramires, P. A.; Romito, A.; Cosentino, F.; Milella, E., The Influence of Titania / Hydroxyapatite Composite Coatings on in Vitro Osteoblasts Behaviour. Biomaterials 2001, 22 (12), 1467–1474. https://doi.org/10.1016/S0142-9612(00)00269-6.

6. CONCLUSION & FUTURE SCOPE

Conclusion

In this present study waste eggshells collected from different household kitchens have been successfully converted to hydroxyapatite. Doped variants (3% and 5%) of zinc, titanium, and magnesium hydroxyapatite from both eggshell (Eggshell HAp) and laboratory sources (Pure HAp) were successfully prepared through the wet precipitation method. During preparation, care must be taken regarding different parameters. The collected eggshell samples were washed repeatedly in boiled water to clear up the mud and debris sticking to them. The dried shell was calcined at 800^0C for about two hours at the heating rate of 5^0C/min. The calcined eggshell was formed into calcium oxide which upon thorough mixing with water and treated with 0.6 (M) orthophosphoric acid produced hydroxyapatite. The pH of the solution was maintained at 10 and the mixing was done at about 80^0C. The formed hydroxyapatite was calcined at 800^0C temperature to get the crystalline sample. The peaks at (0 0 2), (2 1 1), (3 0 0), (2 0 2), (2 1 2), (2 2 2), and (2 1 3) planes were got from XRD study clearly signifies the presence of hydroxyapatite phase and were tallied with the standard JCPD card (09-0432) of hydroxyapatite. In doped variants, the peaks were slightly shifted due to the doping effect. The lattice parameter study showed that on doping with Zn, Ti, and Mg ions, the unit cell value and the percentage of crystallinity were decreased. This might be attributed to smaller atomic radii of the dopants e.g. zinc (134 pm), magnesium (160 pm), and titanium (147 pm) in comparison with calcium (197 pm). The FTIR plot showed the presence of functional groups. At 570 and 1023 the peak signified the presence of phosphate ion whereas at 3752, a stretching band of hydroxyl ion was present. The green density was measured of Eggshell HAp (1.546 gm/cc), Pure HAp (1.53gm/cc), 3% zinc doped pure HAp (1.6 gm/cc), 3% zinc doped Egg shell HAp (1.602 gm/cc), 5% zinc doped Pure HAp (1.644 gm/cc), 5% zinc doped Egg shell HAp (1.628 gm/cc), 3% magnesium doped Pure HAp (1.462 gm/cc), 3% magnesium doped Egg shell HAp (1.504 gm/cc), 5% magnesium doped Pure HAp (1.494 gm/cc), 5% magnesium doped Egg shell HAp (1.526 gm/cc), 3% titanium doped Pure HAp (1.564 gm/cc), 3% titanium doped Egg shell HAp (1.562 gm/cc), 5% titanium doped Pure HAp (1.602 gm/cc), 5% titanium doped Egg shell HAp (1.596 gm/cc). It was noted that the green density values of various composition samples were not significantly changed. A similar kind of bulk volume was noticed. Enhancing the sintering temperature of all the samples from 950^0C to 1050^0C minor changes were noticed. The 5% zinc-doped Pure HAp and 5% zinc-doped Eggshell HAp showed the maximum density at 1050^0C. The magnesium-doped samples showed a lower density whereas titanium-doped samples showed a moderate value. Porosity, a crucial parameter in scaffold synthesis, plays a vital role in bone-tissue implant fixation. Porosity with greater than 150 µm would be beneficial for bone-tissue implant material. The apparent porosity of the prepared pellets was measured through Archimedes principle method and grain size-pore size values were measured by screen ruler software technique. It was noted that a good amount of porosity (>150 µm) was present in all compositions which could promote anchorage of bone cells and bony in-growth. Porosity was

greatly reduced with the increase in temperature. The concentration variation of dopants did not alter any kind of significant changes in grain size, porosity, and crystal structure. The SEM images of all the sintered scaffold samples clearly denoted the presence of nodular-shaped pores and the E-DAX results provided the presence of calcium, phosphorus, oxygen, zinc, magnesium, and titanium ions. Hardness values getting through the Vickers hardness tester instrument provided that the prepared scaffolds were hard enough to withhold the body pressure after implantation. The prepared scaffolds' hardness values were greater than 3.64 GPa. The 5% Zn-doped Pure HAp and 5% Zn-doped Eggshell HAp showed maximum hardness values of 3.86 and 3.97 GPa. It might be due to the higher densification of the ceramic by zinc than other ions in the compositions. The hardness of all doped compositions was higher than pure values. Different biological tests were performed to check the efficacy of the materials. Apatite layer formation was noticed above the pellet surfaces through simulated body fluid (SBF) studies. It was observed that apatite layer formation was started after seven days of immersion. 5% titanium and 5% zinc doped Eggshell HAp were better than other varieties as they gave maximum apatite layer formation. The pellets were degraded in SBF solution after immersion and lost their weight. The weight degradation study showed that the rate of degradation is faster till the 12-15 days, after that the rate becomes slower probably because of apatite layer formation above the pellets. The percentage transmission in the SBF solution was gradually changing up to 12-15 days. After that the change was stable. Another biological test i.e. hemolysis study was done by using human blood. It was observed that all the prepared samples exhibited a percentage of hemolysis less than 5. So, according to the ASTM guidelines the prepared samples were hemocompatible. The Pure HAp and Eggshell HAp showed maximum hemocompatibility. Murine osteoblastic cell study in MTT assay method showed that after 24 hours of incubation period, more than 80% of cells were viable in all the samples. It may predict that the samples were cytocompatibility. Antimicrobial studies were done by using 1 mg/10 ml and 2 mg/10 ml of all the samples in nutrient agar media through bacteria culture addition and incubation at 24 hours. The study showed no zone of inhibition in all the samples. So it was concluded the materials were not bactericidal. In line with the results, a comparative assessment of 5% zinc and 5% titanium of both sourced samples was done in vivo and observed the differences in their impact on living body. The animal studies were conducted in two groups, Group I (control) and Group II (test). In Group I, no samples were implanted whereas for Group II the porous scaffold samples were implanted aseptically in the created defect bone area. The healing effect was evaluated for all the samples after one-month and two-month intervals. No local inflammatory reaction was seen after sixty days postoperatively for all groups of animals. The radiographic study in the control group revealed minor healing at the end of one month and after two-month the gap was reduced but not totally filled up. For the test group after one month, it was found that the Pure HAp implant was degraded to a nearly roundish shape, Egg shell HAp implant degraded to a greater extent and Zn doped Egg shell HAp the defect was healed satisfactorily. In Ti-doped Egg shell HAp, optimum healing was achieved with no radiographic diaphyseal defect along with a minimum amount of callus. After a two-month duration, cortical discontinuity was radio-

graphically evident in Pure HAp and Eggshell HAp, the bony defect was healed completely in Zn doped Egg shell HAp, whereas bone defect was still visible in Ti doped Pure HAp. In Ti-doped Egg shell HAp, the implant was nearly degraded with the establishment of cortical continuity. In a histological study, after a month interval, Pure HAp images showed very few or fewer haversian canals with the presence of moderate red blood cells (RBCs), mononuclear cells, osteoblasts, and some fibrinous threads whereas the shell HAp sample depicted more haversian canals along with RBCs, mononuclear cells, and scanty osteocytes. Ti-doped Eggshell HAp showed centrally a big haversian canal containing angiogenic vessels and mononuclear cells, osteoblasts, and a small amount of osteocytes, and the Zn-doped HAp samples showed the presence of proliferating osteocytes and abundant RBCs mononuclear cells, and fibrinous cells in the medullary cavity indicated that the healing process was started. After a two-month interval, Ti-doped Egg shell HAp microphotograph showed abundant osteoblasts, osteoclasts with haversian canals and angiogenesis and Zn-doped Egg shell HAp showed the presence of abundant osteoblast and osteoclasts cells. In the oxytetracycline labeling study it was noted after a two-month interval that the control sample contained 26.47 ± 1.98% newly formed osseous tissues, Pure HAp contained 31.47 ± 1.86%, Eggshell HAp had 43.30 ± 1.84%, Ti-doped Pure HAp had 54.41 ± 1.93 %, Zn-doped Egg shell HAp had 58.52 ± 2.06%, Ti-doped Egg shell HAp had 59.31 ± 1.89% new osseous tissue. It was concluded that 5% of doped varieties of Eggshell HAp exhibited faster healing rate (radiography study), more amount of osteoblasts, osteoclasts with haversian canal (histological analysis), more percentage of new bone formation (oxytetracycline labeling study).

Scope of the future work:

- Calcined eggshell powder may be chosen instead of synthetic calcium source powder.
- Alternative bone substitutes may be taken into consideration.
- The time span of the application can be altered.
- In-vivo studies in another model can be tried.
- Clinical study can be done if the ethical committee permits.

Report

ORIGINALITY REPORT

10%
SIMILARITY INDEX

PRIMARY SOURCES

1	mswebs.naist.jp Internet	179 words — 1%
2	Sujan Krishna Samanta, Abhijit Chanda. "Study on the Structure and Properties of Crystalline Pure and Doped β-Tri Calcium Phosphate Ceramics", Materials Today: Proceedings, 2018 Crossref	88 words — < 1%
3	louisdl.louislibraries.org Internet	86 words — < 1%
4	dokumen.pub Internet	54 words — < 1%
5	link.springer.com Internet	50 words — < 1%
6	www.researchgate.net Internet	40 words — < 1%
7	www.scribd.com Internet	37 words — < 1%
8	dr.ntu.edu.sg Internet	35 words — < 1%

9	Md Lawshan Habib, Sanjana Afrin Disha, Md Sahadat Hossain, Md Najem Uddin, Samina Ahmed. "Enhancement of antimicrobial properties by metals doping in nano-crystalline hydroxyapatite for efficient biomedical applications", Heliyon, 2023 Crossref	34 words — < 1%
10	Anushika, Prakhar Sharma, Alok Trivedi, Howa Begam. "Synthesis and characterization of pure and titania doped hydroxyapatite", Materials Today: Proceedings, 2019 Crossref	33 words — < 1%
11	www.mdpi.com Internet	31 words — < 1%
12	docplayer.net Internet	30 words — < 1%
13	people.eng.unimelb.edu.au Internet	30 words — < 1%
14	Marjan Safarzadeh, S. Ramesh, C.Y. Tan, Hari Chandran, Ahmad Fauzi Mohd Noor, S. Krishnasamy, U. Johnson Alengaram, S. Ramesh. "Effect of multi-ions doping on the properties of carbonated hydroxyapatite bioceramic", Ceramics International, 2018 Crossref	28 words — < 1%
15	eprints.usm.my Internet	26 words — < 1%
16	Sujan Krishna Samanta, K. Bavya Devi, Piyali Das, Prasenjit Mukherjee, Abhijit Chanda, Mangal Roy, Samit Kumar Nandi. "Metallic ion doped tri-calcium phosphate ceramics: Effect of dynamic loading on in vivo bone	25 words — < 1%

regeneration", Journal of the Mechanical Behavior of Biomedical Materials, 2019
Crossref

17 Dhanaraj Gopi, Louis Kavitha, Subramanian Ramya, Durairajan Rajeswari. "Chemical and green routes for the synthesis of multifunctional pure and substituted nanohydroxyapatite for biomedical applications", Elsevier BV, 2016 — 23 words — < 1%
Crossref

18 www.nature.com — 23 words — < 1%
Internet

19 www.nuklearmalaysia.org — 23 words — < 1%
Internet

20 eprints.uthm.edu.my — 20 words — < 1%
Internet

21 David O. Obada, Semiyou A Osseni, Haziz Sina, Ayodeji N. Oyedeji et al. "Hydroxyapatitematerials-synthesis routes, mechanical behavior, theoreticalinsights, and artificial intelligence models: a review", Journal of the Australian Ceramic Society, 2023 — 19 words — < 1%
Crossref

22 P.A. Ramires, A. Romito, F. Cosentino, E. Milella. "The influence of titania/hydroxyapatite composite coatings on in vitro osteoblasts behaviour", Biomaterials, 2001 — 19 words — < 1%
Crossref

23 Itishree Ratha, Pradyot Datta, Nimu Chand Reger, Himanka Das et al. "In vivo osteogenesis of plasma sprayed ternary-ion doped hydroxyapatite coatings on — 18 words — < 1%

Ti6Al4V for orthopaedic applications", Ceramics International, 2022
Crossref

24 Masayoshi Yamaguchi. "Role of Zinc in Bone Metabolism and Preventive Effect on Bone Disorder", Biomedical Research on Trace Elements, 2007
Publications
18 words — < 1%

25 silo.pub
Internet
18 words — < 1%

26 Cheng, Yili. "Sol-Gel Derived Silica-Titania Porous Coating for the Surface Modification of Dental Implants", The University of Western Ontario (Canada), 2022
ProQuest
17 words — < 1%

27 "Advances in Biomedical Engineering and Technology", Springer Science and Business Media LLC, 2021
Crossref
16 words — < 1%

28 www.science.gov
Internet
16 words — < 1%

29 Sarmita Sinha, Jyotsana Priyadarshani, Karuppasamy Bavya Devi, Anyam Vijay Kishore et al. "In vivo performance analysis of silanized and coated nitinol wires in biological environment", Journal of Materials Research, 2020
Crossref
15 words — < 1%

30 Sabah Taha, Sumayya Begum, Vijaykiran N. Narwade, Devidas I. Halge et al. "Development of alcohol sensor using TiO2-Hydroxyapatite nano-composites", Materials Chemistry and Physics, 2020
Crossref
14 words — < 1%

31	U. Mary Nisha, D. Venkatesh, S. Arulmurugan, A. Kistan, P. Rajeshwaran, P. Siva Karthik. "Assessment of solar light sensitive Chitosan integrated CeO2-CuO ternary composites for the efficient degradation of Malachite Green, Acid Blue 113 dyes and microbial studies", Inorganic Chemistry Communications, 2023 Crossref	14 words — < 1%
32	ir.niist.res.in:8080 Internet	14 words — < 1%
33	Bikramjit Basu, Sourabh Ghosh. "Biomaterials for Musculoskeletal Regeneration", Springer Science and Business Media LLC, 2017 Crossref	13 words — < 1%
34	Chao Li, Hongzhi Lv, Yawei Du, Wenbo Zhu, Weijie Yang, Xiumei Wang, Juan Wang, Wei Chen. "Biologically modified implantation as therapeutic bioabsorbable materials for bone defect repair", Regenerative Therapy, 2022 Crossref	13 words — < 1%
35	Greeshma Ratheesh, Jayarama Reddy Venugopal, Amutha Chinappan, Hariharan Ezhilarasu, Asif Sadiq, Seeram Ramakrishna. "3D Fabrication of Polymeric Scaffolds for Regenerative Therapy", ACS Biomaterials Science & Engineering, 2017 Crossref	13 words — < 1%
36	sahris.sahra.org.za Internet	13 words — < 1%
37	scholarbank.nus.edu.sg Internet	13 words — < 1%
38	www.adb.org	

Internet

13 words — < 1%

39 A. Sindhya, S. Johnson Jeyakumar, M. Jothibas, P. Pugalendhi. "Synthesis and characterization of nanohydroxyapatite (nHAp) from Meretrix Meretrix Clam shells and its in-vitro studies for biomedical applications", Vacuum, 2022

12 words — < 1%

Crossref

40 Balázsi, Csaba, Gréta Gergely, Katalin Balázsi, Chang Hoon Chae, Hye Young Sim, Je Yong Choi, and Seong Gon Kim. "Bone Formation with Nano-Hydroxyapatite from Eggshell", Materials Science Forum, 2012.

12 words — < 1%

Crossref

41 Howa Begam, Somali Mandal, Abhijit Chanda, Jayanta Mukherjee, Samit Kumar Nandi. "Effect of Zinc Doping on Biological Properties of Biphasic Calcium Phosphate Ceramics in Orthopaedic Animal Model", Transactions of the Indian Ceramic Society, 2014

12 words — < 1%

Crossref

42 Kaushik Sarkar, Vinod Kumar, K. Bavya Devi, Debaki Ghosh, Samit Kumar Nandi, Mangal Roy. "Anomalous in Vitro and in Vivo Degradation of Magnesium Phosphate Bioceramics: Role of Zinc Addition", ACS Biomaterials Science & Engineering, 2019

12 words — < 1%

Crossref

43 N. A. Kamel. "Biophysical studies on bone cement composites based on polyester fumarate", Journal of Applied Polymer Science, 2009

12 words — < 1%

Crossref

44 N.A.S. Mohd Pu'ad, P. Koshy, H.Z. Abdullah, M.I. Idris, T.C. Lee. "Syntheses of hydroxyapatite from

12 words — < 1%

natural sources", Heliyon, 2019
Crossref

45 Safarzadeh, Marjan. "Development of B-Type and Multi-Ion Doped Carbonated Hydroxyapatite Bioceramics", University of Malaya (Malaysia), 2023
ProQuest
12 words — < 1%

46 Studies in Mechanobiology Tissue Engineering and Biomaterials, 2011.
Crossref
12 words — < 1%

47 Toufik Sahraoui, Fateh Chouia, Yousf Islem Bourezg, Abdelhamid Guelil. "Effect of natural phosphate content on the growth kinetics of hydroxyapatite crystals grown from kaolin clay", Materials Chemistry and Physics, 2022
Crossref
12 words — < 1%

48 eprints.covenantuniversity.edu.ng
Internet
12 words — < 1%

49 www.hindawi.com
Internet
12 words — < 1%

50 Balamurugan, A.. "Suitability evaluation of sol-gel derived Si-substituted hydroxyapatite for dental and maxillofacial applications through in vitro osteoblasts response", Dental Materials, 200810
Crossref
11 words — < 1%

51 Howa Begam, Samit Kumar Nandi, Abhijit Chanda, Biswanath Kundu. "Effect of bone morphogenetic protein on Zn-HAp and Zn-HAp/collagen composite: A systematic in vivo study", Research in Veterinary Science, 2017
Crossref
11 words — < 1%

52 M. Kavitha, R. Subramanian, K. Somasundara Vinoth, R. Narayanan, G. Venkatesh, N. Esakkiraja. "Optimization of process parameters for solution combustion synthesis of Strontium substituted Hydroxyapatite nanocrystals using Design of Experiments approach", Powder Technology, 2015
Crossref
11 words — < 1%

53 Ramakrishnan, R., P. Wilson, T. Sivakumar, and I. Jemina. "A comparative study of hydroxyapatites synthesized using various fuels through aqueous and alcohol mediated combustion routes", Ceramics International, 2013.
Crossref
11 words — < 1%

54 Zhou, H.. "Nanoscale hydroxyapatite particles for bone tissue engineering", Acta Biomaterialia, 201107
Crossref
11 words — < 1%

55 Amirhossein Esmaeilkhanian, Fariborz Sharifianjazi, Aliasghar Abouchenari, Amirreza Rouhani, Nader Parvin, Mohammad Irani. "Synthesis and Characterization of Natural Nano-hydroxyapatite Derived from Turkey Femur-Bone Waste", Applied Biochemistry and Biotechnology, 2019
Crossref
10 words — < 1%

56 Defne Bayraktar, A.Cüneyt Tas. "Chemical preparation of carbonated calcium hydroxyapatite powders at 37°C in urea-containing synthetic body fluids", Journal of the European Ceramic Society, 1999
Crossref
10 words — < 1%

57 Marium Waheed, Muhammad Yousaf, Aamir Shehzad, Muhammad Inam-Ur-Raheem et al. "Channelling eggshell waste to valuable and utilizable products:
10 words — < 1%

A comprehensive review", Trends in Food Science & Technology, 2020
Crossref

58	Monika Šupová. "Substituted hydroxyapatites for biomedical applications: A review", Ceramics International, 2015 Crossref	10 words — < 1%
59	Venkatesan, Jayachandran, and Se-Kwon Kim. "Hydroxyapatite from Marine Fish Bone : Isolation and Characterization Techniques", Marine Biomaterials Characterization Isolation and Applications, 2013. Crossref	10 words — < 1%
60	Voegeli, Tracy Susan. "The role of Hsp27 in the angiotensin II-induced NF-kappaB signaling pathway in aortic smooth muscle cells and brain endothelial cells", Proquest, 20111003 ProQuest	10 words — < 1%
61	researchbank.swinburne.edu.au Internet	10 words — < 1%
62	theses.lib.polyu.edu.hk Internet	10 words — < 1%
63	www.jmst.org Internet	10 words — < 1%
64	www.maerc.com Internet	10 words — < 1%
65	"Essential Biomechanics for Orthopedic Trauma", Springer Science and Business Media LLC, 2020 Crossref	9 words — < 1%

66 Jingxuan Li, Tianyu Zhang, Ziming Liao, Yan Wei, Ruiqiang Hang, Di Huang. "Engineered functional doped hydroxyapatite coating on titanium implants for osseointegration", Journal of Materials Research and Technology, 2023 — 9 words — < 1%
Crossref

67 Kaygili, O., C. Tatar, and F. Yakuphanoglu. "Structural and dielectrical properties of Mg3â€“Ca3(PO4)2 bioceramics obtained from hydroxyapatite by solâ€“gel method", Ceramics International, 2012. — 9 words — < 1%
Crossref

68 Kevin Lee. "Cell therapy for bone regeneration-Bench to bedside", Journal of Biomedical Materials Research Part B Applied Biomaterials, 04/2009 — 9 words — < 1%
Crossref

69 Pallabi Kayal, Sonali Jana, Pradyot Datta, Himanka Das, Biswanath Kundu, Samit Kumar Nandi. "Microfibers of fish waste-derived collagen and ion-doped bioactive glass in stimulating the healing sequences in full-thickness cutaneous burn injury", Journal of Drug Delivery Science and Technology, 2023 — 9 words — < 1%
Crossref

70 Taotao Liu, Meiqi Jin, Yuzhuo Zhang, Wenxian Weng, Tianlin Wang, Huazhe Yang, Ling Zhou. "K+/Sr2+/Na+ triple-doped hydroxyapatites/GelMA composite hydrogel scaffold for the repair of bone defects", Ceramics International, 2021 — 9 words — < 1%
Crossref

71 Wei Liang, Pengbing Ding, Guan Li, Enhang Lu, Zhenmin Zhao. "Hydroxyapatite Nanoparticles Facilitate Osteoblast Differentiation and Bone Formation Within — 9 words — < 1%

Sagittal Suture During Expansion in Rats", Drug Design, Development and Therapy, 2021
Crossref

72	baadalsg.inflibnet.ac.in Internet	9 words — < 1%
73	gcris.iyte.edu.tr Internet	9 words — < 1%
74	ir-library.egerton.ac.ke Internet	9 words — < 1%
75	jmeche.uitm.edu.my Internet	9 words — < 1%
76	journals.physiology.org Internet	9 words — < 1%
77	www.deepdyve.com Internet	9 words — < 1%
78	www.tdx.cat Internet	9 words — < 1%
79	"Biomaterials in Orthopaedics and Bone Regeneration", Springer Science and Business Media LLC, 2019 Crossref	8 words — < 1%
80	"Developments and Applications of Calcium Phosphate Bone Cements", Springer Science and Business Media LLC, 2018 Crossref	8 words — < 1%
81	A.Cüneyt Tas. "Combustion synthesis of calcium phosphate bioceramic powders", Journal of the	8 words — < 1%

European Ceramic Society, 2000
Crossref

82 D. Dutta Majumdar, V. Kumar, A. Roychowdhury, D.P. Mondal, M. Ghosh, S.K. Nandi. "In vivo analysis of bone-tissue interface in medical grade titanium and porous titanium with and without cenosphere as space holder", Materialia, 2020 — 8 words — < 1%
Crossref

83 Dajana Milovac, Tatiana C. Gamboa-Martínez, Marica Ivankovic, Gloria Gallego Ferrer, Hrvoje Ivankovic. "PCL-coated hydroxyapatite scaffold derived from cuttlefish bone: In vitro cell culture studies", Materials Science and Engineering: C, 2014 — 8 words — < 1%
Crossref

84 Dean-Mo Liu. "Influence of porosity and pore size on the compressive strength of porous hydroxyapatite ceramic", Ceramics International, 1997 — 8 words — < 1%
Crossref

85 Eric M Rivera, Miguel Araiza, Witold Brostow, Victor M Castaño, J.R Díaz-Estrada, R Hernández, J.Rogelio Rodríguez. "Synthesis of hydroxyapatite from eggshells", Materials Letters, 1999 — 8 words — < 1%
Crossref

86 Iwata, N.Y.. "Sintering behavior and apatite formation of diopside prepared by coprecipitation process", Colloids and Surfaces B: Biointerfaces, 20040415 — 8 words — < 1%
Crossref

87 Kunal Pal, S. Pal. "Development of Porous Hydroxyapatite Scaffolds", Materials and Manufacturing Processes, 2006 — 8 words — < 1%
Crossref

88 Lech Pawłowski, Philippe Blanchart. "Industrial Chemistry of Oxides for Emerging Applications", Wiley, 2018
Crossref
8 words — < 1%

89 Mochizuki, Chihiro, Hiroki Hara, Kei Oya, Shun Aoki, Tohru Hayakawa, Hiromichi Fujie, and Mitsunobu Sato. "Behaviors of MC3T3-E1 cells on carbonated apatite films, with a characteristic network structure, fabricated on a titanium plate by aqueous spray coating", Materials Science and Engineering C, 2014.
Crossref
8 words — < 1%

90 Oshida, Yoshiki. "Surface Modifications", Bioscience and Bioengineering of Titanium Materials, 2013.
Crossref
8 words — < 1%

91 Pankaew, Piyapong, Ekachai Hoonnivathana, Pichet Limsuwan, and Kittisakchai Naemchanthara. "Synthesis and Phase Transformation of Calcium Phosphate Prepared from Chicken Eggshells and Ammonium Phosphate", Advanced Materials Research, 2011.
Crossref
8 words — < 1%

92 Sasidharan Pillai, Rahul, and Vincenzo M. Sglavo. "Effect of MgO addition on solid state synthesis and thermal behavior of beta-tricalcium phosphate", Ceramics International, 2015.
Crossref
8 words — < 1%

93 Seong J. Kim. "Phase Transformation Kinetics in the Doped System LiAl5O8-LiFe5O8", Journal of the American Ceramic Society, 10/1988
Crossref
8 words — < 1%

94	Sergey V. Dorozhkin. "Nanosized and nanocrystalline calcium orthophosphates", Acta Biomaterialia, 2010 Crossref	8 words — < 1%
95	Springer Series in Biomaterials Science and Engineering, 2014. Crossref	8 words — < 1%
96	Xiangmei Liu, H.C. Man. "Laser fabrication of Ag-HA nanocomposites on Ti6Al4V implant for enhancing bioactivity and antibacterial capability", Materials Science and Engineering: C, 2017 Crossref	8 words — < 1%
97	archive.org Internet	8 words — < 1%
98	epdf.tips Internet	8 words — < 1%
99	epublications.vu.lt Internet	8 words — < 1%
100	etd.lib.metu.edu.tr Internet	8 words — < 1%
101	hdl.handle.net Internet	8 words — < 1%
102	parasitesandvectors.biomedcentral.com Internet	8 words — < 1%
103	pdffox.com Internet	8 words — < 1%
104	pingpdf.com	

Internet

8 words — < 1%

105 rd.springer.com
Internet

8 words — < 1%

106 repositorio.conare.ac.cr
Internet

8 words — < 1%

107 uvidok.rcub.bg.ac.rs
Internet

8 words — < 1%

108 www.ijsrp.org
Internet

8 words — < 1%

109 www.jeol.com
Internet

8 words — < 1%

110 www.ncbi.nlm.nih.gov
Internet

8 words — < 1%

111 www.tandfonline.com
Internet

8 words — < 1%

112 Diana-Elena Radulescu, Ionela Andreea Neacsu, Alexandru-Mihai Grumezescu, Ecaterina Andronescu. "Novel Trends into the Development of Natural Hydroxyapatite-Based Polymeric Composites for Bone Tissue Engineering", Polymers, 2022
Crossref

7 words — < 1%

113 Ergun, C.. "Synthesis and microstructural characterization of nano-size calcium phosphates with different stoichiometry", Ceramics International, 201104
Crossref

7 words — < 1%

114 IFMBE Proceedings, 2009.
Crossref

7 words — < 1%

115 Paital, S.R.. "Calcium phosphate coatings for bio-implant applications: Materials, performance factors, and methodologies", Materials Science & Engineering R, 20090814 — 7 words — < 1%
Crossref

116 Promita Bhattacharjee, Howa Begam, Abhijit Chanda, Samit Kumar Nandi. "Animal trial on zinc doped hydroxyapatite: A case study", Journal of Asian Ceramic Societies, 2018 — 7 words — < 1%
Crossref

117 R. Sammons. "Biological responses to hydroxyapatite", Elsevier BV, 2015 — 7 words — < 1%
Crossref

118 Samit K. Nandi, Samir K. Ghosh, Biswanath Kundu, Dipak K. De, Debabrata Basu. "Evaluation of new porous β-tri-calcium phosphate ceramic as bone substitute in goat model", Small Ruminant Research, 2008 — 7 words — < 1%
Crossref

119 www.dovepress.com — 7 words — < 1%
Internet

120 Gurbinder Kaur, Vishal Kumar, Francesco Baino, John C. Mauro, Gary Pickrell, Iain Evans, Oana Bretcanu. "Mechanical properties of bioactive glasses, ceramics, glass-ceramics and composites: State-of-the-art review and future challenges", Materials Science and Engineering: C, 2019 — 6 words — < 1%
Crossref

121 Kalita, S.J.. "Nanocrystalline hydroxyapatite bioceramic using microwave radiation: Synthesis and characterization", Materials Science & Engineering C, 20100130
Crossref
6 words — < 1%

122 Khalid Saeed, Idrees Khan, Soo-Young Park. " TiO /amidoxime-modified polyacrylonitrile nanofibers and its application for the photodegradation of methyl blue in aqueous medium ", Desalination and Water Treatment, 2014
Crossref
6 words — < 1%

123 Muhammad Syazwan M.N., Ahmad-Fauzi M.N., W. Balestri, Y. Reinwald, Yanny Marliana B.I.. "Effectiveness of Various Sintering Aids on the Densification and In Vitro Properties of Carbonated Hydroxyapatite Porous Scaffolds Produced by Foam Replication Technique", Materials Today Communications, 2021
Crossref
6 words — < 1%

124 Rahul Verma, Soumya Ranjan Mishra, Vishal Gadore, Md. Ahmaruzzaman. "Hydroxyapatite-based composites: Excellent materials for environmental remediation and biomedical applications", Advances in Colloid and Interface Science, 2023
Crossref
6 words — < 1%

125 Satyabrata Nigamananda Sahoo, Santanu Mandal, Rabiul Khan, Sourav Dutta et al. " Synergistic Effects of Cerium and Hot Forging on Biodegradation, Antibacterial Properties, and Biocompatibility of Microalloyed Mg–Zr–Sr Alloys ", ACS Biomaterials Science & Engineering, 2023
Crossref
6 words — < 1%

126 Sung-Baek Cho. "Dependence of Apatite Formation on Silica Gel on Its Structure: Effect of Heat
6 words — < 1%

Treatment", Journal of the American Ceramic Society, 7/1995
Crossref

EXCLUDE QUOTES	OFF	EXCLUDE SOURCES	OFF
EXCLUDE BIBLIOGRAPHY	ON	EXCLUDE MATCHES	OFF